Subband Adaptive Array for Mobile Communications with Applications to CDMA Systems

Xuan Nam Tran

A dissertation submitted in partial fulfillment
of the requirements for the degree of
Doctor of Engineering
in
Electronic Engineering

The University of Electro-Communications
September 2003

Subband Adaptive Array for Mobile Communications with Applications to CDMA Systems

Xuan Nam Tran

APPROVED BY SUPERVISORY COMMITEE:

Chairperson:	Professor **Yoshio Karasawa**
Member:	Professor **Takeshi Hashimoto**
Member:	Professor **Masashi Hayakawa**
Member:	Professor **Tadashi Fujino**
Member:	Professor **Nobuo Nakajima**

Subband Adaptive Array for Mobile Communications with Applications to CDMA Systems

Xuan Nam Tran

ABSTRACT

In mobile communications inter-symbol interference (ISI) and co-channel interference (CCI) are two main factors which affect the system performance. Tapped delay line adaptive array (TDLAA) has been realized as an effective scheme to suppress both these types of interference. However, TDLAA exposes slow convergence rate in searching for the optimum weights and requires large computational complexity. Subband adaptive array, performing signal processing in the subband frequency domain, has been shown to achieve the comparatively equivalent performance as TDLAA while overcoming those problems of TDLAA. This thesis gives insight into the SBAA performance using theoretical analysis and proposes generalized configurations of SBAA for direct sequence code division multiple access (DS-CDMA).

First, performance of two types of SBAA, namely, critical sampling SBAA and SBAA combining cyclic prefix data transmission, is investigated for multipath fading channel. For both the SBAAs, analytical models providing exact expressions for the subband signals, optimum weights in subband, array output, and output signal-to-interference-plus-noise ratio (SINR) are constructed. Numerical results are presented in comparison with simulation results to validate the analysis.

Next, two generalized configurations of SBAA for DS-CDMA are proposed: one for the DS-CDMA and the other for the wideband multicode DS-CDMA. Performance of the two proposed configurations of SBAA is explored using computer simulation. The so-called cyclic prefix spreading code CDMA is also proposed to use in combination with SBAA to maximize diversity gain in the frequency selective channels.

サブバンド信号処理型アダプティブアレーの理論解析とCDMA 移動通信への応用に関する研究

チャン　スワン　ナム
Tran Xuan Nam

論文概要

移動通信は、広帯域のマルチメディア・サービスを実現する新しい時代に進みつつある。そのような広帯域のネットワークではマルチパスフェージング及び干渉波がシステムパフォーマンスを劣化させる要因になる。このマルチパスフェージング及び干渉波を抑圧するために、タップ付き遅延線 (TDL:Tapped Delay Line) 型アダプティブアレー (TDLAA) がよく使われている。TDLAA は時空間フィルタリングを適応的に行い、受信アンテナの置かれた電波環境の中で不要波や内部雑音に対して所望波の電力比を最大化して受信機に供給するのが特長である。しかし、最適ウェイトを算出する時の演算量が膨大になるのが欠点である。それの対処方法としてサブバンド信号処理型アダプティブアレー (SBAA) が知られている。

SBAA では、各アンテナでの受信した信号をサブバンドに分割して、DFT (または FFT) により周波数領域に変換し、サブバンドごとに適応信号処理を行う。この方法により、分割したサブバンドごとに並列信号処理ができ、計算量を大幅に軽減できる。　また、分割サブバンド数を適当に定めることにより、効率よく遅延波の取り込みを行うことができる。特に、最近、（所属する研究室から）提案されているサイクリックプレフィクス（CP:Cyclic Prefix）を付加するシングルキャリア伝送方式に対する SBAA（SBAA-CP）では、遅延波に対するダイバーシチ利得を最大にすることができることが計算機シミュレーションによって明らかにされている。このように SBAA は、将来のアダプティブアレーのひとつの構成法として期待されているが、その動作解析は計算機シミュレーションによるものが多く、理論解析や最適設計手法に関する研究はまだ十分ではない。

本研究では、マルチパスフェージング環境での SBAA 及び SBAA-CP の理論解析を行い、性能評価や設計法の検討を行う。そして、CDMA における SBAA を提案し、2 次元 RAKE（2D-RAKE）と比較する。さらに、次世代のマルチメディアマルチコード W-CDMA における SBAA の構成法を提案し、その性能を理論解析や計算機シミュレーションにより示す。

この論文は 8 章から構成されており、主な内容は第 2 章のアダプティブアレーの基本、第 3 章の SBAA の構成と原理、第 4 章の SBAA の解析、第 5 章の SBAA-CP の解析、第 6 章の CDMA における SBAA 提案、第 7 章のマルチメディアマルチコード W-CDMA における SBAA の提案に大別される。

第 1 章は、序論であり、本論文の背景及び目的について述べる。

第 2 章では、シングルパス及びマルチパス・フェージング環境におけるアダプティブアレー

の信号モデルを示し、ビーム・フォーミング方法を簡単に説明する。MMSE(Minimum Mean Square Error)、MSN(Maximum Signal-to-Noise ratio)、ML(Maximum Likelihood), そして MV (Minimum Variance) 最適化法をまとめ、LMS(Least Mean Squares)、SMI(Sample Matrix Inversion), RLS(Recursive Least Squares) アルゴリズムなどを詳細に解説する。

第 3 章では、SBAA の構成要素であるサブバンドの分割やマルチレートフィルターなどの概念を説明し、移動通信用 SBAA の構成を述べる。さらに、SBAA の特長と問題点を明らかにする。

第 4 章では、評価基準として信号対干渉波・雑音比（SINR）を用い、相関行列、サブバンド最適ウェイトとその演算に基づく理論的な解析手法を確立する。解析された結果より、SINR がどのように入力 SNR 及び遅延特性に依存するかを明らかにする。

第 5 章では、第 4 章で確立した理論的な解析手法を用い、SBAA-CP の相関行列、サブバンド最適ウェイト、そして SINR の演算を行う。マルチパスフェージング環境では、遅延広がりが CP 長までの場合はダイバーシチ利得が最大になることを理論的な立場から明らかにする。

第 6 章では、CDMA における SBAA（SBAA-CDMA）構成を提案し、この SBAA-CDMA と 2D-RAKE の特性を比較する。遅延広がりがあまり大きくないチャネルでは SBAA-CDMA により 2D-RAKE と同等のパフォーマンスが得られることを示す。

第 7 章では、マルチコード DS-CDMA への SBAA の応用を提案し、これにより、多重アクセスによるマルチユーザ干渉を効果的に抑えて、チャネル容量の大幅増加が可能であることを明らかにする。さらに拡散コードにサイクリックプリフィックスを付ける CDMA 方式を提案し，これを SBAA と併用することでマルチパスフェージングの影響が抑えられ，所望信号に対する最大利得を実現することができることを示す。　　第 8 章では、本研究で得られた結論をまとめるとともに、今後の課題について述べる。

Tặng Bố, Mẹ, Các Anh, Chị, Em,
Huyền, và Khánh Linh, Mỹ Linh!

Tokyo, tháng 9 năm 2003
Trần Xuân Nam

Acknowledgements

First of all, I would like to express my deepest gratitude to my principal advisor Prof. Yoshio Karasawa for his guidance and support throughout the duration of this work. Since I started this work he has always given me motivation and encouragement to excel in research. It has been a pleasure working under his supervision and I would like to maintain this good relationship with him. I am also grateful to my second advisor Prof. Takeshi Hashimoto for his guidance and valuable comments on this work. I would like further to thank other member committees for their helpful comments on this thesis.

I also would like to thank Dr. Tetsuki Taniguchi for many valuable discussions during the course of this work. Working together with him was my pleasure. I would like further to thank Ass. Prof. Yukihiro Kamiya of Tokyo University of Agriculture and Technology and Dr. Yimin Zhang of Villanova University for their helpful discussions on subband adaptive arrays.

Thanks also go to members of Karasawa Laboratory for useful discussions, supports, and fun that I had while working together with them.

Further I would like to thank Ministry of Education, Culture, Sports, Science and Technology (MEXT), Japan for providing me an excellent opportunity to study in Japan and for the Monbukagakusho scholarship that I have received during the time of this research. This work would have been impossible without this financial support.

Finally, I am grateful to my dearest parents for providing me with the best educational opportunities. They have been a vital source driving me to all accomplishments and success. I am thankful to my wife Nguyen Thanh Huyen for being together with me in Japan giving me love and encouragement during the most important time of this work. Especially, I owe many thanks to my lovely twin daughters, Tran Khanh Linh and Tran My Linh, for their love and fun that I have received everyday after school. I could not have done without supports from all of them.

Contents

List of Figures

List of Tables

List of Abbreviations

1D RAKE	one dimensional RAKE
2D RAKE	two dimensional RAKE
AOA	angle of arrival
BPSK	binary phase shift keying
BER	bit error rate
CCI	co-channel interference
CDMA	code division multiple access
CP	cyclic prefix
DOF	degree of freedom
DFT	discrete Fourier transform
DOA	direction of arrival
DS-CDMA	direct sequence code division multiple access
ECF	extended area coverage factor
FFT	fast Fourier transform
i.i.d.	independent and identically distributed
IDFT	inverse discrete Fourier transform
IFFT	inverse fast Fourier transform
INR	interference to noise ratio
ISI	inter-symbol interference
LMS	least mean squares
MAI	multiple access interference
MIMO	multiple input multiple output
ML	maximum likelihood
MMSE	minimum mean square error
MSE	mean square error
MV	minimum variance
OFDM	orthogonal frequency division multiplexing
PN	pseudo-noise
RLS	recursive least squares
SBAA	subband adaptive array
SBAA-CDMA	subband adaptive array for CDMA

SBAA-CP	subband adaptive array combining cyclic prefix data transmission scheme
SINR	sinal to interference plus noise ratio
SIMO	single input multiple output
SISO	single input single output
SMI	sample matrix inversion
SNR	signal to noise ratio
S/P	serial to parallel conversion
SSB	single side band
P/S	parallel to serial conversion
QMF	quadrature mirror filter
QoS	quality of service
TDL	tapped delay line
TDLAA	tapped delay line adaptive array

List of Mathematical Notations

General notations

s	scalar s
$\boldsymbol{s}$	vector $\boldsymbol{s}$
$\boldsymbol{S}$	matrix $\boldsymbol{S}$
$\mathbf{S}$	constant matrix $\mathbf{S}$
$\boldsymbol{S}_{M\times N}$	matrix $\boldsymbol{S}$ with M rows and N columns
$\mathbf{I}$	identity matrix $\mathbf{I}$

Mathematical operation

$(.)^{\mathsf{T}}$	vector or matrix transpose operation
$(.)^{\mathsf{H}}$	complex vector or matrix Hermitian operation
∇	gradient operation
$(.)^*$	complex conjugate
$\det(.)$	matrix determinant
$\mathcal{E}\{.\}$	expectation operation
$\mathcal{L}[.]$	likelihood function
$\downarrow K$	decimating factor
$\uparrow K$	expanding factor

Symbols and variables

$\epsilon(t)$	error signal
j	imaginary number
λ	wavelength
ρ	correlation coefficient
θ	angle of arrival (AOA)
Δf	signal bandwidth
$\boldsymbol{a}(\theta)$	array response
B	relative signal bandwithd
f_c	carrier frequency

$\widetilde{f}^{(n)}$	combined sample at the nth subband
$n_m(t)$	noise at the mth element
$r(t)$	reference signal
$\widetilde{r}^{(n)}$	reference sample at the nth subband
$\boldsymbol{R}$	Covariance matrix
$\widetilde{\boldsymbol{R}}^{(n)}$	covariance matrix at the nth subband
$\boldsymbol{p}$	correlation vector
$\widetilde{\boldsymbol{p}}^{(n)}$	correlation vector at the nth subband
$s(t)$	transmit signal
$\boldsymbol{w}$	weight vector
w_m	weight at the mth element
$\widetilde{\boldsymbol{w}}^{(n)}$	weight vector in subband n
$\boldsymbol{x}(t)$	array input signal vector
$x_m(t)$	array input signal at the mth element
$y(t)$	array output signal

Chapter 1

Introduction

1.1 Context of Work

Mobile communications networks are growing toward a new generation, which provides users with integrated high speed services. In such high speed networks, inter-symbol interference (ISI) due to multipath fading and co-channel interference (CCI) due to frequency reuse are main factors which degrade the system perforamnce.

Adaptive array utilizing space-time signal processing has been realized as an effective scheme to suppress both these types of interference [1]. While suppression of CCI is inherent property of adaptive array, ISI can only be mitigated by use of integrated temporal filters or a certain signal processing method. An M-element adaptive array in essence has $(M-1)$ degrees of freedom (DOF) and thus can eliminate $(M-1)$ interferences. To mitigate multipath fading, tapped delayed line adaptive array (TDLAA), which is typically composed of an M-element array antenna and K tapped delay lines (TDLs)[1], has been considered an effective scheme due to its capability to coherently combine multipath components. The signal correlation between multipath components is always maximized and the signal-to-interference-plus-noise ratio (SINR) of TDLAA is thus improved within the FIR order (TDL length). However, TDLAA exposes slow convergence rate in searching for the optimum weights and difficulty in solving both the effects of ISI and CCI as it requires either large-scale matrix inversion or recursive computation [2, 3]. This problem becomes even more difficult in multipath fading channel with large delay spread as a high order FIR should be utilized.

Subband adaptive array, utilizing multirate filters to perform signal processing in the subband frequency domain, has been recently introduced to replace TDLAA [2–19]. It has been shown to achieve comparatively equivalent performance as TDLAA while overcoming those problems faced by TDLAA. In other words, SBAA can effectively mitigate both ISI

[1]A tapped delayed line with controlled weightes is sometimes also referred to as a temporal finite impulse response (FIR) filter.

and CCI while having at the same time faster convergence rate and reduced computational complexity. Furthermore, the subband structure of SBAA allows parallel processing, which is particularly efficient in the implementation of adaptive arrays with a large number of elements.

Up to the present, several schemes of SBAA have been introduced. These schemes can be classified into critical sampling SBAA, oversampled SBAA and SBAA without decimation based on the selection of the decimating factor. The critical sampling SBAA is the one with decimation factor equal to the number of subbands. When the decimation factor is smaller than the number of subbands, the SBAA is called the oversampled SBAA. Finally, if the decimation factor is zero, the SBAA is referred to as SBAA without decimation, although in essence SBAA without decimation is just the other way to call the frequency domain beamforming. Since the prime objective of subband signal processing is to reduce the computational complexity, the decimation factor should be chosen as large as possible [20], and the maximum decimation corresponding to the critical sampling SBAA is a clever choice. The performance of the critical sampling SBAA was recently explored using computation simulation in [6]. The results of the work show that the output SINR of the SBAA gradually decreases as the delay spread increases. The solution to the improvement of the SBAA performance is to use it in combination with the single carrier cyclic prefix data transmission as proposed by Karasawa and Shinozawa in [12]. However, apart from those obtained using computer simulation, not any results using theoretical analysis have been available for both the critical sampling SBAA and the SBAA combining the cyclic prefix data transmission (SABB-CP). Motivated by this open problem, in this work we *investigate the performance of both the SBAA and SBAA-CP using theoretical analysis.*

Working further toward the application of SBAAs into mobile communications using spread spectrum techniques, we found that except a very simple two-band SBAA for spread spectrum in [4], not any other generalized configurations and performance results were available for the direct sequence code division multiple access (DS-CDMA) scheme. A generalized configuration of SBAA[2] for DS-CDMA and, particularly, for the wideband DS-CDMA of the next generation multimedia mobile communications networks is thus important. We shall address this problem and *propose efficient and flexible configurations of SBAA for both DS-CDMA and wideband multirate multicode DS-CDMA* in this work.

The original contributions of our work is presented in the next section.

[2]From hereafter SBAA otherwise stated means the SBAA using critical sampling.

1.2 Original Contributions

Several contributions on the SBAA configurations and its performance have been made in this work. Parts of these contributions have been published or submitted for publication. The following list summarizes our main contributions within the scope of this work.

- Original contributions on the performance analysis of SBAA:

    1. Firstly, a detailed performance analysis of SBAA in both single path and multipath fading environment is presented in Chapter 4. The results of the analysis was published in the *IEICE Transaction on Fundamentals, Special Section on Digital Signal Processing, vol.E85–A, no.8, August, 2002.* Parts of the results were also presented at *the 2002 IEEE AP-S International Symposium and USNC/URSI National Radio Science Meeting, San Antonio, Texas, USA, June 2002.*
    2. Second is the theoretical analysis of SBAA-CP in multipath fading environment performed in Chapter 5. This analysis was published in the *IEICE Transaction on Communications, Special Issue on Software Defined Radio Technology and Its Applications, vol.E85–B, no.12, December 2002.* Also, portions of the results were presented at *The 8th IEEE International Conference on Communication Systems, Singapore, November 2002.*

- Contributions related to the applications of SBAA to DS-CDMA:

    1. A generalized configuration of SBAA for DS-CDMA and its performance comparison with 2D RAKE in Chapter 6. This material was presented in parts at *2002 Interim International Symposium on Antennas and Propagation, November, Yokosuka Reserach Park, Japan* and submitted to *EURASIP Journal on Applied Signal Processing* for publication.
    2. A flexible configuration of SBAA for wideband multirate multicode DS-CDMA and its performance results presented in Chapter 7. These results were published in the *IEICE Transaction on Fundamentals, Special Section on Multidimensional Mobile Information Networks, vol.E86–A, no.7, July 2003.*

1.3 Thesis Overview

This thesis contains 8 chapters and is organized as follows.

Chapter 2 overviews fundamentals of adaptive arrays. First, the basic concepts and classification of adaptive arrays are presented. Then the array signal model in single path and multipath fading environment is developed. These signal models will be used to analyze the performance of SBAA in the following chapters. Criteria to optimize performance of adaptive arrays and adaptive algorithms to obtain the array optimum weights are also summarized here.

In Chapter 3, basic operations and components in multirate filters are reviewed, followed by the applications of the multirate filters to implementation of SBAAs. Finally, various types of SBAAs are summarized and classified based on the decimation factors and feedback schemes. The motivations are then discussed to see what benefits can be achieved from using SBAA in mobile communications.

The detailed performance analysis of SBAA in both single path and multipath fading environments is presented in Chapter 4. The exact expressions for the subband signals, subband optimum weights, SBAA output and the output SINR are derived. Various performance results of SBAA using the theoretical analysis are also shown and validated using computer simulation.

Chapter 5 is an extension of the theoretical analysis presented in Chapter 4 to the SBAA-CP. Similar to Chapter 4, the derivation of the optimum weights in subbands, SBAA-CP output and the output SINR are presented. Numerical results are shown and verified via using computer simulation. Finally, an example of using the SBAA-CP as a software antenna is also presented.

A generalized configuration of SBAA for DS-CDMA is proposed in Chapter 6. The signal model for the SBAA configuration is developed and performance of the configuration is explored using computer simulation. The RAKE function of the SBAA for DS-CDMA is demonstrated by comparing with the standard 2D RAKE.

The proposed SBAA for DS-CDMA in Chapter 6 is extended to the wideband multirate multicode DS-CDMA in Chapter 7. The proposed scheme's capability to suppress multiple access interferences (MAI), particularly, the effect of high data rate users on the low data rate users are investigated. Furthermore, the combination of the so-called cyclic prefix spreading code CDMA with the proposed scheme is introduced to maximize the diversity gain in multipath fading environment.

Finally, Chapter 8 summarizes the main results of this work and concludes this thesis by suggesting a list of open topics for the future research.

Chapter 2

Fundamentals of Adaptive Arrays

This chapter presents principal concepts of adaptive arrays. In particular, this chapter covers array signal model, different types of adaptive beamforming, criteria to optimize performance, and adaptive signal processing algorithms for adaptive arrays. The benefits of using adaptive arrays in wireless mobile communications are also discussed.

2.1 Basic Concepts

An *adaptive array* is a system consisting of an array of antenna elements and a real-time adaptive processor which controls the beamforming network to automatically adjust its control weights toward optimization of a certain criterion in accordance with a selected algorithm [21–24]. Sometimes adaptive arrays are also referred to as *adaptive antennas* or *smart antennas*. A typical configuration of an adaptive array is illustrated in Figure 2.1.

Antenna elements can be arranged in various geometry configurations of which the most popular are linear, circular and planar (see Figure 2.2). A *linear array* consists of array elements whose centers are aligned along a straight line. If the spacing between consecutive array elements is equal, it is called a *uniformly spaced linear array*. Similarly, a *circular array* contains array elements whose centers lie on a circle. Finally, a *planar array* consists of array elements whose centers are placed on a single plane. While both linear and circular arrays can only perform one-dimensional beamforming (horizontal plane), planar arrays can be used for two-dimension (2-D) beamforming (both in vertical and horizontal planes).

Although the geometry configurations are different the principle of adaptive arrays is the same, and to simplify the analysis and synthesis of arrays the uniformly spaced linear arrays are often considered. The mathematics can be then extended to other geometries [25]. Throughout this work, therefore, we shall restrict our study to the uniformly spaced linear arrays.

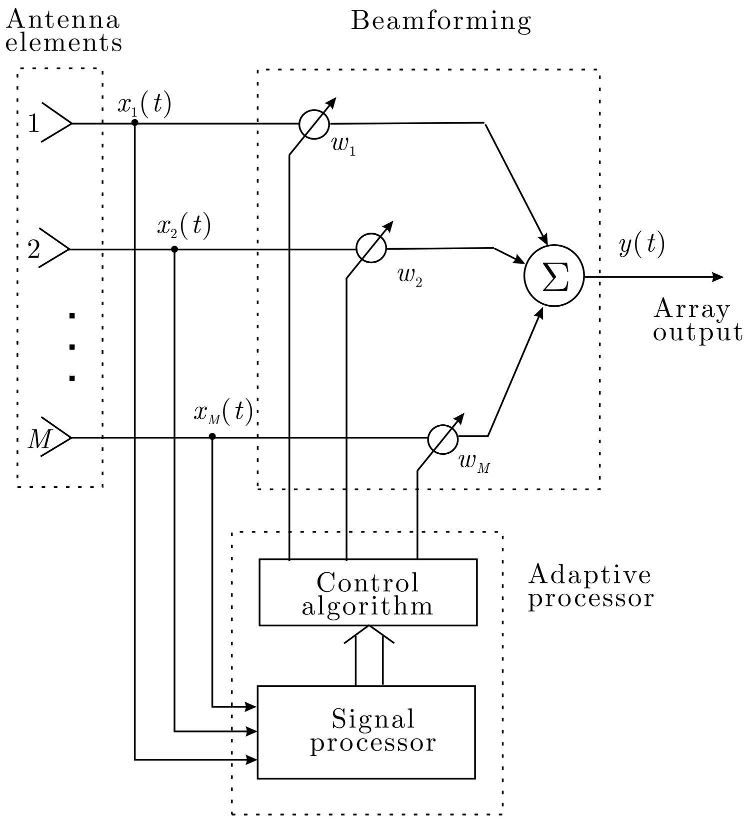

Figure 2.1: An adaptive array with M elements.

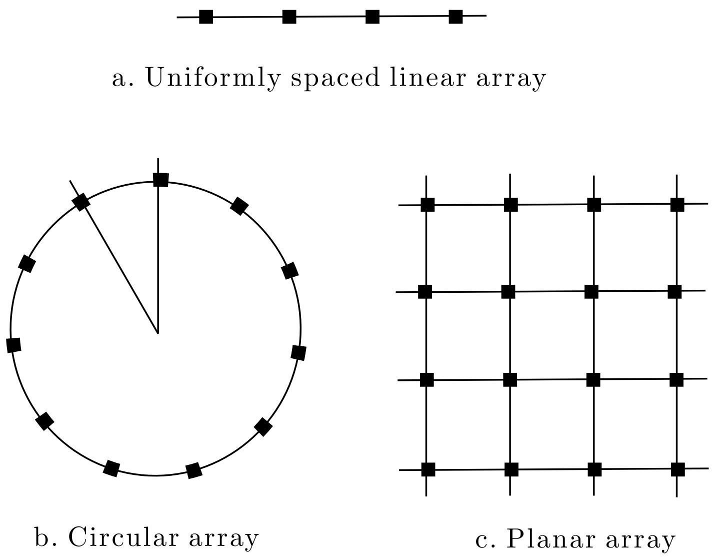

Figure 2.2: Different geometry configurations of adaptive arrays.

2.2 Array Signal Model

Consider a uniformly spaced linear array with M elements as illustrated in Figure 2.3, where d is the distance between adjacent elements.

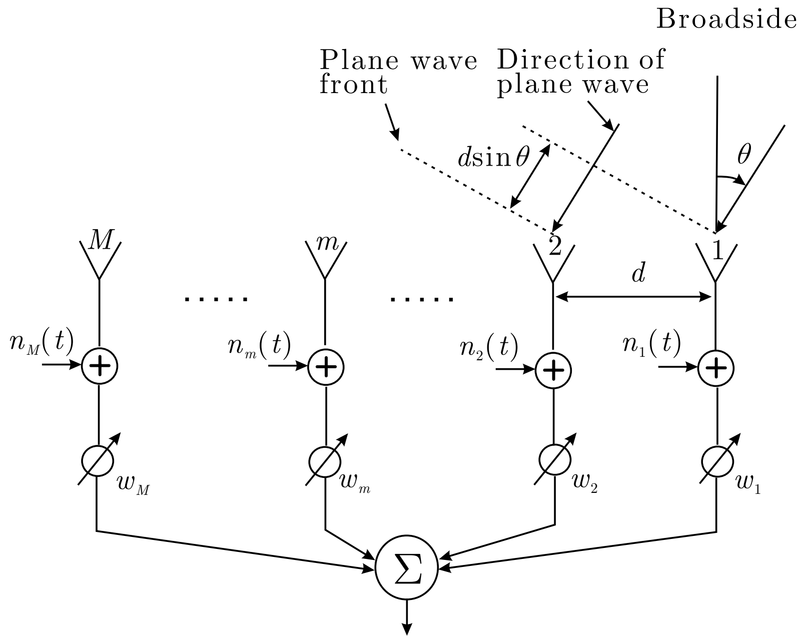

Figure 2.3: Signal model for adaptive arrays.

Assume that a plane wave incident at the array from a direction θ off the array broadside. The angle θ, measured clockwise from the array broadside, is called the *direction of arrival* (DOA) or *angle of arrival* (AOA) of the received signal. The wavefront at the $(m+1)$th element is later than at the mth element a differential distance of $d\sin\theta$. Let us take the first element as the reference element and let the signal at the reference element be $s(t)$, then the phase delay of the signal at element m relative to element 1 is $(m-1)kd\sin\theta$, where $k = \frac{2\pi}{\lambda}$ is the wave number and λ is the wavelength. Consequently, the received signal at the mth element $x_m(t)$ is given as

$$x_m(t) = s(t)e^{-j\frac{2\pi}{\lambda}(m-1)d\sin\theta} \tag{2.1}$$

where $j = \sqrt{-1}$ is the imaginary unit and $m = 1, 2, ..., M$.

Now let us arrange $x_m(t)$ in a vector form as

$$\boldsymbol{x}(t) = \begin{bmatrix} x_1(t) & x_2(t) & \ldots & x_M(t) \end{bmatrix}^{\mathsf{T}} \tag{2.2}$$

and let

$$\boldsymbol{a}(\theta) = \begin{bmatrix} 1 & e^{-j\frac{2\pi}{\lambda}d\sin\theta} & \ldots & e^{-j\frac{2\pi}{\lambda}(M-1)d\sin\theta} \end{bmatrix}^{\mathsf{T}} \tag{2.3}$$

where $[.]^{\mathsf{T}}$ denotes the vector/matrix transpose operation. Then (2.2) can be expressed as

$$\boldsymbol{x}(t) = s(t)\boldsymbol{a}(\theta). \tag{2.4}$$

The vector $\boldsymbol{x}(t)$ is called the array *input data vector* and $\boldsymbol{a}(\theta)$ is referred to as the *array response vector* or *steering vector*. The array response vector in this case depends only on the angle of arrival. In general, it may also depend on individual element response, the array geometry, and signal frequency. The set of array response vectors over all directions and frequencies is known as the *array manifold*. For simple arrays such as uniformly spaced linear array considered here, the array manifold can be analytically computed. In practice, however, it is measured as point source responses over various directions and frequencies and this process of obtaining the array manifold is referred to as *array calibration*.

Now, taking local noise at antenna elements into consideration the input data vector becomes

$$\boldsymbol{x}(t) = s(t)\boldsymbol{a}(\theta) + \boldsymbol{n}(t), \tag{2.5}$$

where the noise vector $\boldsymbol{n}(t)$ has been defined as

$$\boldsymbol{n}(t) = \begin{bmatrix} n_1(t) & n_2(t) & \dots & n_M(t) \end{bmatrix}^{\mathsf{T}}. \tag{2.6}$$

It should be noted that (2.1) holds for signals with bandwidth much smaller than the reciprocal of the propagation time across the array. Any signal which satisfies this condition is referred to as the *narrowband*, otherwise it is called *wideband*.

We now consider the array signal model for a more general case with multipath fading and multiuser effects. Let U denote the total number of users with signals impinging on array and let us assume that the incident signal of the ith user $s_i(t)$ contains P_i multipaths with complex amplitudes $\alpha_{i,p}$, angles of arrival $\theta_{i,p}$ and the excess path delays $\tau_{i,p}$, where p is the path index and $p = 1, 2, ..., P_i$. The received signal vector for the ith user can be expressed as

$$\boldsymbol{x}_i(t) = \sum_{p=1}^{P_i} \alpha_{i,p}\boldsymbol{a}(\theta_{i,p}) s_{i,p}(t - \tau_{i,p}). \tag{2.7}$$

Considering effects of all U users and local noise, the input data vector can be written in a generalized form as

$$\boldsymbol{x}(t) = \sum_{i=1}^{U}\sum_{p=1}^{P_i} \alpha_{i,p}\boldsymbol{a}(\theta_{i,p}) s_{i,p}(t - \tau_{i,p}) + \boldsymbol{n}(t). \tag{2.8}$$

In (2.7) and (2.8), the term $\sum_{p=1}^{P_i} \alpha_{i,p}\boldsymbol{a}(\theta_{i,p})$ is called the *spatial signature vector* of user i.

2.3 Adaptive Beamforming

Beamforming is one type of signal processing used to form the array beams toward the desired signal sources while simultaneously create nulls toward interferences. This process of separating desired user from the interferences based on their spatial characteristics is called *spatial filtering*. In the reverse or uplink (from mobile to basestation), the objective of beamforming is to maximize the signal to interference plus noise ratio (SINR) of the received desired signal. Similarly, beamforming is utilized in the forward or downlink (from basestation to mobile) to maximize the transmit power of basestation to a desired mobile, thereby maximizing SINR of the downlink. When beamforming is controlled using adaptive signal processing, it is called *adaptive beamforming*. In some cases, it is desired to steer not the beams but array nulls toward a specific location to suppress interferences. The beamforming process in those cases is called *null-forming*.

A *beamformer* is a processor used in conjunction with an array to perform versatile form of spatial filtering [26]. There are two types of beamformers, namely, *narrowband beamformer* and *broadband beamformer*.

A narrowband beamformer samples input signals in spatial domain and typically used to process narrowband signals. The configuration of a narrowband beamformer is depicted in Figure 2.4.

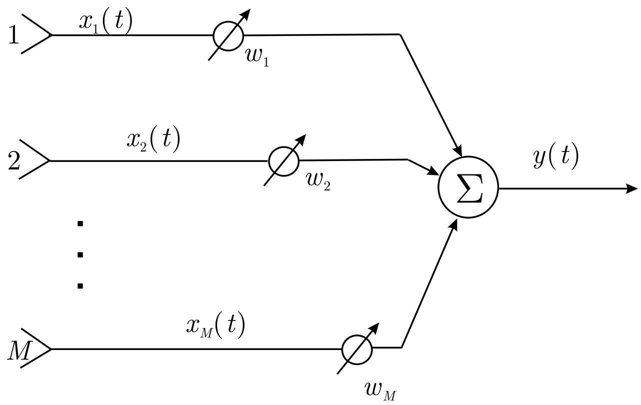

Figure 2.4: Configuration of an adaptive narrowband beamformer.

The output of the narrowband beamformer is weighted linear combination of received signals at each array element, and given by

$$y(t) = \boldsymbol{w}^{\mathsf{H}}\boldsymbol{x}(t), \tag{2.9}$$

where $\boldsymbol{x}(t)$ is input data vector, $(.)^{\mathsf{H}}$ represents Hermitian (complex conjugate transpose) operation of a vector/matrix, and the complex weight vector $\boldsymbol{w}$ is defined as

$$\boldsymbol{w} = \begin{bmatrix} w_1 & w_2 & \dots & w_M \end{bmatrix}^{\mathsf{T}}. \tag{2.10}$$

Different from the narrowband beamformer, a broadband beamformer samples input signals in both spatial and temporal domains and employed to process broadband signals. A broadband beamformer is also called a *spatio-temporal processor* or *spatio-temporal equalizer*. The structure of a broadband beamformer often contains tapped delayed lines (TDLs) or also called transversal filters in individual array elements. If the tap spacing is sufficiently long and the number of taps is large, the TDL approximates an ideal filter that allows exact control of gain and phase at each frequency within the band of interest [27]. The TDL is not only useful for providing desired adjustment of gain and phase over the frequency band of interest for wideband signals but also suited for other purposes such as mitigation of multipath fading and compensation for effects of finite array propagation delay and interchannel mismatch [27]. A typical broadband beamformer using TDLs is shown in Figure 2.5.

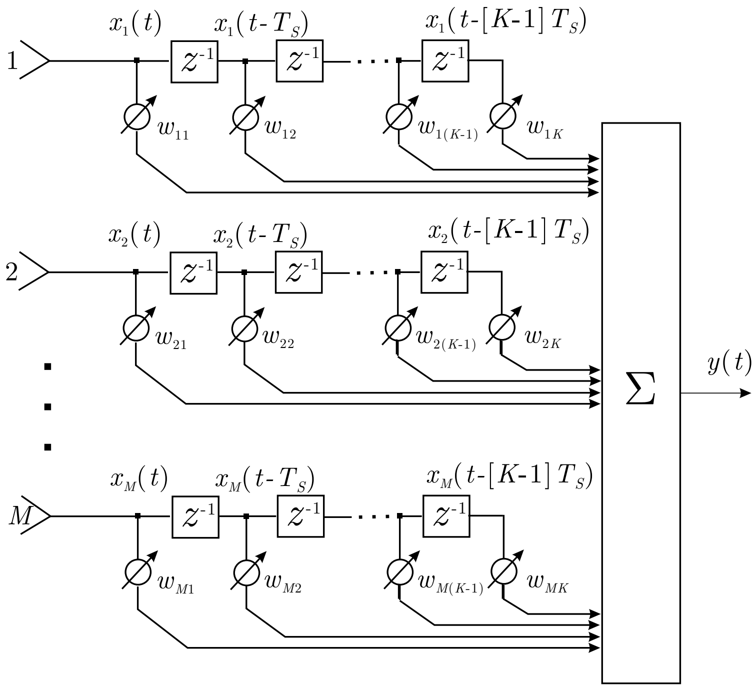

Figure 2.5: Broadband beamformer using tapped delay lines.

To model the broadband beamformer, arrange signals and complex weights at K TDL taps of antenna m as

$$\acute{\boldsymbol{x}}_m(t) = \Big[x_m(t) \quad x_m(t-T_s) \quad \dots \quad x_m(t-[K-1]T_s)\Big]^{\mathsf{T}}, \tag{2.11}$$

$$\acute{\boldsymbol{w}}_m = \Big[w_{m1} \quad w_{m2} \quad \dots \quad w_{mK}\Big]^{\mathsf{T}}, \tag{2.12}$$

and define

$$\boldsymbol{x}(t) = \Big[\acute{\boldsymbol{x}}_1^{\mathsf{T}}(t) \quad \acute{\boldsymbol{x}}_2^{\mathsf{T}}(t) \quad \dots \quad \acute{\boldsymbol{x}}_M^{\mathsf{T}}(t)\Big]^{\mathsf{T}}, \tag{2.13}$$

$$\boldsymbol{w} = \Big[\acute{\boldsymbol{w}}_1^{\mathsf{T}} \quad \acute{\boldsymbol{w}}_2^{\mathsf{T}} \quad \dots \quad \acute{\boldsymbol{w}}_M^{\mathsf{T}}\Big]^{\mathsf{T}}, \tag{2.14}$$

the output of the broadband beamformer can be now expressed in exactly the same form as of the narrowband beamformer in (2.9), that is

$$y(t) = \boldsymbol{w}^{\mathsf{H}}\boldsymbol{x}(t). \tag{2.15}$$

The broadband beamformer using TDLs considered so far is a classical time domain processor. Recently, fast Fourier transform (FFT) has been used to replace TDLs in the beamformer configuration resulting in an equivalent frequency domain broadband beamformer as shown in Figure 2.6 [26][28].

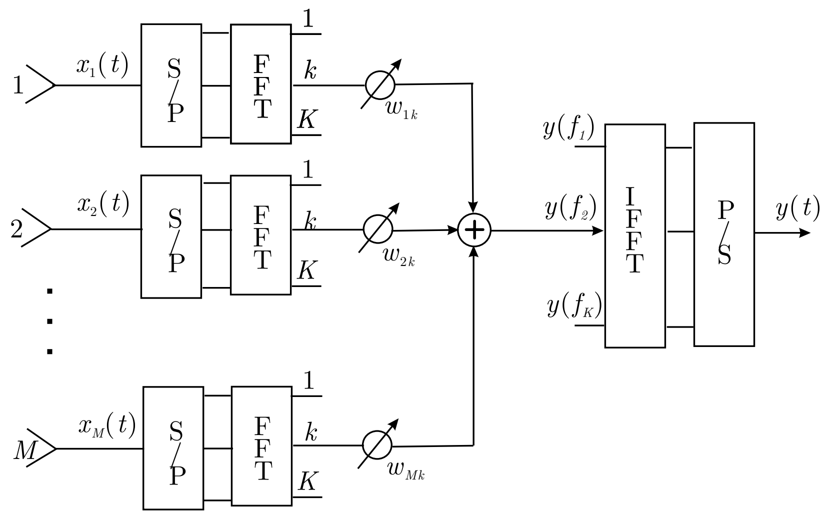

S/P: serial-to-parallel conversion
P/S: parallel-to-serial conversion

Figure 2.6: Frequency domain beamformer using FFT.

The advantage of the frequency domain approach is achievement of reduced computational load and increased convergence rate. Since the control weights are obtained independently for each subband (frequency bin), the process of selecting the weights can be performed in parallel, leading to faster weight update [28]. Moreover, when adaptive algorithms such as the least mean squares (LMS) is used, different step sizes can be applied to each subband, resulting in faster convergence [28]. Study performance of frequency domain beamformer is one of the main objectives of this report and will be presented in details in the following chapters.

2.4 Criteria for Performance Optimization

As we have mentioned earlier in this chapter, the adaptive processor controls the beamforming network to optimize the beamforming weights according to a certain criterion. Four common criteria which are often employed to obtain optimum weights for adaptive arrays in mobile communications are Minimum Mean Square Error (MMSE), Maximum Signal to Interference plus Noise ratio (MSINR), Minimum Variance (MV) and Maximum Likelihood (ML). These optimum criteria will be reviewed below.

2.4.1 Minimum Mean Square Error (MMSE)

The MMSE criterion is first considered by Widrow *et al.* in [21]. The criterion strives to minimize the error between the array output signal $y(t)$ and the desired signal $s(t)$. In practice, the desired signal $s(t)$ is of course not known. However, using some techniques such as training method or estimation based on the desired signal characteristics one can generate a *reference signal* $r(t)$ that closely approximates the desired signal to a certain extent. Consider the input signal vector given by

$$\begin{aligned} \boldsymbol{x}(t) &= s(t)\boldsymbol{a}(\theta) + \boldsymbol{u}(t) \\ &= \boldsymbol{s}(t) + \boldsymbol{u}(t) \end{aligned} \tag{2.16}$$

where $\boldsymbol{a}(\theta)$ is the array response and $\boldsymbol{u}(t)$ is a vector containing zero mean noise and uncorrelated interferences. For a narrowband adaptive array, the output signal is recalled from (2.9) as

$$y(t) = \boldsymbol{w}^{\mathsf{H}}\boldsymbol{x}(t). \tag{2.17}$$

The error signal is defined as

$$\begin{aligned} \epsilon(t) &= r(t) - y(t) \\ &= r(t) - \boldsymbol{w}^{\mathsf{H}}\boldsymbol{x}(t), \end{aligned} \tag{2.18}$$

and the weights are chosen to minimize the mean square error (MSE) of the error signal

$$\mathcal{E}\{|\epsilon(t)|^2\} = \mathcal{E}\{|r(t) - \boldsymbol{w}^{\mathsf{H}}\boldsymbol{x}(t)|^2\}, \tag{2.19}$$

where $\mathcal{E}\{.\}$ denotes the expected operation. Expanding (2.19) we have

$$\begin{aligned}\mathcal{E}\{|\epsilon(t)|^2\} &= \mathcal{E}\{|r(t)|^2\} - \boldsymbol{w}^{\mathsf{T}}\mathcal{E}\{\boldsymbol{x}^*(t)r(t)\} - \boldsymbol{w}^{\mathsf{H}}\mathcal{E}\{\boldsymbol{x}(t)r^*(t)\} + \boldsymbol{w}^{\mathsf{H}}\mathcal{E}\{\boldsymbol{x}(t)\boldsymbol{x}^{\mathsf{H}}(t)\}\boldsymbol{w} \\ &= \mathcal{E}\{|r(t)|^2\} - \boldsymbol{w}^{\mathsf{T}}\boldsymbol{r}_{xr}^* - \boldsymbol{w}^{\mathsf{H}}\boldsymbol{r}_{xr} + \boldsymbol{w}^{\mathsf{H}}\boldsymbol{R}_{xx}\boldsymbol{w},\end{aligned} \tag{2.20}$$

where $\boldsymbol{r}_{xr} = \mathcal{E}\{\boldsymbol{x}(t)r^*(t)\}$ and $\boldsymbol{R}_{xx} = \mathcal{E}\{\boldsymbol{x}(t)\boldsymbol{x}^{\mathsf{H}}(t)\}$ are called the *correlation vector* and the *covariance matrix*, respectively. Here $(.)^*$ denotes the complex conjugate. The optimum weight vector can be found by setting the gradient of (2.20) with respect to $\boldsymbol{w}$ equal to zero [29]

$$\nabla_{\boldsymbol{w}}\mathcal{E}\{|\epsilon(t)|^2\} = -2\boldsymbol{r}_{xr} + 2\boldsymbol{R}_{xx}\boldsymbol{w} = 0 \tag{2.21}$$

which gives the solution

$$\boldsymbol{w}_{\text{MMSE}} = \boldsymbol{w}_{opt} = \boldsymbol{R}_{xx}^{-1}\boldsymbol{r}_{xr}. \tag{2.22}$$

Equation (2.22) is often referred to as the Wiener-Hopf equation or the optimum Wiener solution [29]. By substituting (2.22) into (2.20), we have the optimum MMSE

$$\text{MMSE} = \mathcal{E}\{|\epsilon(t)|^2\} = \mathcal{E}\{|r(t)|^2\} - \boldsymbol{r}_{xr}^{\mathsf{H}}\boldsymbol{R}_{xx}^{-1}\boldsymbol{r}_{xr}. \tag{2.23}$$

2.4.2 Maximum Signal to Interference plus Noise Ratio (MSINR)

The criterion considered in this subsection is the maximum SINR. Recall (2.9) and use (2.16), the output of the array can be expressed as

$$\begin{aligned} y(t) &= \boldsymbol{w}^{\mathsf{H}}\boldsymbol{x}(t) = \boldsymbol{w}^{\mathsf{H}}\boldsymbol{s}(t) + \boldsymbol{w}^{\mathsf{H}}\boldsymbol{u}(t) \\ &= y_s(t) + y_u(t). \end{aligned} \tag{2.24}$$

The average output SINR is given by

$$\text{SINR} = \mathcal{E}\left\{\frac{|y_s(t)|^2}{|y_u(t)|^2}\right\} = \mathcal{E}\left\{\frac{\boldsymbol{w}^{\mathsf{H}}\boldsymbol{s}(t)\boldsymbol{s}^{\mathsf{H}}(t)\boldsymbol{w}}{\boldsymbol{w}^{\mathsf{H}}\boldsymbol{u}(t)\boldsymbol{u}^{\mathsf{H}}(t)\boldsymbol{w}}\right\} = \frac{\boldsymbol{w}^{\mathsf{H}}\boldsymbol{R}_{ss}\boldsymbol{w}}{\boldsymbol{w}^{\mathsf{H}}\boldsymbol{R}_{uu}\boldsymbol{w}}, \tag{2.25}$$

where $\boldsymbol{R}_{ss} = \mathcal{E}\{\boldsymbol{s}(t)\boldsymbol{s}^{\mathsf{H}}(t)\}$ and $\boldsymbol{R}_{uu} = \mathcal{E}\{\boldsymbol{u}(t)\boldsymbol{u}^{\mathsf{H}}(t)\}$. Taking the gradient of (2.25) with respect to $\boldsymbol{w}$ gives

$$\begin{aligned}\nabla_{\boldsymbol{w}}\text{SINR} &= \frac{\nabla_{\boldsymbol{w}}(\boldsymbol{w}^{\mathsf{H}}\boldsymbol{R}_{ss}\boldsymbol{w})(\boldsymbol{w}^{\mathsf{H}}\boldsymbol{R}_{uu}\boldsymbol{w}) - (\boldsymbol{w}^{\mathsf{H}}\boldsymbol{R}_{ss}\boldsymbol{w})\nabla_{\boldsymbol{w}}(\boldsymbol{w}^{\mathsf{H}}\boldsymbol{R}_{uu}\boldsymbol{w})}{(\boldsymbol{w}^{\mathsf{H}}\boldsymbol{R}_{uu}\boldsymbol{w})^2} \\ &= \frac{2\boldsymbol{R}_{ss}\boldsymbol{w}(\boldsymbol{w}^{\mathsf{H}}\boldsymbol{R}_{uu}\boldsymbol{w}) - 2\boldsymbol{R}_{uu}\boldsymbol{w}(\boldsymbol{w}^{\mathsf{H}}\boldsymbol{R}_{ss}\boldsymbol{w})}{(\boldsymbol{w}^{\mathsf{H}}\boldsymbol{R}_{uu}\boldsymbol{w})^2}.\end{aligned} \tag{2.26}$$

The optimum weight $\boldsymbol{w}_{opt}$ can be found by setting $\nabla_{\boldsymbol{w}}\text{SINR} = 0$, which leads to

$$\boldsymbol{R}_{ss}\boldsymbol{w} = \frac{\boldsymbol{w}^{\mathsf{H}}\boldsymbol{R}_{ss}\boldsymbol{w}}{\boldsymbol{w}^{\mathsf{H}}\boldsymbol{R}_{uu}\boldsymbol{w}}\boldsymbol{R}_{uu}\boldsymbol{w} = \text{SINR}\boldsymbol{R}_{uu}\boldsymbol{w}. \tag{2.27}$$

If $\boldsymbol{R}_{uu}$ is invertible, then (2.27) can be rewritten as

$$\boldsymbol{R}_{uu}^{-1}\boldsymbol{R}_{ss}\boldsymbol{w} = \text{SINR}\boldsymbol{w}, \tag{2.28}$$

which is the generalized eigenproblem. Note that the value on the right hand side of (2.26) is bounded by the maximum and minimum eigenvalues of $\boldsymbol{R}_{uu}^{-1}\boldsymbol{R}_{ss}$. The maximum eigenvalue $\lambda_{\max}$ satisfies the following condition

$$\boldsymbol{R}_{uu}^{-1}\boldsymbol{R}_{ss}\boldsymbol{w} = \lambda_{\max}\boldsymbol{w} \tag{2.29}$$

Compare (2.28) with (2.29), it is clear that $\lambda_{\max}$ is the optimum value of SINR. Corresponding to this $\lambda_{\max}$ there is only one eigenvector $\boldsymbol{w}_{opt}$ given by

$$\begin{aligned}\boldsymbol{w}_{opt} &= \frac{\boldsymbol{R}_{uu}^{-1}\boldsymbol{R}_{ss}\boldsymbol{w}_{opt}}{\text{SINR}} = \frac{\boldsymbol{R}_{uu}^{-1}\mathcal{E}\left\{s(t)\boldsymbol{a}(\theta)s(t)\boldsymbol{a}^{\mathsf{H}}(\theta)\right\}\boldsymbol{w}_{opt}}{\text{SINR}} \\ &= \frac{\boldsymbol{R}_{uu}^{-1}\boldsymbol{a}(\theta)\boldsymbol{a}^{\mathsf{H}}(\theta)\boldsymbol{w}_{opt}\mathcal{E}\left\{|s(t)|^2\right\}}{\text{SINR}}.\end{aligned} \tag{2.30}$$

Define

$$\beta = \frac{\boldsymbol{a}^{\mathsf{H}}(\theta)\boldsymbol{w}_{opt}\mathcal{E}\left\{|s(t)|^2\right\}}{\text{SINR}}, \tag{2.31}$$

then the optimum weight vector can be expressed in a similar form of the Wiener-Hopf equation as

$$\boldsymbol{w}_{\text{SINR}} = \boldsymbol{w}_{opt} = \beta\boldsymbol{R}_{uu}^{-1}\boldsymbol{a}(\theta). \tag{2.32}$$

2.4.3 Maximum Likelihood (ML)

Recall again the input signal vector from (2.16)

$$\begin{aligned}\boldsymbol{x}(t) &= s(t)\boldsymbol{a}(\theta) + \boldsymbol{u}(t) \\ &= \boldsymbol{s}(t) + \boldsymbol{u}(t)\end{aligned} \tag{2.33}$$

and define the probability density function for $\boldsymbol{s}(t)$ given $\boldsymbol{x}(t)$ as $p_{\boldsymbol{x}(t)|\boldsymbol{s}(t)}\{\boldsymbol{x}(t)\}$. Given $\boldsymbol{x}(t)$, it is desired to maximize $p_{\boldsymbol{x}(t)|\boldsymbol{s}(t)}\{\boldsymbol{s}(t)\}$. Since the natural logarithm is a monotone function, increasing $p_{\boldsymbol{x}(t)|\boldsymbol{s}(t)}\{\boldsymbol{x}(t)\}$ is equivalent with increasing $\ln\left[p_{\boldsymbol{x}(t)|\boldsymbol{s}(t)}\{\boldsymbol{x}(t)\}\right]$. Thus the likelihood function of $\boldsymbol{x}(t)$ can be defined as

$$\mathcal{L}[\boldsymbol{x}(t)] = -\ln\left[p_{\boldsymbol{x}(t)|\boldsymbol{s}(t)}\{\boldsymbol{x}(t)\}\right] \tag{2.34}$$

Assume that the $\boldsymbol{u}(t)$ is a stationary zero mean Gaussian vector with a covariance matrix $\boldsymbol{R}_{uu}$, and that $\boldsymbol{x}(t)$ is a Gaussian random vector with mean $s(t)\boldsymbol{a}(\theta)$. The likelihood function can be expressed as [27]

$$\mathcal{L}[\boldsymbol{x}(t)] = c\big[\boldsymbol{x}(t) - \boldsymbol{a}(\theta)s(t)\big]^{\mathsf{H}}\boldsymbol{R}_{uu}^{-1}\big[\boldsymbol{x}(t) - \boldsymbol{a}(\theta)s(t)\big] \tag{2.35}$$

where c is a scalar constant independent of $\boldsymbol{x}(t)$ and $\boldsymbol{s}(t)$.

Our objective is to find an estimate $\hat{s}(t)$ of $s(t)$ which minimizes (2.35). Setting the partial derivative of $\mathcal{L}[\boldsymbol{x}(t)]$ with respect to $s(t)$ to zero [27]

$$\frac{\partial\mathcal{L}[\boldsymbol{x}(t)]}{\partial s(t)} = -2\boldsymbol{a}^{\mathsf{H}}(\theta)\boldsymbol{R}_{uu}^{-1}\boldsymbol{x}(t) + 2\hat{s}(t)\boldsymbol{a}^{\mathsf{H}}(\theta)\boldsymbol{R}_{uu}^{-1}\boldsymbol{a}(\theta) = 0 \tag{2.36}$$

and note that $\boldsymbol{a}^{\mathsf{H}}(\theta)\boldsymbol{R}_{uu}^{-1}\boldsymbol{a}(\theta)$ is a scalar, it follows that

$$\hat{s}(t) = \frac{\boldsymbol{a}^{\mathsf{H}}(\theta)\boldsymbol{R}_{uu}^{-1}}{\boldsymbol{a}^{\mathsf{H}}(\theta)\boldsymbol{R}_{uu}^{-1}\boldsymbol{a}(\theta)}\boldsymbol{x}(t). \tag{2.37}$$

Comparing (2.37) with (2.9), it is easy to realize that the optimum weight vector $\boldsymbol{w}_{opt}$ using ML criterion is given by

$$\boldsymbol{w}_{\mathrm{ML}} = \boldsymbol{w}_{opt} = \frac{\boldsymbol{R}_{uu}^{-1}\boldsymbol{a}(\theta)}{\boldsymbol{a}^{\mathsf{H}}(\theta)\boldsymbol{R}_{uu}^{-1}\boldsymbol{a}(\theta)}. \tag{2.38}$$

Define

$$\beta = \frac{1}{\boldsymbol{a}^{\mathsf{H}}(\theta)\boldsymbol{R}_{uu}^{-1}\boldsymbol{a}(\theta)} \tag{2.39}$$

then the optimal weight vector using ML criterion can be expressed in the similar form of the Wiener-Hopf equation as

$$\boldsymbol{w}_{\mathrm{ML}} = \beta\boldsymbol{R}_{uu}^{-1}\boldsymbol{a}(\theta). \tag{2.40}$$

2.4.4 Minimum Variance (MV)

Minimum variance (ML), also known as linear constrained minimum variance (LCMV), is used when the desired signal and its direction are both known. Recall beamformer output from (2.9)

$$\begin{aligned} y(t) &= \boldsymbol{w}^{\mathsf{H}}\boldsymbol{x}(t) = \boldsymbol{w}^{\mathsf{H}}\boldsymbol{s}(t) + \boldsymbol{w}^{\mathsf{H}}\boldsymbol{u}(t) \\ &= \boldsymbol{w}^{\mathsf{H}}\boldsymbol{a}(\theta)s(t) + \boldsymbol{w}^{\mathsf{H}}\boldsymbol{u}(t) \end{aligned} \tag{2.41}$$

In order to obtain the desired signal with a specific gain in a given direction, we can use a constraint [29]

$$\boldsymbol{w}^{\mathsf{H}}\boldsymbol{a}(\theta) = g. \tag{2.42}$$

Substitute (2.42) into (2.41), we obtain the array output subject to the constraint as [30]

$$y(t) = gs(t) + \boldsymbol{w}^{\mathsf{H}}\boldsymbol{u}(t) \tag{2.43}$$

Since $\boldsymbol{u}(t)$ is assumed to be uncorrelated and zero mean Gaussian, we have $\mathcal{E}\{y(t)\} = gs(t)$. The variance of the array output then is given by

$$\begin{aligned} \mathrm{var}\big\{y(t)\big\} &= \mathcal{E}\big\{\big[y(t) - gs(t)\big]\big[y(t) - gs(t)\big]^*\big\} \\ &= \mathcal{E}\Big\{\boldsymbol{w}^{\mathsf{H}}\boldsymbol{u}(t)\big[\boldsymbol{w}^{\mathsf{H}}\boldsymbol{u}(t)\big]^{\mathsf{H}}\Big\} \\ &= \boldsymbol{w}^{\mathsf{H}}\boldsymbol{R}_{uu}\boldsymbol{w} \end{aligned} \tag{2.44}$$

Now using the method of Lagrange, we have

$$\nabla_{\boldsymbol{w}}\Big\{\boldsymbol{w}^{\mathsf{H}}\boldsymbol{R}_{uu}\boldsymbol{w} - \beta\big[g - \boldsymbol{w}^{\mathsf{H}}\boldsymbol{a}(\theta)\big]\Big\} = 0 \tag{2.45}$$

or equivalently,

$$\boldsymbol{R}_{uu}\boldsymbol{w} - \beta\boldsymbol{a}(\theta) = 0. \tag{2.46}$$

If $\boldsymbol{R}_{uu}$ is invertible the optimum weight vector using MV criterion can be expressed as

$$\boldsymbol{w}_{\mathrm{MV}} = \beta\boldsymbol{R}_{uu}^{-1}\boldsymbol{a}(\theta), \tag{2.47}$$

where [29, 30]

$$\beta = \frac{g}{\boldsymbol{a}^{\mathsf{H}}(\theta)\boldsymbol{R}_{uu}^{-1}\boldsymbol{a}(\theta)}. \tag{2.48}$$

When $g = 1$, the MV beamformer is often referred to as the minimum variance distortionless response (MVDR) beamformer, or the Capon beamformer [29].

2.5 Adaptive Algorithms

2.5.1 Least Mean Square (LMS)

The least mean square (LMS) is the most popular adaptive algorithm for continuous adaptation [29]. The algorithm is based on the steepest-descent method [31], which chooses the weight vector to minimize the ensemble average of the error squares toward the MSE. Using the steepest decent method, the updated weight vector at time $(n + 1)$ is given by [29]

$$\boldsymbol{w}(n+1) = \boldsymbol{w}(n) - \frac{\mu}{2}\nabla\mathcal{E}\{\epsilon^2(n)\}, \tag{2.49}$$

where μ is the step size which controls the convergence characteristics of $\boldsymbol{w}(n)$

$$0 < \mu < \frac{1}{\lambda_{max}}. \tag{2.50}$$

Here λ_{max} is the largest eigenvalue of the covariance matrix $\boldsymbol{R}_{xx}$. From (2.21) we have

$$\nabla\mathcal{E}\{\epsilon^2(n)\} = -2\boldsymbol{r}_{xr} + 2\boldsymbol{R}_{xx}\boldsymbol{w}(n) \tag{2.51}$$

Replacing (2.51) into (2.49), we have

$$\boldsymbol{w}(n+1) = \boldsymbol{w}(n) + \mu[\boldsymbol{r}_{xr} - \boldsymbol{R}_{xx}\boldsymbol{w}(n)]. \tag{2.52}$$

In order to update the optimum weight using (2.52), it is necessary to know in advance both $\boldsymbol{R}_{xx}$ and $\boldsymbol{r}_{xr}$, and it is better to use their instantaneous values

$$\begin{aligned}\boldsymbol{R}_{xx}(n) &= \boldsymbol{x}(n)\boldsymbol{x}^{\mathsf{H}}(n)\\ \boldsymbol{r}_{xr}(n) &= \boldsymbol{x}(n)r^*(n)\end{aligned} \tag{2.53}$$

Thus (2.52) now becomes

$$\begin{aligned}\boldsymbol{w}(n+1) &= \boldsymbol{w}(n) + \mu\boldsymbol{x}(n)[r^*(n) - \boldsymbol{x}^{\mathsf{H}}(n)\boldsymbol{w}(n)]\\ &= \boldsymbol{w}(n) + \mu\boldsymbol{x}(n)[r^*(n) - y^*(n)]\\ &= \boldsymbol{w}(n) + \mu\boldsymbol{x}(n)\epsilon^*(n).\end{aligned} \tag{2.54}$$

It is noted that the convergence rate of the LMS algorithm depends on the step size μ and correspondingly on the eigenvalue spread of the covariance matrix $\boldsymbol{R}_{xx}$. An example illustrating the LMS convergence characteristic (learning curve) is shown in Figure 2.7

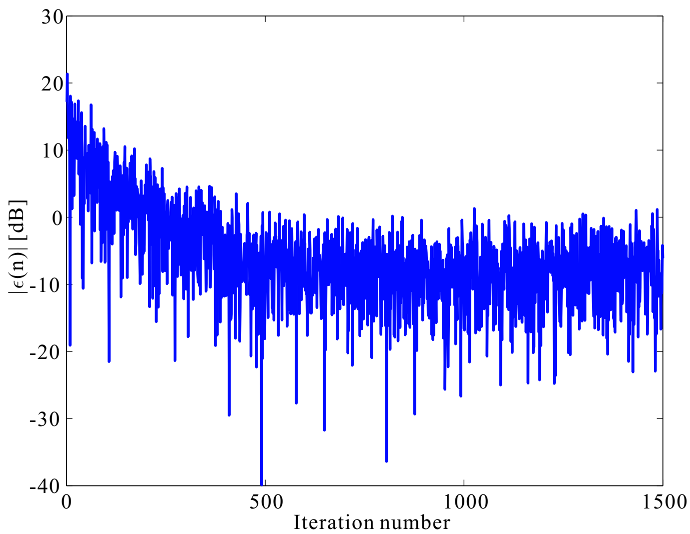

Figure 2.7: An example of the LMS learning curve. Linear array antenna with $d = \lambda/2$, $m = 4$, $\mu = 0.005$, and Input SNR $= 0$dB

2.5.2 Sample Matrix Inversion (SMI)

If the desired and reference signals are both known a priori, then the optimal weights could be computed using the direct inversion of the covariance matrix $\boldsymbol{R}_{xx}$ as in (2.22). Since the desired and reference signals are not known in practice it is possible to use their estimates from the input data vector as [32]

$$\begin{aligned} \boldsymbol{R}_{xx}(n) &= \frac{1}{n}\sum_{i=1}^{n}\boldsymbol{x}(i)\boldsymbol{x}^{\mathsf{H}}(i) \\ \boldsymbol{r}_{xr}(n) &= \frac{1}{n}\sum_{i=1}^{n}\boldsymbol{x}(i)r^{*}(i) \end{aligned} \tag{2.55}$$

From (2.22), it follows that the estimated weight vector using the SMI algorithm is given by

$$\boldsymbol{w}(n) = \boldsymbol{R}_{xx}^{-1}(n)\boldsymbol{r}_{xr}(n). \tag{2.56}$$

It is noted that the SMI is a block-adaptive algorithm and has been shown to be the fastest algorithm for estimating the optimum weight vector [23]. However, it suffers the problems of increased computational complexity and numerical instability due to inversion of a large matrix [29].

2.5.3 Recursive Least Squares (RLS)

The RLS algorithm uses least squares to estimates the weight vector, that is to choose the weight vector which minimizes a cost function of the sum of the error squares over a time window

$$Q(n) = \sum_{i=1}^{n}\gamma^{n-i}|\epsilon(i)|^{2} \tag{2.57}$$

where the error function $\epsilon(i)$ is defined in (2.18) and $0 < \gamma < 1$ is the forgetting factor. Using the least squares method, the covariance matrix and correlation vector are given by [29]

$$\boldsymbol{R}_{xx}(n) = \sum_{i=1}^{n}\gamma^{n-i}\boldsymbol{x}(i)\boldsymbol{x}^{\mathsf{H}}(i) \tag{2.58}$$

$$\boldsymbol{r}_{xr}(n) = \sum_{i=1}^{n}\gamma^{n-i}\boldsymbol{x}(i)r^{*}(i), \tag{2.59}$$

Factoring out the terms corresponding to $i = n$, (2.58) and (2.59) become

$$\boldsymbol{R}_{xx}(n) = \sum_{i=1}^{n-1} \gamma^{(n-1)-i} \gamma \boldsymbol{x}(i)\boldsymbol{x}^{\mathsf{H}}(i) + \boldsymbol{x}(n)\boldsymbol{x}^{\mathsf{H}}(n) = \gamma \boldsymbol{R}_{xx}(n-1) + \boldsymbol{x}(i)\boldsymbol{x}^{\mathsf{H}}(i) \tag{2.60}$$

$$\boldsymbol{r}_{xr}(n) = \sum_{i=1}^{n-1} \gamma^{(n-1)-i} \gamma \boldsymbol{x}(i) r^*(i) + \boldsymbol{x}(i) r^*(i) = \gamma \boldsymbol{r}(n-1) + \boldsymbol{x}(n) r^*(n). \tag{2.61}$$

Apply Woodbury's Identity, we can obtain the inversion of the covariance matrix as follows [29]

$$\boldsymbol{R}_{xx}^{-1}(n) = \gamma^{-1} \Big[\boldsymbol{R}_{xx}^{-1}(n-1) - \boldsymbol{q}(n)\boldsymbol{x}(n)\boldsymbol{R}_{xx}^{-1}(n-1) \Big] \tag{2.62}$$

where,

$$\boldsymbol{q}(n) = \frac{\gamma^{-1} \boldsymbol{R}_{xx}^{-1}(n-1)\boldsymbol{x}(n)}{1 + \gamma^{-1} \boldsymbol{x}^{\mathsf{H}}(n) \boldsymbol{R}_{xx}^{-1}(n-1)\boldsymbol{x}(n)}. \tag{2.63}$$

The estimated weight vector can be updated using (2.22) as

$$\begin{aligned} \boldsymbol{w}(n) &= \boldsymbol{R}_{xx}^{-1}(n)\boldsymbol{r}_{xr}(n) \\ &= \gamma^{-1} \Big[\boldsymbol{R}_{xx}^{-1}(n-1) - \boldsymbol{q}(n)\boldsymbol{x}(n)\boldsymbol{R}_{xx}^{-1}(n-1) \Big] \Big[\gamma \boldsymbol{r}(n-1) + \boldsymbol{x}(n) r^*(n) \Big] \end{aligned} \tag{2.64}$$

which finally gives us [29]

$$\boldsymbol{w}(n) = \boldsymbol{w}(n-1) + \boldsymbol{q}(n) \Big[r^*(n) - \boldsymbol{w}^{\mathsf{H}}(n-1)\boldsymbol{x}(n) \Big] \tag{2.65}$$

Since the RLS algorithm utilizes information from the initial sample to estimate the weight, it is an order of magnitude faster then that of the LMS algorithm [33]. However, this convergence improvement is achieved at the expense of the increased computational complexity. An example of the convergence characteristic of the RLS algorithm is depicted in Figure 2.8

2.6 Benefits of Using Adaptive Arrays

Use of adaptive arrays brings various benefits for mobile communications and has been widely discussed in the literature [29, 34, 35]. Some of the benefits are summarized below.

2.6.1 Improved Signal Quality

Due to using multiple elements adaptive arrays can provide additional antenna (array) gain, which depends on the number of utilized array elements. This, consequently, leads to improved SINR. Define the input SNR as SNR_{in} than if the number of interferences is

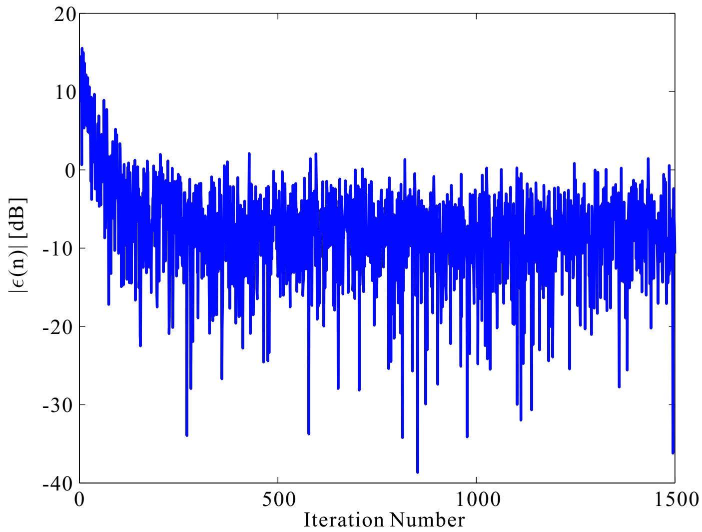

Figure 2.8: An example of the RLS learning curve. Linear array antenna with $d = \lambda/2$, $m = 4$, $\gamma = 0.999$, and Input SNR $= 0$dB

smaller than the number of degree of freedom DoF $= M - 1$ the output SINR in a single propagation environment (without multipath fading) can be found as

$$\text{SINR}_{out} = M \cdot \text{SNR}_{in}, \tag{2.66}$$

or

$$\text{SINR}_{out}[\text{dB}] = 10 \log_{10} M + \text{SNR}_{in}[\text{dB}], \tag{2.67}$$

where M is the number of array elements.

In the multipath fading environment, if signal processing is used in both the spatial and temporal domains such as the case of the broadband beamformer more diversity gain could be achieved depending on the number of taps in the employed TDLs and fading characteristics. Take a simple case of 2-path model as an example. When the two paths are spatially uncorrelated, for example, the preceding and delayed rays coming from $0°$ and $30°$, respectively, the output SINR is estimated as

$$\text{SINR}_{out}[\text{dB}] = 10 \log_{10} M + 10 \log_{10}(2) + \text{SNR}_{in}[\text{dB}]. \tag{2.68}$$

This means that additional 3dB diversity gain has been obtained in multipath fading environment. The richer the multipath fading environment is, the more diversity gain can be achieved. Figure 2.9 plots the output SNR versus the number of employed array elements.

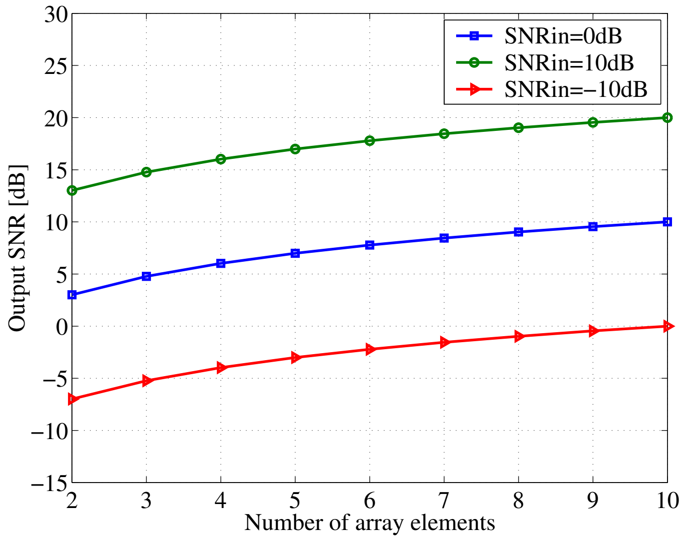

Figure 2.9: Output SNR versus number of array elements

2.6.2 Extended Coverage

From (2.67), it is clear that the array gain achieved by an adaptive array is

$$G = 10 \log_{10} M. \tag{2.69}$$

This additional gain allows to extend the coverage of the basestation. When the angular spread is small and the path loss is modelled with exponent α, the range extension factor (REF) is given by [34]

$$\text{REF} = \frac{r_{array}}{r_{conv}} = M^{\frac{1}{\alpha}}, \tag{2.70}$$

where r_{conv} and r_{array} are the range covered by the conventional antenna (with single element) and the array antenna (with multiple elements), respectively. The extended area coverage factor (ECF) is [34]

$$\text{ECF} = \left(\frac{r_{array}}{r_{conv}}\right)^2 = \text{REF}^2. \tag{2.71}$$

Figure 2.10 shows that with an 6 element array, the coverage area is almost double compared with single antenna case for $\alpha = 5$. Since the inverse of the ECF represents the reduction factor in number of basestation required to cover the same area using a single antenna [34], it is clear that using adaptive arrays can significantly reduce the number of basestations. For example, for the above mentioned case with $\alpha = 5$, the number of basestation can be reduced to only one half of the original number.

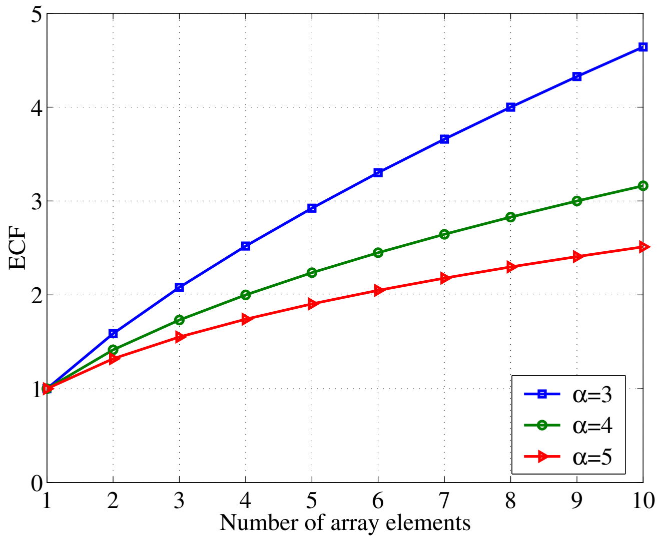

Figure 2.10: Improvement of area coverage by adaptive arrays.

2.6.3 Reduced Transmit Power

We have seen in section 2.6.1 that use of adaptive arrays can provide a large array gain. This gain, consequently leads to the reduction in required transmit power of the basestation. If the required reception sensitivity is kept the same, then the power requirement of a basestation employed an M-element array is reduced to M^{-1} and correspondingly the required output power of the basestation power amplifier can be reduced to M^{-2}[34]. The reduction in the transmit power is beneficial to user's health and implementation cost since high frequency power amplifiers are often very expensive.

2.7 Summary

We have provided an overview of adaptive arrays for mobile communications. The array signal models for both single and multipath fading environments were developed. Moreover, structures of both the narrowband and broadband beamforming were described. It was shown that the array output of both the beamformer can be expressed in the same multiplication form of the input signal and array weight vectors. The conventional time domain broadband beamforming was also shown to be equivalently replaced by a frequency domain beamformer having reduced computational load and faster convergence rate.

Discussing on how to optimize the optimum array performance, four criteria, namely, MMSE, MSINR, MV and ML were taken for investigation. It was shown that all the four criteria can be expressed in the same form of the well-known Wiener-Hopf equation.

In addition, three common adaptive algorithms were discussed. It was shown that the

SMI algorithm is the fastest algorithm sacrificing computational complexity and instability. Although the convergence rate is slow and depends on the eigenvalue spread of the signal covariance matrix, the LMS algorithm is most efficient in term of the computational complexity.

Finally, we have shown that using adaptive arrays can bring great benefits for mobile communications. Improvement of signal quality, coverage area, channel capacity and reduced transmit power was explained.

Chapter 3

Subband Adaptive Arrays for Mobile Communications

This chapter presents the principle of SBAA for mobile communications. Basic operations and components in the multirate filter structure such as decimator, expander, analysis and synthesis filters are introduced. Different representations of analysis and synthesis filters using polyphase decomposition and noble identities are also presented. Furthermore, different configurations of SBAA are reviewed to show the most suitable one for mobile communications. Finally, motivation to use SBAA in mobile communications is discussed.

3.1 Basic Theory of Multirate Filters

Subband adaptive arrays are built on *multirate digital filters*, which comprise of *analysis* and *synthesis* parts [33, 36]. The analysis part contains a bank of *decimators* $\downarrow K$ and an *analysis filter*. The synthesis part, operated inversely, includes a *synthesis filter* and a bank of *expanders* $\uparrow K$. Figure 3.1 depicts a multirate digital filter.

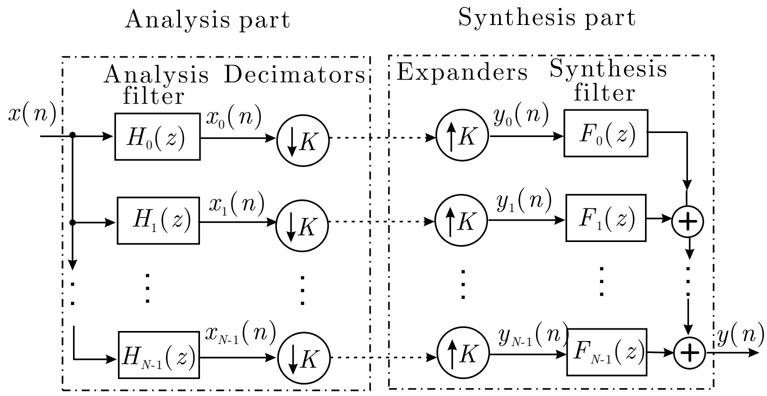

Figure 3.1: Multirate digital filter.

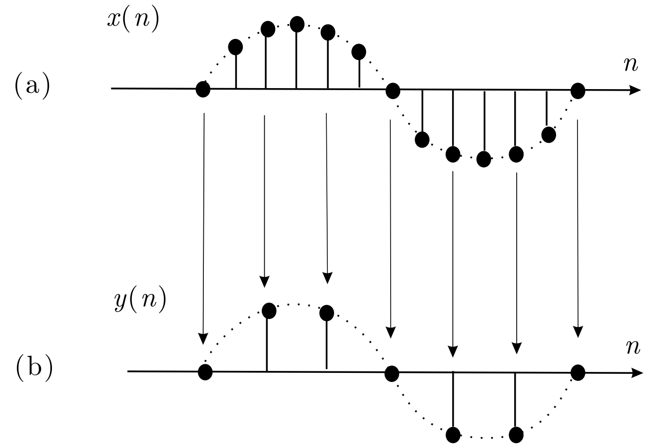

Figure 3.2: Decimation process with $K = 2$. (a) Original signal. (b) Decimated signal.

3.1.1 Decimators and Expanders

The decimators down-sample the input signals with decimation rate K. Using the discrete time notation, if the signal $x(n)$ is put through a decimator with decimation rate K as in Figure 3.3.a then only every Kth sample is retained at the output signal $y(n)$, that is

$$y(n) = x(Kn). \tag{3.1}$$

The decimation operation with $K = 2$ is depicted in Figure 3.2, where the output signal $y(n)$ contains only odd samples of the input signal $x(n)$.

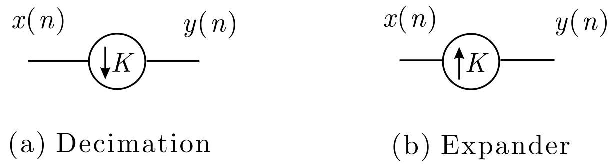

Figure 3.3: Basic multirate operations.

Contrary to the decimator, the expanders up-sample the input signal with expansion rate K. The expanded signal $y(n)$ from the input signal $x(n)$ is

$$y(n) = \begin{cases} x(\frac{n}{K}) & \text{if } n \text{ is an integer multiple of } K \\ 0 & \text{otherwise} \end{cases}. \tag{3.2}$$

Figure 3.4 shows an example of expansion process with $K = 2$, where the expander inserts $(K-1)$ zeros between adjacent original samples. A filter is followed to convert zero-valued samples of the expanders into interpolated samples and complete the interpolation.

Table 3.1: Classification of multirate filters.

Decimation rate	Type of multirate filters
$K = N$	Critically sampled filters
$K < N$	Oversampled filters
$K = 1$	Filters without decimation. (Frequency domain filter)

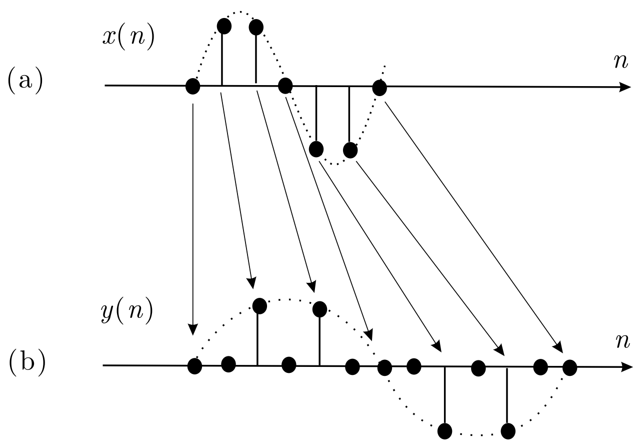

Figure 3.4: Expansion process with $K = 2$. (a) Original signal. (b) Expended signal.

In (3.1) and (3.2), the decimation and expansion rate K is often selected as an integer. The fractional values of K which correspond to the non-uniform sampling [37] is also possible, however, not considered in this work. Since each subband signal covers only a portion of frequency spectrum, in order to avoid aliasing and thus reconstruct perfectly the output signal $y(t)$, the selection of the decimation rate K should meet the condition $K \leq N$. Based on the relation between the decimation rate K and the number of subbands N, multirate filters can be classified into 3 types as in Table 3.1. Since the main objective of subband signal processing is to reduce the computational complexity, the decimation rate K should be equal (critical sampling multirate filter [38–40]) or closely equal (oversampled subband adaptive filter [20, 41]) to the number of subbands N. For this reason, this work will mainly focus on the critical sampling, *i.e.*, $K = N$.

3.1.2 Analysis and Synthesis Filter Banks

The analysis and synthesis filter banks are banks comprised of K digital filters with the transfer function $H_k(z)$ and $F_k(z)$, respectively [33, 36, 42]. Since we are considering the critical sampling case, *i.e.*, $K = N$, the analysis filter bank splits the input signal $x(n)$ into K subband signals $x_k(n)$ as shown in Figure 3.1. The synthesis filter banks, on

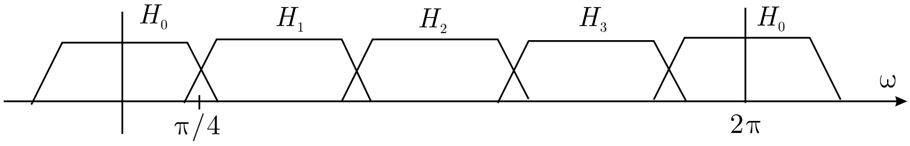

Figure 3.5: A typical response of a uniform DFT filter bank.

the other hand, combines K subband signals $y_k(n)$ into the reconstructed signal $y(n)$. There are several types of filter banks among which the most popular one is the *discrete fourier transform (DFT) uniform filter bank* in which all the channels have the same bandwidths and sampling rates [42]. This is because uniform filter banks can be practically implemented with the aid of a fast transform algorithm such as fast Fourier transform (FFT) resulting in *uniform FFT filter banks.* A typical response of a DFT filter bank with $K = 4$ is illustrated in Figure 3.5. The combination of DFT filter bank and critical sampling results in *the frequency domain block processing* which is of our particular interest in this work. Other types of filter banks such as nonuniform, uniform single side-band (SSB) and quadrature mirror filter (QMF) banks will not be considered.

3.1.3 Polyphase Decomposition and Noble Identities

Let $H_k(z) = \sum_{n=-\infty}^{\infty} h(n)z^{-n}$ be the transfer function of a digital filter. $H_k(z)$ can be rewritten as

$$\begin{aligned} H_k(z) =&[\ldots + h(-4)z^4 + h(-2)z^2 + h(0) + h(2)z^{-2} + h(4)z^{-4} + \ldots] \\ &+z^{-1}[\ldots + h(-3)z^4 + h(-1)z^2 + h(1) + h(3)z^{-2} + \ldots] \end{aligned} \tag{3.3}$$

Denote $H_{k|0}(z) = \sum_{n=-\infty}^{\infty} h(2n)z^{-n}$ and $H_{k|1}(z) = \sum_{n=-\infty}^{\infty} h(2n+1)z^{-n}$, then we can express (3.3) as

$$H_k(z) = H_{k|0}(z^2) + z^{-1}H_{k|1}(z^2), \tag{3.4}$$

where we have grouped the impulse response coefficients into even numbered samples $h(2n)$ and odd numbered samples $h(2n+1)$. Similarly, it is possible to write $H_k(z)$ in a form of K components as [36]

$$H_k(z) = \sum_{n=0}^{K-1} z^{-n} H_{k|n}(z^N), \tag{3.5}$$

where index n has been redefined from previous equations. This representation of $H_k(z)$ is called *polyphase decompositions* and $H_{k|n}(z^N)$ are called *polyphase components.* Using the polyphase representations, the analysis filter bank can be expressed as [20]

$$\boldsymbol{h}(z) = \boldsymbol{H}(z^K)\begin{bmatrix}1 & z^{-1} \ldots z^{-(K-1)}\end{bmatrix}^{\mathsf{T}} \tag{3.6}$$

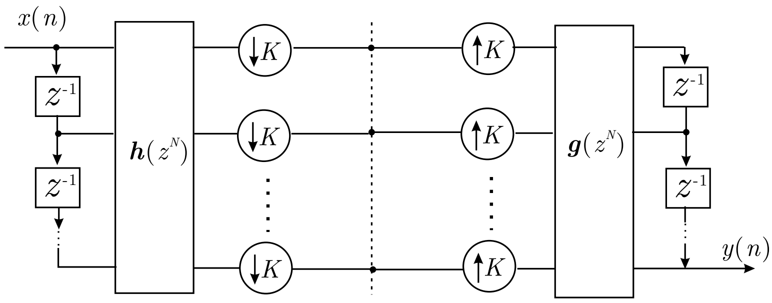

(a) Polyphase decomposition of analysis and synthesis filter banks

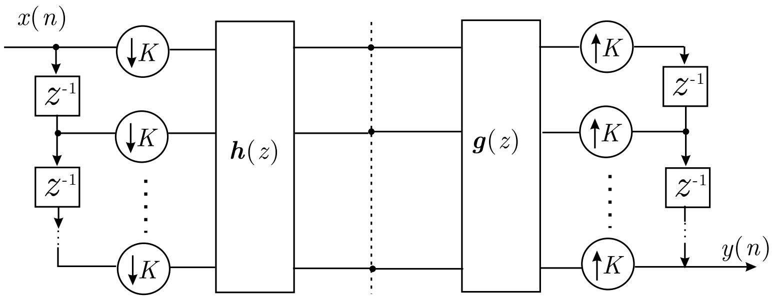

(b) Rearrangement using noble identities

Figure 3.6: Representation of analysis and synthesis filter banks using polyphase and noble identities.

where

$$\boldsymbol{H}(z) = \begin{bmatrix} H_{0|0}(z) & H_{0|1}(z) & \dots & H_{0|K-1}(z) \\ H_{1|0}(z) & H_{1|1}(z) & \dots & H_{1|K-1}(z) \\ \vdots & \vdots & \ddots & \vdots \\ H_{K-1|0}(z) & H_{K-1|1}(z) & \dots & H_{K-1|K-1}(z) \end{bmatrix} \tag{3.7}$$

Using the similar approach, the synthesis filter bank with

$$G_k(x) = \sum_{n=0}^{K-1} z^{-(N-1-n)} G_{n|k}(z^N) \tag{3.8}$$

can be express as [20]

$$\boldsymbol{g}^{\mathsf{T}}(z) = \left[z^{-(N-1)} \quad z^{-(N-2)} \dots 1\right] \boldsymbol{G}(z^N) \tag{3.9}$$

where

$$\boldsymbol{G}(z) = \begin{bmatrix} G_{0|0}(z) & G_{0|1}(z) & \dots & G_{0|K-1}(z) \\ G_{1|0}(z) & G_{1|1}(z) & \dots & G_{1|K-1}(z) \\ \vdots & \vdots & \ddots & \vdots \\ G_{K-1|0}(z) & G_{K-1|1}(z) & \dots & G_{K-1|K-1}(z) \end{bmatrix} \tag{3.10}$$

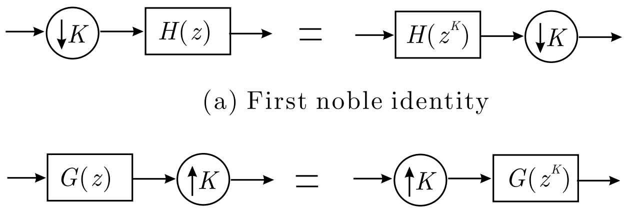

(a) First noble identity

(b) Second noble identity

Figure 3.7: Noble identities

The polyphase representations of a K-channel analysis and synthesis filter banks are shown in Figure 3.6.(a).

Noble identities: The first noble identity states that a cascade of a decimator $\downarrow K$ followed by a transfer function $H(z)$ is equivalent to a cascade of a transfer function $H(z^K)$ followed by a decimator $\downarrow K$. The identity is depicted in Figure 3.7.a. The second noble identity can be stated similarly and illustrated in Figure 3.7.b. The representation of analysis and synthesis filter banks using polyphase and noble identities is shown in Figure 3.6.(b).

3.2 Subband Adaptive Arrays for Mobile Communications

3.2.1 Subband Adaptive Array Configurations

A typical configuration of SBAA is illustrated in Figure 3.8. The received signals from each array element are first put through receive modules to convert to baseband and then converted into digital samples using an analog-to-digital (A/D) converter. For simplicity, we have simplified the receive modules and A/D converters from the configuration of the SBAA. Also, to keep the signal model similar with that used in Chapter 2 we use t as the discrete time notation for SBAA. Denote the receive signal at the mth array element at time t as $x_m(t)$. Each signal $x_m(t)$ is decomposed into K subband signals and converted into the frequency domain using the FFT filter bank. The adaptive signal processing is then carried out in subbands to obtain the optimum weight vector for each subband $\tilde{\boldsymbol{w}}^{(k)}$. To do so the reference signal is also converted into the frequency domain subband signal using the same method for the received signal. After being multiplied with the optimum weights, the weighted samples are combined corresponding to each subband. The combined samples are then converted back into the time domain using the IFFT filter bank. Finally, the interpolation with expansion rate K is applied to get the array output signal $y(t)$. Based on the selection of the decimation rate, SBAAs can be classified into the SBAA with decimation and SBAA without decimation [43]. Similar to the classification

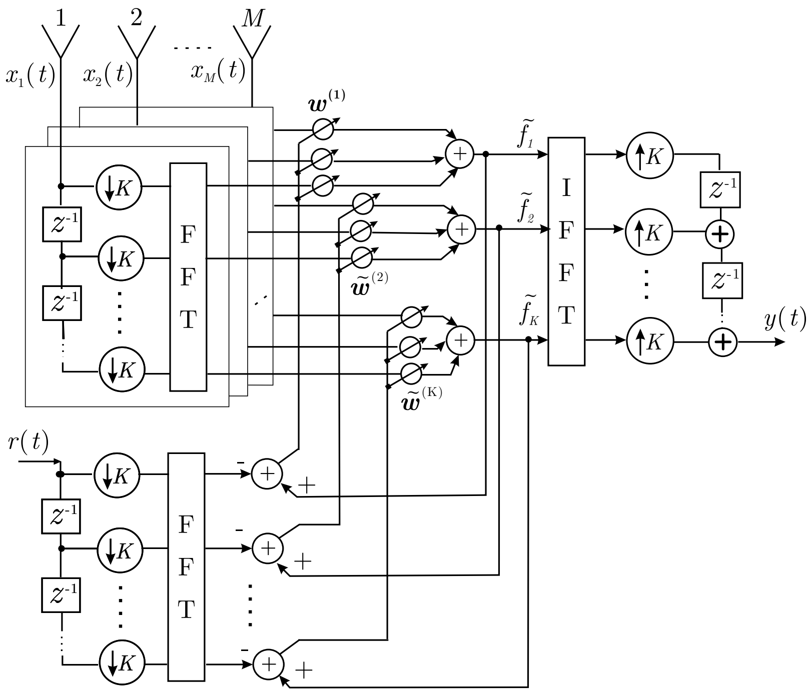

Figure 3.8: Subband adaptive array configuration.

Table 3.2: Classification of subband adaptive arrays.

	Global	**Local**	**Partial**
Without decimation	Type 1	Type 2	Type 3
With decimation	NR[a]	Type 4	NR

[a]NR: Not realizable

of the multirate filters, in the case of SBAAs with decimation, if the decimation rate is equal to the number of subbands, *i.e.*, $K = N$, it is called the critical sampling SBAAs; otherwise it is the oversampled SBAAs for $K < N$.

Another method to classify SBAA is based on the definition of the feedback signal to update weights in subbands. Using this method, SBAAs are divided into three different groups, namely, global feedback, local feedback and partial feedback schemes [10, 13]. In the global feedback SBAAs, the feedback signal is taken from the array output signal $y(t)$. Thus the reference signal in this case is not necessarily converted into subbands. This type of SBAAs, however, is only realized for the SBAA without decimation. When the feedback is extracted from the combined signals such as shown in Figure 3.8, it is called the local feedback SBAA. The so-called partial feedback, where a certain number of subbands are grouped with one another, is a generalization of both the local feedback and global feedback schemes. As with the global feedback type, the partial feedback SBAA exists only for the SBAA without decimation.

In implementation when both the criteria are considered, there are four distinct types of SBAAs as summarized in Table 3.2. Since performance of of Types 1, 2, and 3 was analyzed in [10], our interest in this work is mainly focused on Type 4 and, particularly, for the critical sampling SBAA with local feedback scheme.

3.2.2 Motivations

ISI and ICI mitigation capability

As we have mentioned earlier, in mobile communications ISIs and CCIs are two main factors which degrade the system performance. Adaptive arrays as a spatial filter have been shown to have capability to suppress CCIs within the array degree of freedom (DOF) [23, 24]. For an M-element array, the DOF is

$$\mathrm{DOF} = M - 1 \tag{3.11}$$

and the array can effectively cancel $(M-1)$ interferences. For ISIs, since the conventional adaptive arrays using narrowband beamforming processes the input signal only in spatial domain it does not have capability to mitigate delay spread in the frequency selective channels. The solution is to use adaptive arrays in combination with temporal filters using TDLs such as broadband beamforming adaptive arrays [27, 43]. The TDL adaptive arrays (TDLAAs) work as a spatio-temporal equalizer and thus can effectively suppress both CCIs and ISIs. However, resolving simultaneously both CCI and ISI is a difficult task for TDLAAs since it requires either large-scale matrix inversion or recursive computation [2]. Moreover, as the adaptive processing is done in full band, TDLAAs suffer slow convergence in searching for optimum weights [16]. In severe multipath fading environments these problems become even more serious as longer order temporal filters are required. In such cases, SBAA has been shown to outperform the conventional TDLAA [2, 4–10, 13–19, 44, 45].

Subband adaptive array, which is comprised of an integrated adaptive array and mutirate filter banks , was shown to achieve the same objective as TDLAA while more efficient in implementation [2]. In SBAA, the frequency band of the received signal is first decomposed into smaller subbands and then adaptive signal processing is performed in subbands to obtain the optimum weights. Due to the subband decomposition, the spatio-temporal equalization is converted into a number of simple spatial equalizers which can be implemented in parallel [2]. As a result, both the problems of the slow convergence rate and the computational complexity can be resolved. Furthermore, if the multirate filter banks

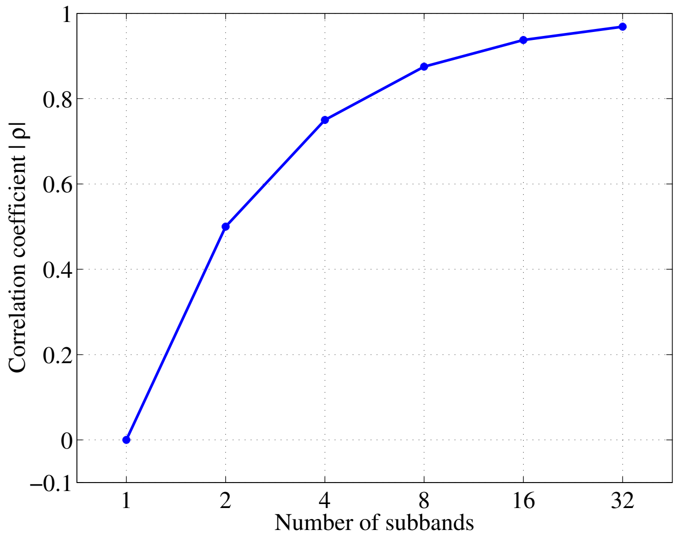

Figure 3.9: Signal correlation enhancement versus number of subbands

are properly designed then signal correlation can be significantly increased. This helps to mitigate the effect of multipath fading occurred in both the desired and interference signals [2].

In order to show how SBAAs can enhance the signal correlation, let us use the auto-correlation function $r^{(k)}(\tau)$ and signal correlation coefficient $\rho^{(k)}(\tau)$ at the kth subband derived in [2] for the DFT filter banks as

$$r^{(k)}(\tau) = \sum_{n=0}^{K-1} \sum_{n=0}^{K-1} B\text{sinc}(B\tau - n + m)e^{-j2\pi(m-n)k/K}, \tag{3.12}$$

and

$$\rho^{(k)}(\tau) = \alpha r^{(k)}(\tau)/r^{(k)}(0), \tag{3.13}$$

where B is the signal bandwidth and K is number of subbands. Figure 3.9 illustrates the signal correlation coefficient at the first subband ($k = 0$), with $B\tau = 1$. It is noticed from the figure that as the number of subband increases, signal correlation is greatly improved. When the number of subbands equals to 32, we can obtain almost full signal correlation.

Reduced computational complexity

The main difference between TDLAA and SBAA is their processing modes. While TDLAA processes the input signal on sample-by-sample basis, this is done on subband block-by-block mode by SBAA. As a result, SBAA requires less computational operations and than TDLAA. For a K-tap and M-element array antenna, the TDLAA employing the sample

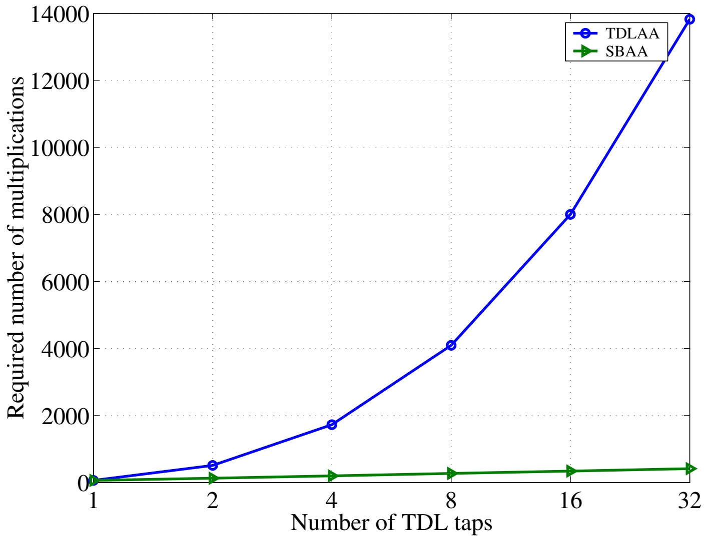

Figure 3.10: Computational complexity of TDLAA and SBAA. $M = 4$, SMI algorithm.

matrix inversion (SMI) algorithm requires $(KM)^3$ multiplications for each weight update. The SBAA with K subbands, on the other hand, needs only KM^3 multiplications [43]. As DFT/IDFT are often implemented using efficient FFT/IFFT filter banks, $2K \log_2 K$ more multiplications are needed by the SBAA. The total computational load required by the SBAA is $K(M^3 + 2\log_2 K)$. In wideband communications, the propagation channel often encounters multipath fading with large delay spread. This leads to the use of high order temporal filters, that is, with a large number of taps K. In this case $(KM)^3 \gg K(M^3 + 2\log_2 K)$ and thus use of SBAA can help to reduce a significant amount of computational complexity. Figure 3.10 compares the computational complexity of the TDLAA and SBAA using SMI algorithm with $M = 4$. As can be seen in the figure, when 32 TDL taps are employed, the TDLAA requires 13824 multiplication, while that of SBAA is only about 415. The resulting complexity reduction by the SBAA is thus approximately 33 times.

3.3 Summary

Basic operations and components of multirate filters and SBAA were presented. It was shown that the critical sampling is the most suitable choice for SBAA. Different configurations of SBAA were reviewed to see that in case the critical sampling is used, only the local feedback is realizable. The critical sampling SBAA using local feedback scheme will be focused in this work.

The motivations of using SBAA in mobile communications were also discussed. It was shown that SBAA can effectively mitigate both ISI and CCI while having greatly reduced computational complexity. The use of SBAA is thus of great benefits.

Chapter 4

Performance of Subband Adaptive Array

In this chapter, the output SINR is taken as a criterion to investigate the performance of SBAA using critical sampling and local feedback scheme in both the single path propagation and multipath frequency selective fading channel. For both the cases, the exact expressions for the subband signals, optimal subband weights and the output SINR of the SBAA are derived. The output SINR of the SBAA is also compared with that of the SBAA without using decimation.

4.1 Performance of SBAA in Single Path Environment.

4.1.1 Assumptions

Consider a general case of a critical sampling SBAA with local feedback scheme as illustrated in Figure 4.1. The linear array is comprised of M isotropic elements which are uniformly placed apart a distance of d. The subband decomposition is done by decimating the received signal with decimation rate K, which is equal to the number of subbands. The analysis and synthesis filter banks employ the FFT and the IFFT as efficient implementations of DFT and IDFT filters.

To reduce the complexity in analyzing the performance of SBAA, we strict our analysis to the T-spaced equalization, *i.e.*, the received signal is sampled at the symbol rate [33, 46]. The principle of the SBAA is thus analogous to the block FFT processing adaptive array considered by Compton in [43]. The initial assumptions for the analysis are as follows:

(A1) The received signals at the mth element $s_m(t)$ with arrival angle θ measured clockwise from the broadside of the array is a zero mean stationary process with average power $\xi^2 = \mathcal{E}\{|s_m(t)|^2\}$. The received signal is also assumed narrowband with the relative bandwidth $B = \Delta f / f_c \ll 1$, where f_c is the carrier frequency and Δf is the signal bandwidth.

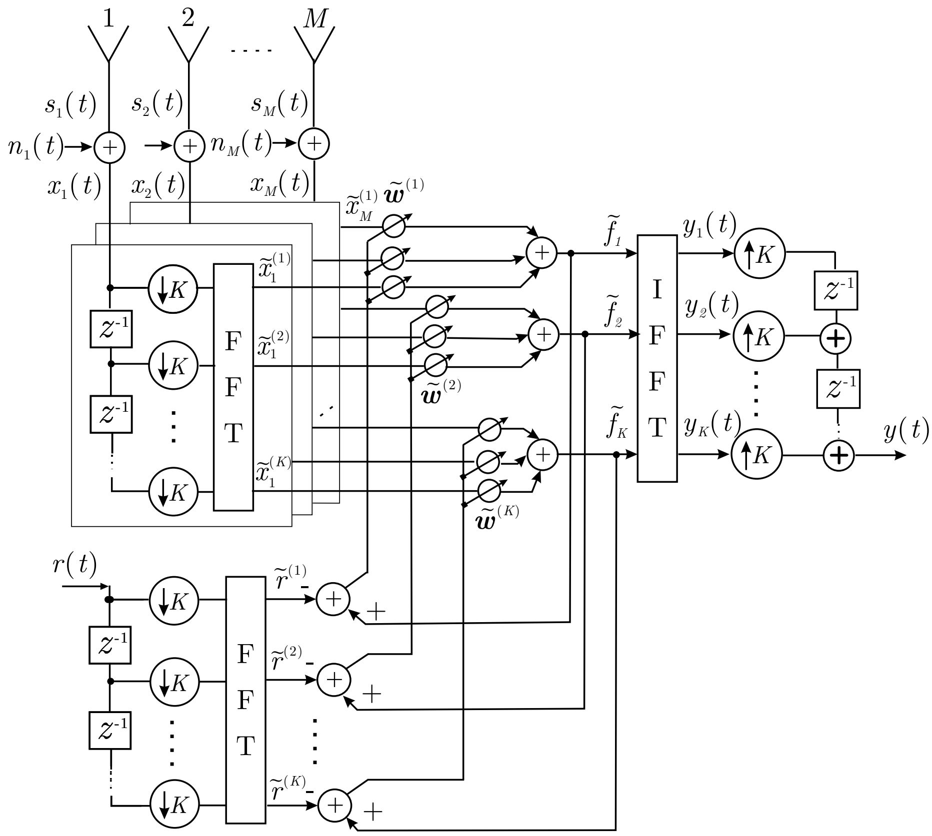

Figure 4.1: Subband adaptive array using FFT/IFFT filter banks

(A2) Noise in each array element $n_m(t)$ contains only the thermal noise and is statistically independent and identically distributed (i.i.d.) Gaussian process with average power $\sigma^2 = \mathcal{E}\{|n_m(t)|^2\}$.

(A3) The reference signal $r(t)$ is assumed available, and is an ideal replica of the received signal at the first antenna $s_1(t)$ with normalized power so that the amplitude change of $s_1(t)$ does not affect the reference signal, *i.e.*, $r(t) = \frac{1}{\xi}s_1(t)$.

(A4) The delay of each TDL tap is equal to the symbol duration, *i.e.*, $z^{-1} = T_s$, where T_s is symbol duration.

4.1.2 Signal Model

Since the received signal is assumed stationary, the output of the antenna array is thus also stationary. The output SINR of the SBAA at each data block of signal is thus the same, and the overall output SINR of SBAA is equal to the mean value of the SINR at each block of the received signal. Assume that, at time t, the received signal at the mth antenna is given by $s_m(t)$. The vector of signal arriving at the array is given by

$$\begin{aligned}\boldsymbol{x}(t) &= s_1(t)\boldsymbol{a}(\theta) + \boldsymbol{n}(t)\\ &= \boldsymbol{s}(t) + \boldsymbol{n}(t),\end{aligned} \tag{4.1}$$

where the array response vector $\boldsymbol{a}(\theta)$ is given by

$$\boldsymbol{a}(\theta) = \begin{bmatrix}1 & e^{-j\frac{2\pi d}{\lambda}\sin(\theta)} & \dots & e^{-j(M-1)\frac{2\pi d}{\lambda}\sin(\theta)}\end{bmatrix}^{\mathsf{T}}. \tag{4.2}$$

Let us define the phase components in the array response vector by

$$\psi = \frac{2\pi d}{\lambda}\sin(\theta), \tag{4.3}$$

then $\boldsymbol{a}(\theta)$ can be expressed in a simpler form as

$$\boldsymbol{a}(\theta) = \begin{bmatrix}1 & e^{-j\psi} & \dots & e^{-j(M-1)\psi}\end{bmatrix}^{\mathsf{T}}. \tag{4.4}$$

In (4.1) the complex signal vector $\boldsymbol{s}(t)$ and noise vector $\boldsymbol{n}(t)$ are given by

$$\boldsymbol{s}(t) = \begin{bmatrix}s_1(t) & s_2(t) & \cdots & s_M(t)\end{bmatrix}^{\mathsf{T}}, \tag{4.5}$$

$$\boldsymbol{n}(t) = \begin{bmatrix}n_1(t) & n_2(t) & \cdots & n_M(t)\end{bmatrix}^{\mathsf{T}}. \tag{4.6}$$

Because the critical sampling is assumed, the process of decomposing the received signal into subbands is equivalent to the operation of serial to parallel conversion. The element signal vectors of the received signal $\boldsymbol{s}_m(t)$ and local noise $\boldsymbol{n}_m(t)$ at the mth array element after decimation can be expressed as

$$\begin{aligned}\boldsymbol{s}_m(t) &= \begin{bmatrix} s_1(t)e^{-j(m-1)\psi} \\ s_1(t-T_s)e^{-j(m-1)\psi} \\ \vdots \\ s_1(t-[K-1]T_s)e^{-j(m-1)\psi} \end{bmatrix}\\ &= \bar{\boldsymbol{s}}(t)e^{-j(m-1)\psi},\end{aligned} \tag{4.7}$$

and

$$\boldsymbol{n}_m(t) = \begin{bmatrix} n_m(t) \\ n_m(t-T_s) \\ \vdots \\ n_m(t-[K-1]T_s) \end{bmatrix}, \tag{4.8}$$

respectively.

The element signal vector is then given by

$$\boldsymbol{x}_m(t) = \boldsymbol{s}_m(t) + \boldsymbol{n}_m(t). \tag{4.9}$$

After taking FFT, the frequency samples at the nth subband of the mth array element are given by

$$\begin{aligned} \tilde{x}_m^{(n)} &= \sum_{k=1}^{K} x_m(t-[k-1]T_s)E_{n,k} \\ &= \sum_{k=1}^{K} \Big\{ s_m(t-[k-1]T_s) + n_m(t-[k-1]T_s) \Big\} E_{n,k}, \end{aligned} \tag{4.10}$$

where we have defined

$$E_{n,k} = e^{-j\frac{2\pi}{K}(n-1)(k-1)}. \tag{4.11}$$

The subband signal vectors at the nth subband in the frequency domain can be now written as

$$\widetilde{\boldsymbol{x}}^{(n)} = \widetilde{\boldsymbol{s}}^{(n)} + \widetilde{\boldsymbol{n}}^{(n)}, \tag{4.12}$$

where

$$\widetilde{\boldsymbol{s}}^{(n)} = \begin{bmatrix} \sum_{k=1}^{K} s_1(t-[k-1]T_s)E_{n,k} \\ \sum_{k=1}^{K} s_1(t-[k-1]T_s)E_{n,k}e^{-j\psi} \\ \vdots \\ \sum_{k=1}^{K} s_1(t-[k-1]T_s)E_{n,k}e^{-j(M-1)\psi} \end{bmatrix}, \tag{4.13}$$

and

$$\widetilde{\boldsymbol{n}}^{(n)} = \begin{bmatrix} \sum_{k=1}^{K} n_1(t-[k-1]T_s)E_{n,k} \\ \sum_{k=1}^{K} n_2(t-[k-1]T_s)E_{n,k} \\ \vdots \\ \sum_{k=1}^{K} n_M(t-[k-1]T_s)E_{n,k} \end{bmatrix}. \tag{4.14}$$

4.1.3 Subband Optimum Weights

When the MMSE is taken as a criterion to maximize the output SINR, the optimal weight vectors in subbands can be calculated by using the Wiener-Hopf solution given by

$$\widetilde{\boldsymbol{w}}^{(n)} = \left(\widetilde{\boldsymbol{R}}^{(n)}\right)^{-1} \widetilde{\boldsymbol{p}}^{(n)}, \tag{4.15}$$

where $\widetilde{\boldsymbol{R}}^{(n)}$ and $\widetilde{\boldsymbol{p}}^{(n)}$ are the covariance matrices and the correlation vectors at subband n, respectively. The signal covariance matrices $\widetilde{\boldsymbol{R}}^{(n)}$ which has $M \times M$ dimensions can be expressed as

$$\widetilde{\boldsymbol{R}}^{(n)} = \mathcal{E}\left\{\left(\widetilde{\boldsymbol{x}}^{(n)}\right)^*\left(\widetilde{\boldsymbol{x}}^{(n)}\right)^{\mathsf{T}}\right\}$$
$$= \begin{bmatrix} \mathcal{E}\left\{\left(\widetilde{x}_1^{(n)}\right)^*\widetilde{x}_1^{(n)}\right\} & \mathcal{E}\left\{\left(\widetilde{x}_1^{(n)}\right)^*\widetilde{x}_2^{(n)}\right\} & \dots & \mathcal{E}\left\{\left(\widetilde{x}_1^{(n)}\right)^*\widetilde{x}_M^{(n)}\right\} \\ \mathcal{E}\left\{\left(\widetilde{x}_2^{(n)}\right)^*\widetilde{x}_1^{(n)}\right\} & \mathcal{E}\left\{\left(\widetilde{x}_2^{(n)}\right)^*\widetilde{x}_2^{(n)}\right\} & \dots & \mathcal{E}\left\{\left(\widetilde{x}_2^{(n)}\right)^*\widetilde{x}_M^{(n)}\right\} \\ \vdots & \vdots & \ddots & \vdots \\ \mathcal{E}\left\{\left(\widetilde{x}_M^{(n)}\right)^*\widetilde{x}_1^{(n)}\right\} & \mathcal{E}\left\{\left(\widetilde{x}_M^{(n)}\right)^*\widetilde{x}_2^{(n)}\right\} & \dots & \mathcal{E}\left\{\left(\widetilde{x}_M^{(n)}\right)^*\widetilde{x}_M^{(n)}\right\} \end{bmatrix} \tag{4.16}$$

with $\varepsilon_{mv}^{(n)}$ being the element at the mth row and vth column computed as

$$\varepsilon_{mm}^{(n)} = \mathcal{E}\left\{\left(\widetilde{x}_m^{(n)}\right)^*\widetilde{x}_m^{(n)}\right\} = K\xi^2 + K\sigma^2, \tag{4.17}$$

$$\varepsilon_{mv}^{(n)} = \mathcal{E}\left\{\left(\widetilde{x}_m^{(n)}\right)^*\widetilde{x}_v^{(n)}\right\} = K\xi^2 e^{j(m-v)\psi}, (m \neq v). \tag{4.18}$$

After some mathematical manipulations, the signal covariance matrices in subbands are straightforwardly given by

$$\widetilde{\boldsymbol{R}}^{(n)} = \begin{bmatrix} K\xi^2 + K\sigma^2 & K\xi^2 e^{-j\psi} & \dots & K\xi^2 e^{-j(M-1)\psi} \\ K\xi^2 e^{j\psi} & K\xi^2 + K\sigma^2 & \dots & K\xi^2 e^{-j(M-2)\psi} \\ \vdots & \vdots & \ddots & \vdots \\ K\xi^2 e^{j(M-1)\psi} & K\xi^2 e^{j(M-2)\psi} & \dots & K\xi^2 + K\sigma^2 \end{bmatrix}. \tag{4.19}$$

From (4.19) the determinants of the signal covariance matrices $\widetilde{\boldsymbol{R}}^{(n)}$ are given by

$$\det\left(\widetilde{\boldsymbol{R}}^{(n)}\right) = K^M\left(M\xi^2\sigma^{2(M-1)} + \sigma^{2M}\right). \tag{4.20}$$

Now using (4.19) and (4.20) the inverse signal covariance matrices are calculated and given by

$$\left(\widetilde{\boldsymbol{R}}^{(n)}\right)^{-1} = \frac{K^{M-1}\sigma^{2(M-2)}}{\det\left(\widetilde{\boldsymbol{R}}^{(n)}\right)} \begin{bmatrix} (M-1)\xi^2 + \sigma^2 & -\xi^2 e^{-j\psi} & \dots & -\xi^2 e^{-j(M-1)\psi} \\ -\xi^2 e^{j\psi} & (M-1)\xi^2 + \sigma^2 & \dots & -\xi^2 e^{-j(M-2)\psi} \\ \vdots & \vdots & \ddots & \vdots \\ -\xi^2 e^{j(M-1)\psi} & -\xi^2 e^{j(M-2)\psi} & \dots & (M-1)\xi^2 + \sigma^2 \end{bmatrix} \tag{4.21}$$

Next, we consider the reference correlation vectors $\widetilde{\boldsymbol{p}}^{(n)}$ which are calculated from the correlation between the subband signal and reference samples in the frequency domain

$$\widetilde{\boldsymbol{p}}^{(n)} = \mathcal{E}\left\{\left(\widetilde{\boldsymbol{x}}^{(n)}\right)^*\widetilde{r}^{(n)}\right\}, \tag{4.22}$$

where

$$\widetilde{r}^{(n)} = \frac{1}{\xi}\sum_{k=1}^{K} s_1(t-[K-1]T_s)E_{n,k} \tag{4.23}$$

are the reference samples at subband n in the frequency domain. Using (4.12) and (4.23) the reference correlation vectors are then calculated and given by

$$\begin{aligned}\widetilde{\boldsymbol{p}}^{(n)} &= \mathcal{E}\Big\{\Big(\widetilde{\boldsymbol{x}}^{(n)}\Big)^{*}\widetilde{r}^{(n)}\Big\} = \mathcal{E}\Big\{\Big[\Big(\widetilde{\boldsymbol{s}}^{(n)}\Big)^{*} + \Big(\widetilde{\boldsymbol{n}}^{(n)}\Big)^{*}\Big]\widetilde{r}^{(n)}\Big\} \\ &= K\xi\boldsymbol{a}^{*}(\theta).\end{aligned} \tag{4.24}$$

Combining (4.21) and (4.24), we can obtain the optimal weight vectors in subbands as

$$\widetilde{\boldsymbol{w}}^{(n)} = \frac{\xi}{M\xi^2+\sigma^2}\boldsymbol{a}^{*}(\theta). \tag{4.25}$$

Denote

$$Q = \frac{\xi}{M\xi^2+\sigma^2}, \tag{4.26}$$

then (4.25) can be rewritten in a shorter form as

$$\widetilde{\boldsymbol{w}}^{(n)} = Q\boldsymbol{a}^{*}(\theta). \tag{4.27}$$

It is noted that (4.27) does not depend on the subband index n. Therefore, the subband optimal weight vectors of the SBAA in the case of single path propagation are the same for all subbands.

4.1.4 Output Signal

In the case of the SBAA with local feedback, after being weighted by the optimum weights, the frequency domain samples are combined in corresponding subbands to give

$$\widetilde{f}_n = \Big(\widetilde{\boldsymbol{w}}^{(n)}\Big)^{\mathsf{T}}\widetilde{\boldsymbol{x}}^{(n)} = Q\boldsymbol{a}^{\mathsf{H}}(\theta)\widetilde{\boldsymbol{x}}^{(n)}. \tag{4.28}$$

Since the outputs of SBAA at tap ℓ in time domain are the inverse Fourier transform of $\widetilde{f}_n$, they are given by

$$y_\ell(t) = \frac{1}{K}\sum_{n=1}^{K}\widetilde{f}_n E^{*}_{n,\ell} = \frac{Q}{K}\sum_{n=1}^{K}\boldsymbol{a}^{\mathsf{H}}(\theta)\widetilde{\boldsymbol{x}}^{(n)}E^{*}_{n,\ell}, \tag{4.29}$$

where $E^{*}_{n,\ell} = e^{j\frac{2\pi}{K}(n-1)(\ell-1)}$. The output signal $y(t)$ is finally obtained using interpolation on the outputs signals $y_\ell(t)$.

4.1.5 Output SINR

Since the output SINR is equivalent to the mean SINR at each data block of output signal, instead of using the output signal $y(t)$ to calculate the output SINR , we use the output signals at each IFFT tap $y_\ell(t)$. In order to find the expression for the output SINR, we adopt the cross-correlation coefficient defined as

$$\rho = \frac{\mathcal{E}\Big\{ \sum_{\ell=1}^{K} y_\ell(t) r_\ell^*(t) \Big\}}{\sqrt{\mathcal{E}\Big\{\sum_{\ell=1}^{K} |y_\ell(t)|^2\Big\}\mathcal{E}\Big\{ \sum_{\ell=1}^{K} |r_\ell(t)|^2\Big\}}}, \tag{4.30}$$

where $r_\ell(t)$ are the reference signal samples in time domain, and given by

$$r_\ell(t) = \frac{1}{\xi} s_1(t - [\ell-1]T_s). \tag{4.31}$$

Components in (4.30) are calculated and given in equations (4.32) to (4.34) below

$$\begin{aligned} \mathcal{E}\Big\{ \sum_{\ell=1}^{K} y_\ell(t) r_\ell^*(t) \Big\} &= \mathcal{E}\Big\{ \sum_{\ell=1}^{K} \frac{Q}{K} \sum_{n=1}^{K} \boldsymbol{a}^{\mathsf{H}}(\theta) \Big(\widetilde{\boldsymbol{s}}^{(n)} + \widetilde{\boldsymbol{n}}^{(n)}\Big) E_{n,\ell}^* \frac{1}{\xi} s_1^*(t - [\ell-1]T_s) \Big\} \\ &= KQM \end{aligned} \tag{4.32}$$

$$\begin{aligned} \mathcal{E}\Big\{ \sum_{\ell=1}^{K} |y_\ell(t)|^2 \Big\} &= \mathcal{E}\Big\{ \sum_{\ell=1}^{K} \Big[\frac{Q}{K} \sum_{n=1}^{K} \boldsymbol{a}^{\mathsf{H}}(\theta) \big(\widetilde{\boldsymbol{s}}^{(n)} + \widetilde{\boldsymbol{n}}^{(n)}\big) \frac{Q}{K} \sum_{n=1}^{K} \boldsymbol{a}^{\mathsf{T}}(\theta) \big\{ (\widetilde{\boldsymbol{s}}^{(n)})^* + (\widetilde{\boldsymbol{n}}^{(n)})^* \big\} \Big] \Big\} \\ &= KQ^2 \big[M^2 \xi^2 + M\sigma^2 \big] \end{aligned} \tag{4.33}$$

$$\begin{aligned} \mathcal{E}\Big\{ \sum_{\ell=1}^{K} |r_\ell(t)|^2 \Big\} &= \mathcal{E}\Big\{ \frac{1}{\xi} \sum_{\ell=1}^{K} s_1(t - [\ell-1]T_s) \frac{1}{\xi} s_1^*(t - [\ell-1]T_s) \Big\} \\ &= K \frac{1}{\xi^2} \end{aligned} \tag{4.34}$$

Replacing equations (4.32) to (4.34) into (4.30), we obtain the cross-correlation coefficient

$$\rho = \frac{KQM}{\sqrt{KQ^2[M^2\xi^2 + M\sigma^2]K/\xi^2}} = \frac{M\xi}{\sqrt{M^2\xi^2 + M\sigma^2}} \tag{4.35}$$

The output SINR then can be calculated via the cross-correlation coefficient using the relation

$$\mathrm{SINR}_{\mathrm{out}} = \frac{|\rho|^2}{1 - |\rho|^2}, \tag{4.36}$$

which gives us

$$\mathrm{SINR}_{\mathrm{out}} = M\frac{\xi^2}{\sigma^2} = M \cdot \mathrm{SNR}_{\mathrm{in}}. \tag{4.37}$$

Now we have shown the analytical results of the performance of the SBAA in the case of single path propagation. It is noted from (4.37) that the output SINR of the SBAA depends only on the number of antennas and the input SNR. This observation is the same with the SINR of an adaptive array without using subband signal processing, which is shown in [43]. Consequently, it is concluded that in the case of single path propagation, subband signal processing does not produce any improvement to the output SINR. However, the practical mobile channels are often frequency selective, which contain multiple paths with different time delays, and thus subband signal processing is necessarily employed to perform temporal equalization.

In the next section, we shall explore the effects of multipath frequency selective fading on the performance of SBAA. We shall show how subband signal processing effects the output SINR of SBAA in the multipath frequency selective fading channel.

4.2 Performance of SBAA in Multipath Frequency Selective Fading Channel

4.2.1 Assumptions

In this section, we analyze the performance of SBAA for the case of multipath frequency selective fading channel. Assume that the received signal contains P paths arriving at the array from different angles θ_p, with different delays $T_p = L_p \cdot T_s$, where $L_p \in [0, 1, 2, ..., K]$, and p is path index, $p = 0, 1, 2 \ldots (P-1)$. Each path has average power ξ_p^2. The direct path with path index $p = 0$ arrives at the array without any delays, *i.e.*, $L_0 = 0$ and $T_0 = 0 \cdot T_s = 0$. For $q > p$ we assume that $L_q \geq L_p$.

For simplicity, let us further assume that the reference signal is available and an ideal replica of the direct path at the first antenna $s_{1,0}(t)$ with normalized power, *i.e.*, $r(t) = \frac{1}{\xi_0} s_{1,0}(t)$.

4.2.2 Signal Model

Similar to Section 2, denote the received signal from path p at the first antenna as $s_{1,p}(t)$, the vector of the received signal arriving at the array at time t can be then set up as

$$\boldsymbol{x}(t) = \sum_{p=0}^{P-1} s_{1,p}(t)\boldsymbol{a}(\theta_p) + \boldsymbol{n}(t) \tag{4.38}$$

where

$$\boldsymbol{a}(\theta_p) = [1 \quad e^{-j\psi_p} \ldots e^{-j(M-1)\psi_p)}]^{\mathsf{T}}, \tag{4.39}$$

and

$$\psi_p = \frac{2\pi d}{\lambda}\sin(\theta_p). \tag{4.40}$$

We now can write the element signal vectors at the mth array element as

$$\boldsymbol{x}_m(t) = \sum_{p=0}^{P-1} \bar{\boldsymbol{s}}_p(t)e^{-j(m-1)\psi_p} + \boldsymbol{n}_m(t), \tag{4.41}$$

where

$$\bar{\boldsymbol{s}}_p(t) = \begin{bmatrix} s_{1,p}(t) \\ s_{1,p}(t-T_s) \\ \vdots \\ s_{1,p}(t-[K-1]T_s) \end{bmatrix} \tag{4.42}$$

and $\boldsymbol{n}_m(t)$ is defined as in (4.8).

In SBAA the frequency domain sample vectors of the received signal at the nth subband can be built by performing FFT transform on the element signal vectors, given by

$$\widetilde{\boldsymbol{x}}^{(n)} = \sum_{p=0}^{P-1} \widetilde{\boldsymbol{s}}_p^{(n)} + \widetilde{\boldsymbol{n}}^{(n)} \tag{4.43}$$

where

$$\widetilde{\boldsymbol{s}}_p^{(n)} = \begin{bmatrix} \sum_{k=1}^{K} s_{1,p}(t-[k-1]T_s)E_{n,k} \\ \sum_{k=1}^{K} s_{1,p}(t-[k-1]T_s)e^{-j\psi_p}E_{n,k} \\ \vdots \\ \sum_{k=1}^{K} s_{1,p}(t-[k-1]T_s)e^{-j(M-1)\psi_p}E_{n,k} \end{bmatrix}, \tag{4.44}$$

and $\widetilde{\boldsymbol{n}}^{(n)}$ are the same as in (4.14).

4.2.3 Subband Optimum Weights

In multipath fading environment, since there are P paths of the received signal arriving at the array, the signal covariance matrices $\widetilde{\boldsymbol{R}}^{(n)}$ and the reference correlation vectors $\widetilde{\boldsymbol{p}}^{(n)}$ are affected by multipath parameters such as powers, arrival angles and delays of multipath rays. The signal covariance matrices $\widetilde{\boldsymbol{R}}^{(n)}$ in this case contain powers of the multipath rays, noise power and also correlations between multipath rays. Components of the covariance matrices $\widetilde{\boldsymbol{R}}^{(n)}$ defined by (4.16) for the multipath frequency selective fading case are calculated and given by

$$\varepsilon_{mv}^{(n)} = \sum_{p=0}^{P-1}\sum_{q=p}^{P-1} R_{mv,pq}^{(n)} + \begin{cases} K\sigma^2 & \text{if } m = v \\ 0 & \text{if } m \neq v \end{cases}, \tag{4.45}$$

where $R_{pq,mv}^{(n)}$ are the cross-correlations between path p and path q in subband n of the mth and vth antennas, and given respectively by

$$R_{pq,mm}^{(n)} = \begin{cases} K\xi_p^2, & \text{if } p = q \\ 2\big[K - (L_q - L_p)\big]\xi_p\xi_q \cos\Big[(m-1)(\psi_q - \psi_p) - \frac{2\pi}{K}(n-1)(L_q - L_p)\Big], & \text{if } p \neq q \end{cases} \tag{4.46}$$

$$R_{pq,mv}^{(n)} = \begin{cases} K\xi_p^2 e^{j(m-v)\psi_p}, & \text{if } p = q \\ 2\big[K - (L_q - L_p)\big]\xi_p\xi_q & \\ \quad \cdot \cos\Big[\frac{(m+v-2)(\psi_q-\psi_p)}{2} - \frac{2\pi}{K}(n-1)(L_q - L_p)\Big] e^{\frac{j(m-v)(\psi_p+\psi_q)}{2}}, & \text{if } p \neq q \end{cases} \tag{4.47}$$

Similarly, the reference correlation vectors are given by

$$\begin{aligned} \widetilde{\boldsymbol{p}}^{(n)} &= \mathcal{E}\Big\{\Big(\widetilde{\boldsymbol{x}}^{(n)}\Big)^*\widetilde{r}^{(n)}\Big\} \\ &= \sum_{p=0}^{P-1} \xi_p(K - L_p)\boldsymbol{a}^*(\theta_p)e^{-j\frac{2\pi}{K}(n-1)L_p}, \end{aligned} \tag{4.48}$$

where in this case $\widetilde{r}^{(n)}$ are given by

$$\widetilde{r}^{(n)} = \frac{1}{\xi_0}\sum_{k=1}^{K} s_{1,0}(t - [K-1]T_s)E_{n,k}. \tag{4.49}$$

The optimal weight vectors in subbands can be now obtained by applying Wiener-Hopf solution given in (4.15). It is immediately realized that in the case of multipath frequency selective fading channel, the optimal subband weight vectors depend on the subband index n and thus are different for each subband. Furthermore, values of the subband optimal weights depend on the powers of the multipath rays and noise, the number of employed subbands K and the delays L_p of multipath rays.

4.2.4 Output Signal

Since the local feedback scheme is considered, as explained in Section 2, the weighted samples in frequency domain are combined according to each subband to give

$$\widetilde{f}_n = \left(\boldsymbol{w}^{(n)}\right)^{\mathsf{T}} \widetilde{\boldsymbol{x}}^{(n)} = \left(\widetilde{\boldsymbol{w}}^{(n)}\right)^{\mathsf{T}} \left(\sum_{p=0}^{P-1} \widetilde{\boldsymbol{s}}_p^{(n)} + \widetilde{\boldsymbol{n}}^{(n)} \right), \tag{4.50}$$

and the array outputs at the array output (IFFT) taps in the time domain are given by

$$\begin{aligned} y_\ell(t) &= \frac{1}{K} \sum_{n=1}^{K} \widetilde{f}_n e^{j\frac{2\pi}{K}(n-1)(\ell-1)} \\ &= \frac{1}{K} \sum_{n=1}^{K} \left(\widetilde{\boldsymbol{w}}^{(n)}\right)^{\mathsf{T}} \left(\sum_{p=0}^{P-1} \widetilde{\boldsymbol{s}}_p^{(n)} + \widetilde{\boldsymbol{n}}^{(n)} \right) E_{n,\ell}^{*}. \end{aligned} \tag{4.51}$$

In order to solve (4.51) to get a more convenient form of $y_\ell(t)$ so that the output SINR of the SBAA can be easily computed, let us consider the following term

$$\begin{aligned} \sum_{n=1}^{K} \left(\widetilde{\boldsymbol{w}}^{(n)}\right)^{\mathsf{T}} \widetilde{\boldsymbol{s}}_p^{(n)} E_{n,\ell}^{*} &= \sum_{n=1}^{K} \left(\widetilde{\boldsymbol{w}}^{(n)}\right)^{\mathsf{T}} \sum_{k=1}^{K} s_{1,p}(t-[k-1]T_s) \boldsymbol{a}(\theta_p) E_{n,\ell}^{*} E_{n,k} \\ &= \sum_{k=1}^{K} s_{1,p}(t-[k-1]T_s) \sum_{n=1}^{K} \left(\widetilde{\boldsymbol{w}}^{(n)}\right)^{\mathsf{T}} \boldsymbol{a}(\theta_p) \chi(\ell,k,n,K), \end{aligned} \tag{4.52}$$

where

$$\chi(\ell,k,n,K) = e^{-j\frac{2\pi}{K}(n-1)(k-\ell)}. \tag{4.53}$$

Now define the following vectors

$$\bar{\boldsymbol{a}}(\theta_p) = \Big[\underbrace{\boldsymbol{a}^{\mathsf{T}}(\theta_p) \quad \boldsymbol{a}^{\mathsf{T}}(\theta_p) \quad \ldots \quad \boldsymbol{a}^{\mathsf{T}}(\theta_p)}_{K} \Big]^{\mathsf{T}}, \tag{4.54}$$

$$\bar{\boldsymbol{w}}_k^{(\ell)} = \begin{bmatrix} \widetilde{\boldsymbol{w}}^{(1)} \chi(\ell,k,1,K) \\ \widetilde{\boldsymbol{w}}^{(2)} \chi(\ell,k,2,K) \\ \vdots \\ \widetilde{\boldsymbol{w}}^{(K)} \chi(\ell,k,K,K) \end{bmatrix}, \tag{4.55}$$

and

$$\boldsymbol{u}_p^{(\ell)} = \begin{bmatrix} \bar{\boldsymbol{a}}^{\mathsf{T}}(\theta_p) \bar{\boldsymbol{w}}_1^{(\ell)} \\ \bar{\boldsymbol{a}}^{\mathsf{T}}(\theta_p) \bar{\boldsymbol{w}}_2^{(\ell)} \\ \vdots \\ \bar{\boldsymbol{a}}^{\mathsf{T}}(\theta_p) \bar{\boldsymbol{w}}_K^{(\ell)} \end{bmatrix}, \tag{4.56}$$

then (4.52) becomes

$$\sum_{n=1}^{K}\left(\widetilde{\boldsymbol{w}}^{(n)}\right)^{\mathsf{T}}\widetilde{\boldsymbol{s}}_p^{(n)}E_{n,\ell}^{*}=\bar{\boldsymbol{s}}_p^{\mathsf{T}}(t)\boldsymbol{u}_p^{(\ell)}. \tag{4.57}$$

By doing similarly for the local noise, define

$$\boldsymbol{u}_N^{(\ell)}=\begin{bmatrix}\widetilde{\boldsymbol{w}}^{(1)}\chi(\ell,1,1,K)+\ldots+\widetilde{\boldsymbol{w}}^{(K)}\chi(\ell,1,K,K)\\ \widetilde{\boldsymbol{w}}^{(1)}\chi(\ell,2,1,K)+\ldots+\widetilde{\boldsymbol{w}}^{(K)}\chi(\ell,2,K,K)\\ \vdots\\ \widetilde{\boldsymbol{w}}^{(1)}\chi(\ell,K,1,K)+\ldots+\widetilde{\boldsymbol{w}}^{(K)}\chi(\ell,K,K,K)\end{bmatrix}, \tag{4.58}$$

and

$$\bar{\boldsymbol{n}}(t)=\begin{bmatrix}\boldsymbol{n}^{\mathsf{T}}(t) & \boldsymbol{n}^{\mathsf{T}}(t-T_s)\ldots\boldsymbol{n}^{\mathsf{T}}(t-[K-1]T_s)\end{bmatrix}^{\mathsf{T}} \tag{4.59}$$

then we have

$$\sum_{n=1}^{K}\left(\widetilde{\boldsymbol{w}}^{(n)}\right)^{\mathsf{T}}\widetilde{\boldsymbol{n}}^{(n)}E_{n,\ell}^{*}=\bar{\boldsymbol{n}}^{\mathsf{T}}(t)\boldsymbol{u}_N^{(\ell)}. \tag{4.60}$$

By replacing (4.57) and (4.60) into (4.51), we have a simpler form of the array outputs as

$$y_\ell(t)=\sum_{p=0}^{P-1}\bar{\boldsymbol{s}}_p^{\mathsf{T}}(t)\boldsymbol{u}_p^{(\ell)}+\bar{\boldsymbol{n}}^{\mathsf{T}}(t)\boldsymbol{u}_N^{(\ell)}. \tag{4.61}$$

4.2.5 Output SINR

From (4.61) the output power of the array is given by

$$\begin{aligned}P_{\text{out}}&=\mathrm{E}\left[\Big|\sum_{p=0}^{P-1}\bar{\boldsymbol{s}}_p^{\mathsf{T}}(t)\boldsymbol{u}_p^{(\ell)}\Big|^2\right]+\mathrm{E}\left[\Big|\bar{\boldsymbol{n}}^{\mathsf{T}}(t)\boldsymbol{u}_N^{(\ell)}\Big|^2\right]\\&=P_{S+I}+P_N\end{aligned} \tag{4.62}$$

Since the power P_{I+N} contains both desired signal power P_S and ISI power P_I, it is not easy to extract P_S and P_I from P_{S+I} to get $\text{SINR}_{\text{out}}=\frac{P_S}{P_I+P_N}$. In this paper we again calculate the output SINR via the cross-coefficient defined in (4.30), where in this case

$$r_\ell(t)=\frac{1}{\xi_0}s_{1,0}(t-[\ell-1]T_s). \tag{4.63}$$

In order to solve the equation of ρ, let us define the following weight vectors

$$\hat{\boldsymbol{w}}_p=\begin{bmatrix}(K-L_p)\widetilde{\boldsymbol{w}}^{(1)}e^{j\frac{2\pi}{K}(1-1)(K-L_p)}\\(K-L_p)\widetilde{\boldsymbol{w}}^{(2)}e^{j\frac{2\pi}{K}(2-1)(K-L_p)}\\ \vdots\\(K-L_p)\widetilde{\boldsymbol{w}}^{(K)}e^{j\frac{2\pi}{K}(K-1)(K-L_p)}\end{bmatrix}, \tag{4.64}$$

and the following matrices

$$\boldsymbol{R}_p = \xi_p^2 \mathbf{I}_{K\times K}, \tag{4.65}$$

$$\boldsymbol{R}_N = \sigma^2 \mathbf{I}_{MK\times MK}, \tag{4.66}$$

$$\boldsymbol{R}_{pq} = \xi_p \xi_q \mathbf{H}_{K\times K}, \tag{4.67}$$

where $\mathbf{I}_{K\times K}$ is a $K \times K$ identity matrix and

$$\mathbf{H} = \begin{bmatrix} 0 & 0 & 0 & \dots & 0 & \dots & 0 \\ \vdots & \dots & \vdots & \dots & \vdots & \dots & \vdots \\ 1 & 0 & 0 & \dots & 0 & \dots & 0 \\ 0 & 1 & 0 & \dots & 0 & \dots & 0 \\ \vdots & \vdots & \vdots & \dots & \vdots & \dots & \vdots \\ 0 & 0 & 0 & \dots & 1 & \dots & 0 \end{bmatrix} \tag{4.68}$$

is the $K \times K$ identity shift matrix with shift step equal to the difference in delay lengths between two multipath rays p and q , *i.e.*, $L = (L_q - L_p)$. If we define $\mathbf{H}_{L+1:K,1:K-L}$ as elements from row $L+1$ to row K and column 1 to column $K-L$ of vector $\mathbf{H}$ then (4.68) can be expressed as

$$\mathbf{H} \Rightarrow \begin{cases} \mathbf{H}_{L+1:K,1:K-L} & = \mathbf{I}_{(K-L)\times(K-L)} \\ \text{elsewhere} & = 0 \end{cases}. \tag{4.69}$$

The components of the correlation coefficient ρ in (4.30) are finally computed as

$$\mathcal{E}\left\{\sum_{\ell=1}^{K} y_\ell(t) r_\ell^*(t)\right\} = \sum_{p=0}^{P-1} \big(K - L_p\big)\xi_p \bar{\boldsymbol{a}}^\mathsf{T}(\theta_p)\hat{\boldsymbol{w}}_p, \tag{4.70}$$

$$\mathcal{E}\left\{\sum_{\ell=1}^{K} |r_\ell(t)|^2\right\} = K\frac{1}{\xi_0^2}, \tag{4.71}$$

$$\mathcal{E}\left\{\sum_{\ell=1}^{K} |y_\ell(t)|^2\right\} = \sum_{\ell=1}^{K}\left[\sum_{p=0}^{P-1}\sum_{q=p}^{P-1} \mathcal{R}_{pq}^{(\ell)} + \mathcal{R}_N^{(\ell)}\right], \tag{4.72}$$

where

$$\mathcal{R}_{pq}^{(\ell)} = \begin{cases} \left(\boldsymbol{u}_p^{(\ell)}\right)^\mathsf{T} \boldsymbol{R}_p \left(\boldsymbol{u}_p^{(\ell)}\right)^*, & \text{if } p = q \\ \left(\boldsymbol{u}_p^{(\ell)}\right)^\mathsf{T} \boldsymbol{R}_{pq} \left(\boldsymbol{u}_q^{(\ell)}\right)^* + \left(\boldsymbol{u}_q^{(\ell)}\right)^\mathsf{T} \boldsymbol{R}_{pq}^\mathsf{T} \left(\boldsymbol{u}_p^{(\ell)}\right)^*, & \text{if } p \neq q \end{cases} \tag{4.73}$$

$$\mathcal{R}_N^{(\ell)} = \big(\boldsymbol{u}_N^{(\ell)}\big)^\mathsf{T} \boldsymbol{R}_N \big(\boldsymbol{u}_N^{(\ell)}\big)^*. \tag{4.74}$$

Table 4.1: Simulation model for SBAA

Parameters	**Value**
Type of array	linear ($d = \lambda/2$)
Number of antennas	$M = 4$
Number of subbands	$K = 8$
Type of modulation	BPSK
Signal length	10^4 symbols
Sampling type	T-spaced (1 sample/symbol)
Adaptive algorithm	SMI
Input SNR	0dB

The output SINR of SBAA in multipath frequency selective fading channel is then finally calculated using (4.36).

It is observed that in multipath frequency selective fading channel, the output SINR of the SBAA depends on not only the input SNR and the number of array elements as in the case of single path propagation, but also the number of employed subbands and multipath parameters such as delays, powers and arrival angles of multipath components.

We have presented an efficient and simple method to analyze the performance of SBAA in multipath frequency selective fading channel. The verification of the method is considered in the next section by computer simulation.

4.3 Numerical and Simulation Results

4.3.1 Validation of Analysis

In order to verify the proposed method, we use a simulation model (see Table 4.1) which is comprised of $M = 4$ array elements and $K = 8$ subbands. The transmit signal contains 10^4 BPSK samples, 1 sample per symbol. The multipath rays are assumed to have the same power $\xi_p^2 = 1$. The input SNR, which is defined by the power ratio of each ray to the noise, is set by varying the noise power σ^2. The subband adaptive processing employs the SMI algorithm for the sake of simplicity. The verification of the method is done for the following cases.

Case 1: In this case, we adopt the simple 2–path model for simulation. The array receives 2 multipath rays ($P = 2$): one is the preceding (direct) ray, *i.e.*, $L_0 = 0$, with arrival angle $\theta_0 = 0°$, the other is the delayed ray with delay $L_1 = 0, 1, 2, 3$ and arrival angle θ_1. The input SNR is set equal to 0 dB. The arrival angle of the delayed ray is varied to get the output SINR of SBAA. Simulation and numerical results are compared and illustrated in Figure 4.2.

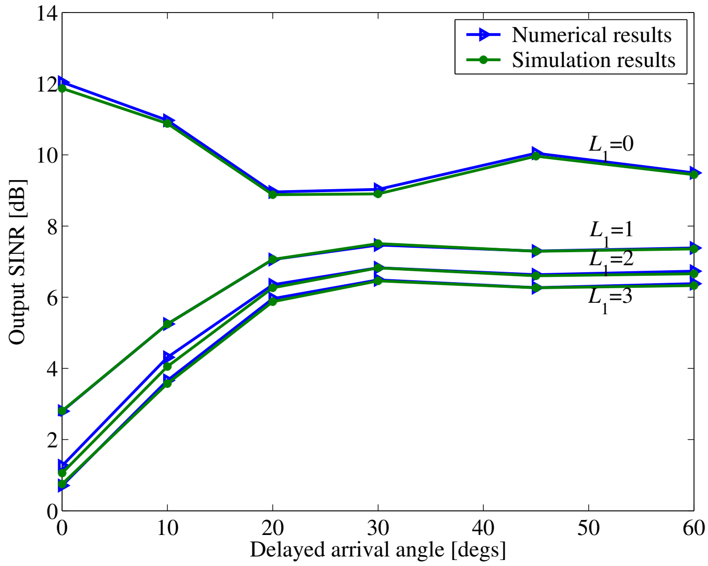

Figure 4.2: SBAA output SINR versus AOA of delayed ray. $M = 4$, $d = \lambda/2$, $K = 8$, 10^4 BPSK symbols, Input SNR=0dB, SMI algorithm, 2–path model: $\theta_0 = 0°$, $L_0 = 0$.

Case 2: In the second simulation, we verify if the proposed method can be applied for different values of input SNRs. The input SNRs are thus set to different values as -10dB, 0dB and 10dB. Similar to Case 1, it is assumed that there are 2 multipath rays arriving at the array. The AOA of the preceding (direct) ray and the delayed ray are set to $\theta_0 = 0°$ and $\theta_1 = 30°$, respectively. The delay of the delayed ray is then varied to get the output SINR of SBAA. Results by the simulation and the numerical method are shown in Figure 4.3.

Case 3: We verify the method for a more general case of frequency selective fading channel, *i.e.*, the received signal contains 3 multipath rays: the preceding ray with $\theta_0 = 0°$ and $L_0 = 0$, the first delayed ray with $L_1 = 1$ and the second delayed ray with $L_2 = 2$. For the arrival angles of the other two rays, it is assumed that $\theta_2 = -\theta_1$ with θ_1 changing from from $0°$ to $60°$. The numerical and simulation results for input SNR=0 dB are plotted in Figure 4.4.

From Figures 4.2 to 4.4, it is noticed that the theoretical and simulation results match well with each other. Therefore, the presented analysis can be considered an accurate method for analyzing the performance of the SBAA.

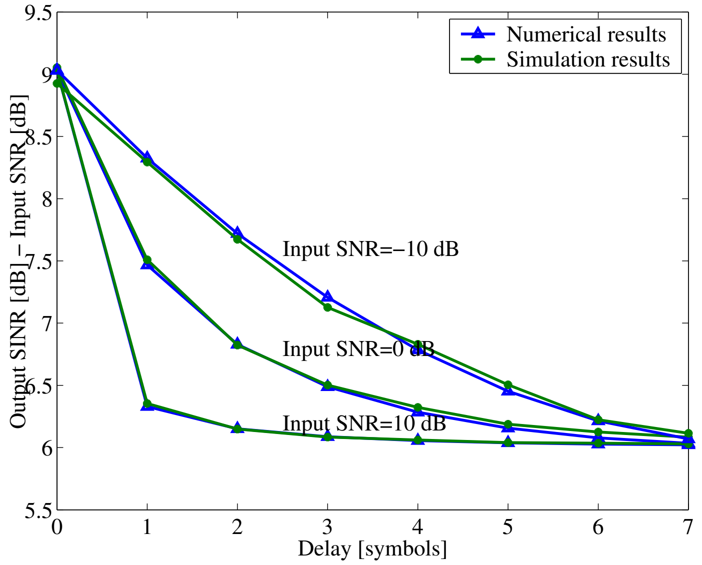

Figure 4.3: SBAA output SINR versus delay of delayed ray. $M = 4$, $d = \lambda/2$, $K = 8$, 10^4 BPSK symbols, SMI algorithm, 2–path model: $\theta_0 = 0°$, $L_0 = 0$, $\theta_1 = 30°$.

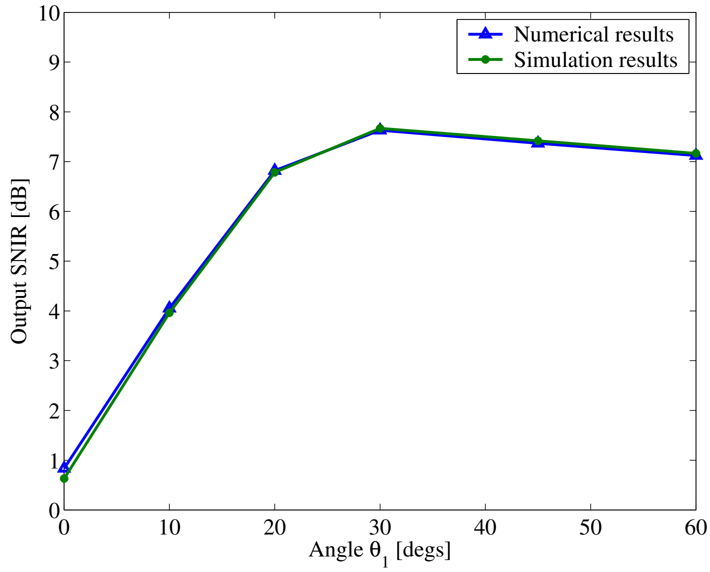

Figure 4.4: SINR of SBAA in the frequency selective fading channel. $M = 4$, $d = \lambda/2$, $K = 8$, 10^4 BPSK symbols, Input SNR=0dB, SMI algorithm, 3–path model: $\theta_0 = 0°$, $L_0 = 0$, $L_1 = 1$, $L_2 = 2$, $\theta_2 = -\theta_1$.

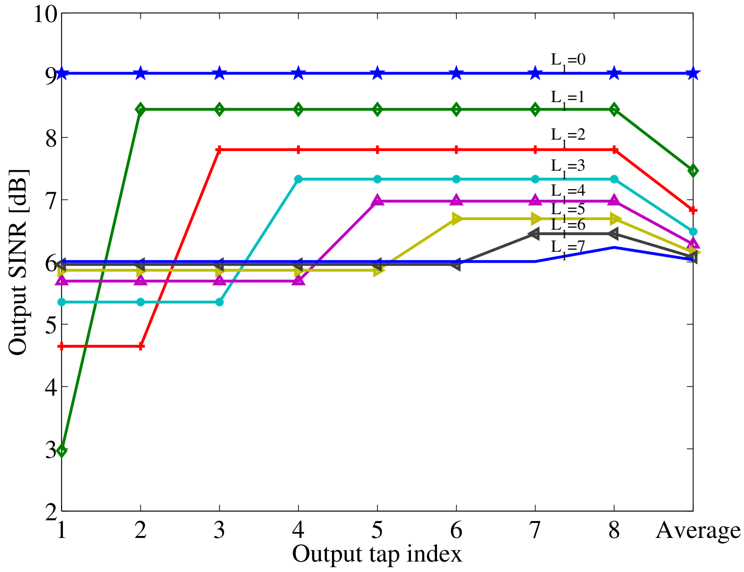

Figure 4.5: SINR of SBAA at each output tap. $M = 4$, $d = \lambda/2$, $K = 8$, 10^4 BPSK symbols, Input SNR=0dB, SMI algorithm, 2–path model: $\theta_0 = 0°$, $L_0 = 0$, $\theta_1 = 30°$.

4.3.2 Output SINRs at Different Output Taps

Next, we apply the method for different evaluations of the SBAA performance. For simplicity, we use the same model as in Case 2 with input SNR equal to 0dB. In Figure 4.5, we show the output SINRs of the SBAA at different output taps using the theoretical method. The overall output SINR of SBAA is shown with "Average" tag. It is noticed that the overall output SINR of the SBAA is simply the average of SINRs at all the output taps.

4.3.3 SINR Comparison with SBAA without Decimation

Figure 4.6 compares the output SINRs of the critical sampling SBAA using the local feedback scheme with the SBAA without using decimation. It is clear that the output SINR of SBAA without using decimation is equal to SINR at the last output tap of SBAA using critical sampling with local feedback. We can also see that the output SINR of the SBAA without decimation is better than that of the SBAA with decimation. However, as we have mentioned above, SBAA with decimation is often preferably chosen because it requires less computation complexity than that of SBAA without decimation.

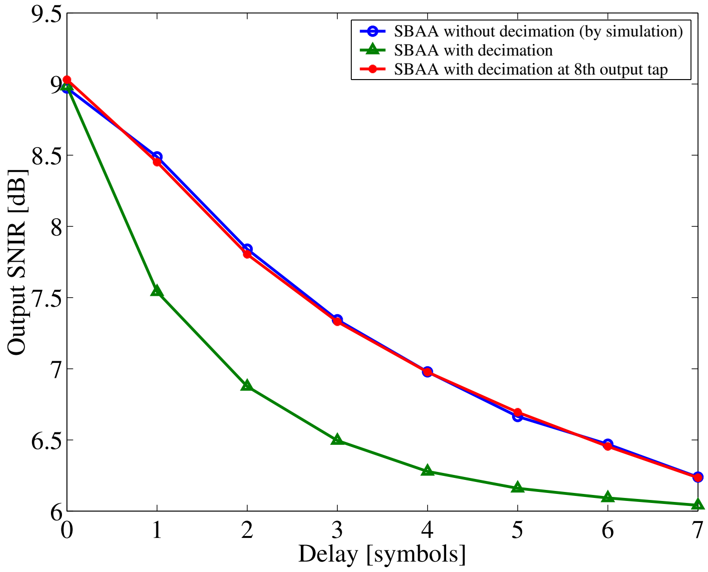

Figure 4.6: SINR of SBAAs with and without decimation. $M = 4$, $d = \lambda/2$, $K = 8$, 10^4 BPSK symbols, Input SNR=0db, SMI algorithm, 2-path model: $\theta_0 = 0°$, $L_0 = 0$, $\theta_1 = 30°$

4.4 Summary

The performance of the SBAA has been investigated. It was shown that the subband optimum weights and the SINR of the SBAA do not depend on the number of subbands in the case of the single path propagation. That is subband signal processing does not contribute any SINR improvement in the single path propagation channel. However, in multipath frequency selective fading channel, the SINR becomes dependent of the input SNR, and multipath parameters such as AOA and delays of the multipath components. We showed that the output SINR of SBAA gradually degrades as the delay spread increases. Moreover, the SINR at the last output (IFFT) tap of the critical sampling SBAA with local feedback is simply equal to the SINR of SBAA without using decimation.

In the next chapter we are going to perform theoretical analysis of another type of SBAA, *i.e.*, SBAA-CP. We shall see how cyclic prefix improves the performance of SBAA-CP.

Chapter 5

Performance of SBAA Combining Cyclic Prefix Transmission Scheme

This chapter presents the theoretical analysis of the integrated subband adaptive array with cyclic prefix transmission scheme (SBAA-CP) in multipath frequency selective fading channel. The exact expressions for the subband signals, optimal weights, array outputs and the output SINR are derived. The analysis shows that use of the cyclic prefix data transmission scheme can significantly improve the performance of SBAA. An example of implementing SBAA-CP as a software antenna which has capability to reconfigure itself to adapt to multipath fading conditions is also presented.

5.1 Single Carrier Cyclic Prefix Transmission Scheme

The cyclic prefix data transmission scheme has been well known as an effective way to mitigate multipath fading, and is widely used in the multicarrier OFDM systems [47]. The basic idea of the cyclic prefix data transmission scheme is as follows. The transmission data is first divided into successive blocks (frames) of a certain length K. At the ith block, the last L_{CP} samples are copied and inserted into the front of the block as a guard interval. The new block of data has length $D = K + L_{CP}$ as shown in Figure 5.1. To

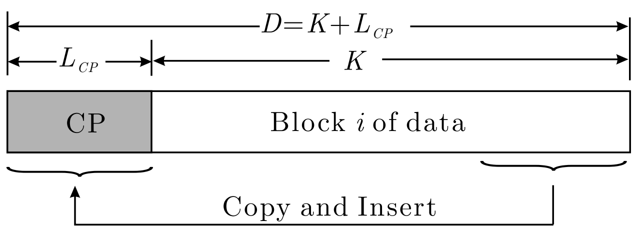

Figure 5.1: Transmit frame with a cyclic prefix.

eliminate ideally the ISI, the cyclic prefix length should be chosen larger then the expected delay spread or the channel order. Although it was initially introduced to work with the multicarrier transmission, recent works [48–50] showed that it can be well integrated with the single carrier frequency domain equalization to combat the ISI.

5.2 SBAA Combining Cyclic Prefix Transmission Scheme

5.2.1 Configuration Description

Since SBAA performs both the spatial and temporal equalizations in the frequency domain, the combination of the cyclic prefix transmission with SBAA was shown to achieve the maximum diversity gain in the multipath fading environment [12, 15, 17]. The configuration of the SBAA-CP is depicted in Figure 5.2.

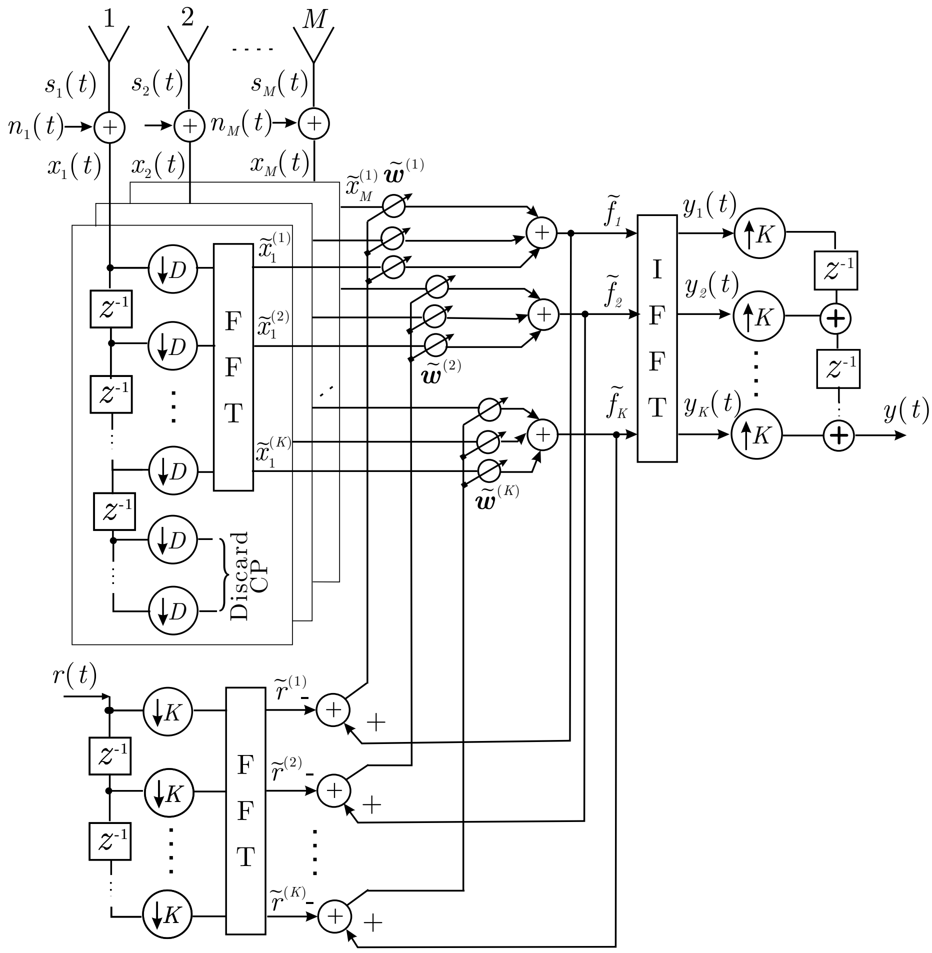

Figure 5.2: Configuration of SBAA-CP.

The principle of SBAA-CP is explained as follows. At the transmit side, the original transmit data is processed as in Figure 5.1 to create the new data stream with cyclic prefix. At the receiver the received signal is first decimated by a factor D. The L_{CP} sample cyclic prefix are then discarded and the FFT is applied to convert the time domain samples into the K subband samples in the frequency domain. Next the subband adaptive signal processing is done and the output signal is reconstructed in the same way as in the conventional SBAA presented in Chapter 4.

Since both critical sampling and local feedback are employed in SBAA-CP, we can certainly apply the analytical method presented for the conventional SBAA presented in Chapter 4 to the SBAA-CP.

5.3 Performance of SBAA-CP in Multipath Fading Channel

5.3.1 Assumptions

Similar to Chapter 4, we now consider a uniformly spaced linear array antenna with M elements. Assume that the received signal contains P multipath rays arriving at the array from different angles θ_p measured clockwise from the array broadside and with different delays $T_p = L_p \cdot T_s$, where $p = 0, 1, 2, ..., (P-1)$ is the path index, $L_p \in [0, 1, 2, ..., D]$, and T_s is the sampling period. For simplicity, we also adopt the initial assumptions used in Chapter 4.

5.3.2 Signal Model

Using (4.38) of Chapter 4, the received signal vector $\boldsymbol{x}(t)$ at time t are given by

$$\boldsymbol{x}(t) = \sum_{p=0}^{P-1} \boldsymbol{s}_p(t) + \boldsymbol{n}(t). \tag{5.1}$$

After decomposing the received signal into subbands and discarding the L_{CP} sample cyclic prefix, the vectors of frequency domain samples at subband n can be built as

$$\widetilde{\boldsymbol{x}}^{(n)} = \sum_{p=0}^{P-1} \widetilde{\boldsymbol{s}}_p^{(n)} + \widetilde{\boldsymbol{n}}^{(n)} \tag{5.2}$$

where $\widetilde{\boldsymbol{s}}_p^{(n)}$ and $\widetilde{\boldsymbol{n}}^{(n)}$ were defined in (4.44) and (4.14), respectively.

Now from (5.2), (4.44) and (4.14) we can write the frequency samples at the nth subband of the mth antenna, *i.e.*, the mth component of the subband signal vector $\widetilde{\boldsymbol{x}}^{(n)}$, as

$$\widetilde{x}_m^{(n)} = \sum_{k=1}^{K} \left\{ \sum_{p=1}^{P} s_{1,p}(t - [k-1]T_s) e^{-j(m-1)\psi_p} + n_m(t - [k-1]T_s) \right\} E_{n,k}. \tag{5.3}$$

In order to calculate the optimal weight vectors and the output SINR of SBAA-CP, let us consider the correlation between multipaths in subbands. In multipath fading environment, since we have assumed that there are P paths arriving at the array, the correlation among P paths is the summation of the correlation between each couple of paths p and q. Since each frame is inserted with a cyclic prefix, the correlation between multipaths in subbands now depends significantly on the utilized cyclic prefix L_{CP}, which is different from the case of the conventional SBAA. Analyzing SBAA-CP is thus also more complicated than SBAA, and it is convenient to divide the analysis into different cases based on the relations between the cyclic prefix length L_{CP} and the delays of delayed rays L_p.

In the next sub-sections, we perform our analysis in the following steps: analyzing the optimal weight vector in subbands using the well known Wiener-Hopf equation, finding the expression for the array output, and calculating the output SINR of SBAA-CP. In each step, we divide the calculations into different small cases based on the relations between the cyclic prefix length L_{CP} and the delays of delayed rays L_p as mentioned above.

5.3.3 Subband Optimum Weights

The optimal weight vector in subbands of SBAA-CP can be calculated using the well known Wiener-Hopf equation, given by (4.15)

$$\widetilde{\boldsymbol{w}}^{(n)} = \left(\widetilde{\boldsymbol{R}}^{(n)}\right)^{-1} \widetilde{\boldsymbol{p}}^{(n)}, \tag{5.4}$$

where $\widetilde{\boldsymbol{R}}^{(n)}$ and $\widetilde{\boldsymbol{p}}^{(n)}$ are the covariance matrices and the reference correlation vectors at the nth subband, respectively. The calculations of $\widetilde{\boldsymbol{R}}^{(n)}$ and $\widetilde{\boldsymbol{p}}^{(n)}$ for the SBAA-CP are presented below.

Covariance Matrix $\widetilde{\boldsymbol{R}}^{(n)}$

For an M-element array antenna, recall the $M \times M$ covariance matrices $\widetilde{\boldsymbol{R}}^{(n)}$ given in (4.16)

$$
\begin{aligned}
\widetilde{\boldsymbol{R}}^{(n)} &= \mathcal{E}\left\{\left(\widetilde{\boldsymbol{x}}^{(n)}\right)^*\left(\widetilde{\boldsymbol{x}}^{(n)}\right)^{\mathsf{T}}\right\} \\
&= \begin{bmatrix}
\mathcal{E}\left\{\left(\widetilde{x}_1^{(n)}\right)^*\widetilde{x}_1^{(n)}\right\} & \mathcal{E}\left\{\left(\widetilde{x}_1^{(n)}\right)^*\widetilde{x}_2^{(n)}\right\} & \dots & \mathcal{E}\left\{\left(\widetilde{x}_1^{(n)}\right)^*\widetilde{x}_M^{(n)}\right\} \\
\mathcal{E}\left\{\left(\widetilde{x}_2^{(n)}\right)^*\widetilde{x}_1^{(n)}\right\} & \mathcal{E}\left\{\left(\widetilde{x}_2^{(n)}\right)^*\widetilde{x}_2^{(n)}\right\} & \dots & \mathcal{E}\left\{\left(\widetilde{x}_2^{(n)}\right)^*\widetilde{x}_M^{(n)}\right\} \\
\vdots & \vdots & \ddots & \vdots \\
\mathcal{E}\left\{\left(\widetilde{x}_M^{(n)}\right)^*\widetilde{x}_1^{(n)}\right\} & \mathcal{E}\left\{\left(\widetilde{x}_M^{(n)}\right)^*\widetilde{x}_2^{(n)}\right\} & \dots & \mathcal{E}\left\{\left(\widetilde{x}_M^{(n)}\right)^*\widetilde{x}_M^{(n)}\right\}
\end{bmatrix}
\end{aligned} \tag{5.5}
$$

Let the element at row m and column v of $\widetilde{\boldsymbol{R}}^{(n)}$ be $\varepsilon_{mv}^{(n)} = \mathcal{E}\left\{\left(\widetilde{x}_m^{(n)}\right)^*\widetilde{x}_v^{(n)}\right\}$, then we have

$$
\varepsilon_{mv}^{(n)} = \sum_{p=0}^{P-1}\sum_{q=p}^{P-1} R_{mv,pq}^{(n)} + \begin{cases} K\sigma^2 & \text{if } m = v \\ 0 & \text{if } m \neq v \end{cases}, \tag{5.6}
$$

where $R_{mv,pq}^{(n)}$ are the cross-correlations between path p and path q in subband n of antennas m and v.

Assume that path p and path q have delays L_p and L_q, respectively. For $q > p$ it is assumed that $L_q \geq L_p$. In order to calculate the cross-correlations $R_{mv,pq}^{(n)}$ let us consider the following cases: (i) $p = q$, (ii) $p \neq q$, $L_p \leq L_{CP}$ and $L_q \leq L_{CP}$, (iii) $p \neq q$, $L_p \leq L_{CP}$ and $L_q > L_{CP}$, and (iv) $p \neq q$, $L_p > L_{CP}$ and $L_q > L_{CP}$. The values of $R_{mv,pq}^{(n)}$ are calculated for these cases and given below. For detailed derivation of $R_{mv,pq}^{(n)}$ see Appendix.

(i) **Case 1:** $p = q$

In this case, the cross-correlations $R_{mv,pq}^{(n)}$ are in effect the correlation between samples of path p in subband n of antenna m with samples of path p itself in subband n of antenna v. Since the received signals from path p in antennas m and v are only different in phase with the phase difference $\Delta\psi_p = e^{j(m-v)\psi_p}$, it follows that

$$
R_{mv,pp}^{(n)} = K\xi_p^2 e^{j(m-v)\psi_p}. \tag{5.7}
$$

(ii) **Case 2**: $p \neq q$ and $L_p \leq L_{CP}$, $L_q \leq L_{CP}$

Since both the paths have delays smaller than L_{CP}, the utilized cyclic prefix can cover the delays to enhance the correlation between the two paths in subbands. The cross-correlations $R^{(n)}_{mv,pq}$ becomes

$$R^{(n)}_{mv,pq} = 2K\xi_p\xi_q e^{j\frac{(m-v)(\psi_p+\psi_q)}{2}} \cos\left[\frac{(m+v-2)(\psi_q-\psi_p)}{2} - \frac{2\pi}{K}(n-1)(L_q-L_p)\right]. \quad (5.8)$$

It can be seen from (5.8) that in this case the cross-correlations $R^{(n)}_{mv,pq}$ are independent of the utilized cyclic prefix L_{CP}.

(iii) **Case 3:** $p \neq q$ and $L_p \leq L_{CP}$, $L_q > L_{CP}$

In this case, since $L_q > L_{CP}$, the utilized cyclic prefix cannot cover the delay, and thus cross-correlations $R^{(n)}_{mv,pq}$ are reduced compared with Case 2. The cross-correlations in this case also depend on the cyclic prefix L_{CP} and are given by

$$\begin{aligned} R^{(n)}_{mv,pq} = {} & 2(K - L_q + L_{CP})\xi_p\xi_q e^{j\frac{(m-v)(\psi_p+\psi_q)}{2}} \\ & \cdot \cos\left[\frac{(m+v-2)(\psi_q-\psi_p)}{2} - \frac{2\pi}{K}(n-1)(L_q-L_p)\right]. \end{aligned} \quad (5.9)$$

(iv) **Case 4:** $p \neq q$ and $L_p > L_{CP}$, $L_q > L_{CP}$

Since the delays of both the multipaths exceed L_{CP}, the utilized cyclic prefix cannot cover both delays L_p and L_q. The cross-correlations $R^{(n)}_{mv,pq}$ between the two multipaths in this case are not affected by the cyclic prefix L_{CP}, and given by

$$\begin{aligned} R^{(n)}_{mv,pq} = {} & 2(K - L_q + L_p)\xi_p\xi_q e^{j\frac{(m-v)(\psi_p+\psi_q)}{2}} \\ & \cdot \cos\left[\frac{(m+v-2)(\psi_q-\psi_p)}{2} - \frac{2\pi}{K}(n-1)(L_q-L_p)\right]. \end{aligned} \quad (5.10)$$

It is noted from (5.10) that the cross-correlations $R^{(n)}_{mv,pq}$ in this case are the same with that calculated for the conventional SBAA given in (4.47).

Now in order to summarize the calculations from the above 4 cases, let us denote

$$\delta^{(n)}_{mv,pq} = \xi_p\xi_q e^{j\frac{(m-v)(\psi_p+\psi_q)}{2}} \cos\left[\frac{(m+v-2)(\psi_q-\psi_p)}{2} - \frac{2\pi}{K}(n-1)(L_q-L_p)\right] \quad (5.11)$$

so that (5.7)–(5.10) can be written in a single equation as

$$R^{(n)}_{mv,pq} = \begin{cases} K\delta^{(n)}_{mv,pq} & \text{if } p = q \\ 2K\delta^{(n)}_{mv,pq} & \text{if } p \neq q,\ L_p \leq L_{CP},\ L_q \leq L_{CP} \\ 2(K - L_q + L_{CP})\delta^{(n)}_{mv,pq} & \text{if } p \neq q,\ L_p \leq L_{CP},\ L_q > L_{CP} \\ 2(K - L_q + L_p)\delta^{(n)}_{mv,pq} & \text{if } p \neq q,\ L_p > L_{CP},\ L_q > L_{CP} \end{cases} \quad (5.12)$$

Reference Correlation Vector $\widetilde{\boldsymbol{p}}^{(n)}$

The reference correlation vector is calculated using the correlation between the subband signal vector $\widetilde{\boldsymbol{x}}^{(n)}$ and the reference signal in frequency domain $\widetilde{r}^{(n)}$ defined in (4.22) as

$$\widetilde{\boldsymbol{p}}^{(n)} = \mathcal{E}\Big\{\Big(\widetilde{\boldsymbol{x}}^{(n)}\Big)^{*}\widetilde{r}^{(n)}\Big\}, \tag{5.13}$$

where $\widetilde{r}^{(n)}$ are the reference signal samples at subband n in frequency domain, and were defined in (4.49)

$$\widetilde{r}^{(n)} = \frac{1}{\xi_0}\sum_{k=1}^{K} s_{1,0}(t-[K-1]T_s)E_{n,k}. \tag{5.14}$$

Since noise is assumed uncorrelated with signals, (5.13) becomes

$$\widetilde{\boldsymbol{p}}^{(n)} = \mathrm{E}\left\{\sum_{p=0}^{P-1}\Big(\widetilde{\boldsymbol{s}}_p^{(n)}\Big)^{*}\widetilde{r}^{(n)}\right\}, \tag{5.15}$$

where $\widetilde{\boldsymbol{s}}_p^{(n)}$ can be rewritten from (4.44) as

$$\widetilde{\boldsymbol{s}}_p^{(n)} = \sum_{k=1}^{K} s_{1,p}(t-[k-1]T_s)E_{n,k}\boldsymbol{a}(\theta_p). \tag{5.16}$$

Replacing (5.16) and (5.14) into (5.15) gives us

$$\widetilde{\boldsymbol{p}}^{(n)} = \sum_{p=0}^{P-1}\frac{\boldsymbol{a}^{*}(\theta_p)}{\xi_0}\mathcal{E}\left\{\sum_{k=1}^{K} s_{1,p}^{*}(t-[k-1]T_s)E_{n,k}^{*}\sum_{k=1}^{K} s_{1,0}(t-[k-1]T_s)E_{n,k}\right\}. \tag{5.17}$$

As the preceding path $s_{1,0}(t)$ is assumed incident at the array without delay, the calculation of the expectation in (5.17) is similar to that presented in Appendix for $L_0 = 0$ and given by

$$\begin{aligned}\mathrm{E}\Big[\sum_{k=1}^{K} s_{1,p}^{*}(t-[k-1]T_s)E_{n,k}^{*}&\sum_{k=1}^{K} s_{1,0}(t-[k-1]T_s)E_{n,k}\Big]\\ &= \begin{cases} K\xi_p\xi_0 e^{-j\frac{2\pi}{K}(n-1)L_p} & \text{if } L_p \le L_{CP} \\ (K-L_p+L_{CP})\xi_p\xi_0 e^{-j\frac{2\pi}{K}(n-1)L_p} & \text{if } L_p > L_{CP} \end{cases}.\end{aligned} \tag{5.18}$$

Now if we define

$$\hat{\boldsymbol{p}}^{(n)} = \sum_{p=0}^{P-1}\xi_p\boldsymbol{a}^{*}(\theta_p)e^{-j\frac{2\pi}{K}(n-1)L_p}, \tag{5.19}$$

then $\widetilde{\boldsymbol{p}}^{(n)}$ will be finally given by a short form as

$$\widetilde{\boldsymbol{p}}^{(n)} = \begin{cases} K\hat{\boldsymbol{p}}^{(n)} & \text{if } L_p \le L_{CP} \\ (K-L_p+L_{CP})\hat{\boldsymbol{p}}^{(n)} & \text{if } L_p > L_{CP} \end{cases}. \tag{5.20}$$

5.3.4 Array Output Signal

Since the local feedback scheme [10] is utilized for SBAA-CP, after being multiplied by the optimal weights the frequency domain samples are combined according to each subband to give $\widetilde{f}_n$, the array outputs at the array output taps in the time domain are then the IFFT of $\widetilde{f}_n$, and given by (4.51)

$$y_\ell(t) = \frac{1}{K} \sum_{n=1}^{K} \left(\widetilde{\boldsymbol{w}}^{(n)} \right)^{\mathsf{T}} \left(\sum_{p=0}^{P-1} \widetilde{\boldsymbol{s}}_p^{(n)} + \widetilde{\boldsymbol{n}}^{(n)} \right) E_{n,\ell}^{*}. \tag{5.21}$$

Using the method introduced in Chapter 4, we can write (5.21) in a simpler form as

$$y_\ell(t) = \sum_{p=0}^{P-1} \bar{\boldsymbol{s}}_p^{\mathsf{T}}(t) \boldsymbol{u}_p^{(\ell)} + \bar{\boldsymbol{n}}^{\mathsf{T}}(t) \boldsymbol{u}_N^{(\ell)}, \tag{5.22}$$

where $\bar{\boldsymbol{s}}_p(t)$, $\boldsymbol{u}_p^{(\ell)}$, $\boldsymbol{u}_N^{(\ell)}$ and $\bar{\boldsymbol{n}}^{\mathsf{T}}(t)$ were defined in (4.42) (4.56), (4.58) and (4.59), respectively.

5.3.5 Output SINR

The output SINR of SBAA-CP can be calculated using the same approach in Section 4.2.5, where for the SBAA-CP the multipath correlation matrix $\mathbf{H}$ is given for 4 different cases as below.
(i) **Case 1**: $p = q$
Since 2 multipaths are fully correlated in this case, the multipath correlation matrix $\mathbf{H}$ becomes a $K \times K$ identity matrix $\mathbf{I}$ as shown in Fig.5.3.(i), that is

$$\mathbf{H}_{K\times K} = \mathbf{I}_{K\times K} \tag{5.23}$$

(ii) **Case 2**: $p \neq q$, and $L_p \leq L_{CP}$, $L_q \leq L_{CP}$
In this case, since both the multipaths have delays smaller than L_{CP}, the utilized cyclic prefix can compensate the delays making the 2 paths fully correlated at the array output. That is the number of "1" in the multipath correlation matrix is equal to the signal frame length K. However, the multipath correlation matrix $\mathbf{H}$ is no longer a diagonal but modified as in Fig.5.3.(ii). Let $\mathbf{H}_{L+1:K,1:K-L}$ be the elements from row $(L+1)$ to row K, and from column 1 to column $(K-L)$ of the matrix $\mathbf{H}$. The multipath correlation matrix $\mathbf{H}$ can be now expressed as

$$\mathbf{H} \Rightarrow \begin{cases} \mathbf{H}_{L+1:K,1:K-L} & = \mathbf{I}_{(K-L)\times(K-L)} \\ \mathbf{H}_{1:L,K-L+1:K} & = \mathbf{I}_{L\times L} \\ \text{elsewhere} & = 0 \end{cases}. \tag{5.24}$$

$$\mathbf{H} = \begin{bmatrix} 1 & 0 & \dots & 0 & 0 & 0 & \dots & 0 \\ 0 & 1 & \dots & 0 & 0 & 0 & \dots & 0 \\ \vdots & \vdots & \dots & \vdots & \vdots & \vdots & \dots & \vdots \\ 0 & 0 & \dots & 1 & 0 & 0 & \dots & 0 \\ 0 & 0 & \dots & 0 & 1 & 0 & \dots & 0 \\ 0 & 0 & \dots & 0 & 0 & 1 & \dots & 0 \\ \vdots & \vdots & \dots & \vdots & \vdots & \vdots & \dots & 0 \\ 0 & 0 & \dots & 0 & 0 & 0 & \dots & 1 \end{bmatrix}$$

(i) Case 1: $p = q$

$$\mathbf{H} = \begin{bmatrix} 0 & 0 & \dots & 0 & 1 & 0 & \dots & 0 \\ 0 & 0 & \dots & 0 & 0 & 1 & \dots & 0 \\ \vdots & \vdots & \dots & \vdots & \vdots & \vdots & \dots & \vdots \\ 1 & 0 & \dots & 0 & 0 & 0 & \dots & 1 \\ 0 & 1 & \dots & 0 & 0 & 0 & \dots & 0 \\ 0 & 0 & \dots & 0 & 0 & 0 & \dots & 0 \\ \vdots & \vdots & \dots & \vdots & \vdots & \vdots & \dots & 0 \\ 0 & 0 & \dots & 1 & 0 & 0 & \dots & 0 \end{bmatrix}$$

(ii) Case 2: $p \neq q$ and $L_p \leq L_{CP}$, $L_q \leq L_{CP}$

$$\mathbf{H} = \begin{bmatrix} 0 & 0 & \dots & 0 & 0 & 0 & \dots & 0 \\ 0 & 0 & \dots & 0 & 0 & 1 & \dots & 0 \\ \vdots & \vdots & \dots & \vdots & \vdots & \vdots & \dots & \vdots \\ 0 & 0 & \dots & 0 & 0 & 0 & \dots & 1 \\ 1 & 0 & \dots & 0 & 0 & 0 & \dots & 0 \\ 0 & 1 & \dots & 0 & 0 & 0 & \dots & 0 \\ \vdots & \vdots & \dots & \vdots & \vdots & \vdots & \dots & 0 \\ 0 & 0 & \dots & 1 & 0 & 0 & \dots & 0 \end{bmatrix}$$

(iii) Case 3: $p \neq q$ and $L_p \leq L_{CP}$, $L_q > L_{CP}$

$$\mathbf{H} = \begin{bmatrix} 0 & 0 & \dots & 0 & 0 & 0 & \dots & 0 \\ 0 & 0 & \dots & 0 & 0 & 0 & \dots & 0 \\ \vdots & \vdots & \dots & \vdots & \vdots & \vdots & \dots & \vdots \\ 0 & 0 & \dots & 0 & 0 & 0 & \dots & 0 \\ 1 & 0 & \dots & 0 & 0 & 0 & \dots & 0 \\ 0 & 1 & \dots & 0 & 0 & 0 & \dots & 0 \\ \vdots & \vdots & \dots & \vdots & \vdots & \vdots & \dots & 0 \\ 0 & 0 & \dots & 1 & 0 & 0 & \dots & 0 \end{bmatrix}$$

(iv) Case 4: $p \neq q$ and $L_p > L_{CP}$, $L_q > L_{CP}$

Figure 5.3: Multipath correlation matrix of SBAA-CP

Note from (5.24) that the multipath correlation matrix is independent of the cyclic prefix L_{CP}.

(iii) **Case 3**: $p \neq q$ and $L_p \leq L_{CP}$, $L_q > L_{CP}$
Since the utilized cyclic prefix can cover only the delay of path p, the correlation between the two paths at the array output decreases compared with Case 2. The structure of $\mathbf{H}$ is thus the modified version of $\mathbf{H}$ in Case 2, and given by

$$\mathbf{H} \Rightarrow \begin{cases} \mathbf{H}_{L+1:K,1:K-L} & = \mathbf{I}_{(K-L)\times(K-L)} \\ \mathbf{H}_{Lq-L_{CP}+1:L,K-L_{CP}+Lp+1:K} & = \mathbf{I}_{(L_{CP}-L_p)\times(L_{CP}-L_p)} \\ \text{elsewhere} & = 0 \end{cases} . \tag{5.25}$$

An example of $\mathbf{H}$ in this case is shown in Fig.5.3.(iii).

(iv) **Case 4**: $p \neq q$ and $L_p > L_{CP}$, $L_q > L_{CP}$
Since delays of both multipaths exceed the cyclic prefix length L_{CP}, the effect of multipath

fading is thus not eliminated. As a result, the correlation matrix in this case is the same with the identity shift matrix for the conventional SBAA given in (4.68), that is

$$\mathbf{H} \Rightarrow \begin{cases} \mathbf{H}_{L+1:K,1:K-L} & = \mathbf{I}_{(K-L)\times(K-L)} \\ \text{elsewhere} & = 0 \end{cases}. \tag{5.26}$$

The illustration of $\mathbf{H}$ for this case is given in Fig.5.3.(iv).

Now by replacing (5.23)–(5.26) into (4.67), we can obtain $\boldsymbol{R}_{pq}$ for the above four cases. Using $\boldsymbol{R}_{pq}$ together with $\boldsymbol{R}_p$ and $\boldsymbol{R}_N$ defined by (4.65) and (4.66) gives us

$$\mathcal{R}_{pq}^{(\ell)} = \begin{cases} \left(\boldsymbol{u}_p^{(\ell)}\right)^{\mathsf{T}} \boldsymbol{R}_p \left(\boldsymbol{u}_p^{(\ell)}\right)^*, & \text{if } p = q \\ \left(\boldsymbol{u}_p^{(\ell)}\right)^{\mathsf{T}} \boldsymbol{R}_{pq} \left(\boldsymbol{u}_q^{(\ell)}\right)^* + \left(\boldsymbol{u}_q^{(\ell)}\right)^{\mathsf{T}} \boldsymbol{R}_{pq}^{T} \left(\boldsymbol{u}_p^{(\ell)}\right)^*, & \text{if } p \neq q \end{cases} \tag{5.27}$$

and

$$\mathcal{R}_N^{(\ell)} = \left(\boldsymbol{u}_N^{(\ell)}\right)^{\mathsf{T}} \boldsymbol{R}_N \left(\boldsymbol{u}_N^{(\ell)}\right)^*. \tag{5.28}$$

The components of the cross-correlation coefficient ρ defined in (4.30) are then given by

$$\mathcal{E}\left\{\sum_{\ell=1}^{K} y_\ell(t) r_\ell^*(t)\right\} = \sum_{p=0}^{P-1} (K - L_p)\xi_p \bar{\boldsymbol{a}}^{\mathsf{T}}(\theta_p)\hat{\boldsymbol{w}}_p, \tag{5.29}$$

$$\mathcal{E}\left\{\sum_{\ell=1}^{K} |r_\ell(t)|^2\right\} = K\frac{1}{\xi_0^2}, \tag{5.30}$$

$$\mathcal{E}\left\{\sum_{\ell=1}^{K} |y_\ell(t)|^2\right\} = \sum_{\ell=1}^{K}\left\{\sum_{p=0}^{P-1}\sum_{q=p}^{P-1} \mathcal{R}_{pq}^{(\ell)} + \mathcal{R}_N^{(\ell)}\right\}. \tag{5.31}$$

Finally, the output SINR of SBAA-CP is calculated via the cross-correlation (4.36) as

$$\mathrm{SINR}_{\mathrm{out}} = \frac{|\rho|^2}{1 - |\rho|^2}. \tag{5.32}$$

5.4 Performance Comparison of SBAA-CP with SBAA

Since the performance of an adaptive array is mainly affected by the optimal weight vector, it is possible to compare the performance of SBAA-CP with that of the conventional SBAA by comparing their optimal weight vectors in subbands accordingly. This is equivalent to compare the covariance matrices $\widetilde{\boldsymbol{R}}^{(n)}$ and the reference correlation vectors $\widetilde{\boldsymbol{p}}^{(n)}$ of both the SBAA schemes. However, this method requires the comparison for various cases as we have done above, and thus results in complicated analysis. Because the output SINR of SBAA-CP is taken as the criterion for our analysis, we thus compare the performance of the two SBAA schemes by directly considering their output SINR. As we have discussed earlier in this paper, the purpose of combining the cyclic prefix data transmission scheme with SBAA is to enhance the correlation between multipath components and thus help to improve the output SINR of SBAA-CP. By comparing the output SINR equation of SBAA-CP given in (5.32) with that of SBAA obtained in Section 4.2.5, we can see that the only different component in both SINRs is the multipath correlation matrix. This, finally, leads us to make the performance comparison by comparing the multipath correlation matrices $\mathbf{H}$.

Now let us rewrite the multipath correlation matrix $\grave{\mathbf{H}}$ of the conventional SBAA given in (4.68) as [1]

$$\grave{\mathbf{H}} = \mathbf{I}_{K\times K} \tag{5.33}$$

for $p = q$, and

$$\grave{\mathbf{H}} \Rightarrow \begin{cases} \grave{\mathbf{H}}_{L+1:K,1:K-L} & = \mathbf{I}_{(K-L)\times(K-L)} \\ \text{elsewhere} & = 0 \end{cases} \tag{5.34}$$

for $p \neq q$. The illustrations of (5.33) and (5.34) correspond to $\mathbf{H}$ in Fig.5.3.(i) and Fig.5.3.(iv), respectively.

By comparing $\grave{\mathbf{H}}$ in (5.33) and (5.34) with $\mathbf{H}$ given in (5.23)–(5.26), it is apparent that $\mathbf{H} = \grave{\mathbf{H}}$ in Case 1 and Case 4, and $\mathbf{H}$ is better than $\grave{\mathbf{H}}$ in Case 2 and Case 3. Thus it is concluded that the output SINR of SBAA-CP is always equal or better than that of the conventional SBAA. In other words, the performance of SBAA-CP is improved compared with that of the conventional SBAA due to use of the cyclic prefix in the transmit data.

Now let us consider a special case when the delays $\grave{L}_p$, $\grave{L}_q$ of multipath rays of SBAA, and the delays L_p, L_q of the multipath rays of SBAA-CP are related with one another as $L_p = \grave{L}_p + L_{CP}$ and $L_q = \grave{L}_q + L_{CP}$. In this case, since $L = L_q - L_p$ and $\grave{L} = \grave{L}_q - \grave{L}_p = L_q - L_{CP} - L_p + L_{CP} = L_q - L_p$, then it is clear that $\mathbf{H} = \grave{\mathbf{H}}$. As a result, it is concluded that when the delay of the delayed path is larger than the utilized cyclic prefix, the output SINR of SBAA-CP is the same with that of SBAA. To be more specific, if the output SINR is plotted versus the delay of the delayed paths, we can realize that the output SINR of

[1] Note that we have changed the notation for the multipath correlation matrices of SBAA from $\mathbf{H}$ to $\grave{\mathbf{H}}$ to avoid misunderstanding with that of SBAA-CP.

SBAA-CP in this case is actually the output SINR of the conventional SBAA being shifted by L_{CP} samples to the right in the time axis.

Our conclusions in this section will be supported by the numerical and simulation results in Section 5.6

5.5 SBAA-CP as a Software Antenna

In this section, we discuss the application of using SBAA-CP as a software antenna [51],[52]. The idea of the software antenna using SBAA-CP is that the antenna has capability to reconfigure itself to adapt to multipath fading conditions so that its performance is always optimized. Figure 5.4 describes a block diagram of the proposed software antenna configuration combining with the adaptive transmission scheme. Since the critical sampling is assumed for SBAA-CP, the process of decomposing the received signal into subbands is equivalent to the serial-to-parallel (S/P) conversion process which is shown in the figure. The operation of the software antenna is explained as follows. At the receiver, the so-called "Measure channel response" block keeps sensing the propagation environment to obtain the channel response of the transmission channel which is given by

$$h(t) = \sum_{p=0}^{P-1} \xi_p \delta(t - L_p), \tag{5.35}$$

where $\delta(t)$ is the Dirac delta function. Based on the obtained channel response, the block "Decide number of subband K and cyclic prefix L_{CP}" selects the optimal number of subband K and cyclic prefix length L_{CP}, and then adjusts the software antenna and transmitter configuration accordingly. The optimal subband number K and cyclic prefix L_{CP} are chosen such that a predefined number of multipath rays can be covered and the efficiency of the cyclic prefix transmission scheme, which is given by

$$\eta = \frac{K}{K + L_{CP}}, \tag{5.36}$$

is satisfied. By doing so, the performance of the software antenna is always maintained optimal.

Since the process to adjust the transmitter configuration is done via a feedback channel from the receiver to the transmitter, there exists an inevitable feedback delay τ_{fb} which is actually the propagation delay from the receiver to the transmitter. In study the performance of the adaptive transmission scheme, this delay should not be neglected. However, in this work as we focus our analysis on the performance of SBAA-CP, the effect of the delay τ_{fb} is not discussed here.

In the next section, we shall show effects of selecting various cyclic prefix lengths L_{CP} on the SBAA-CP performance.

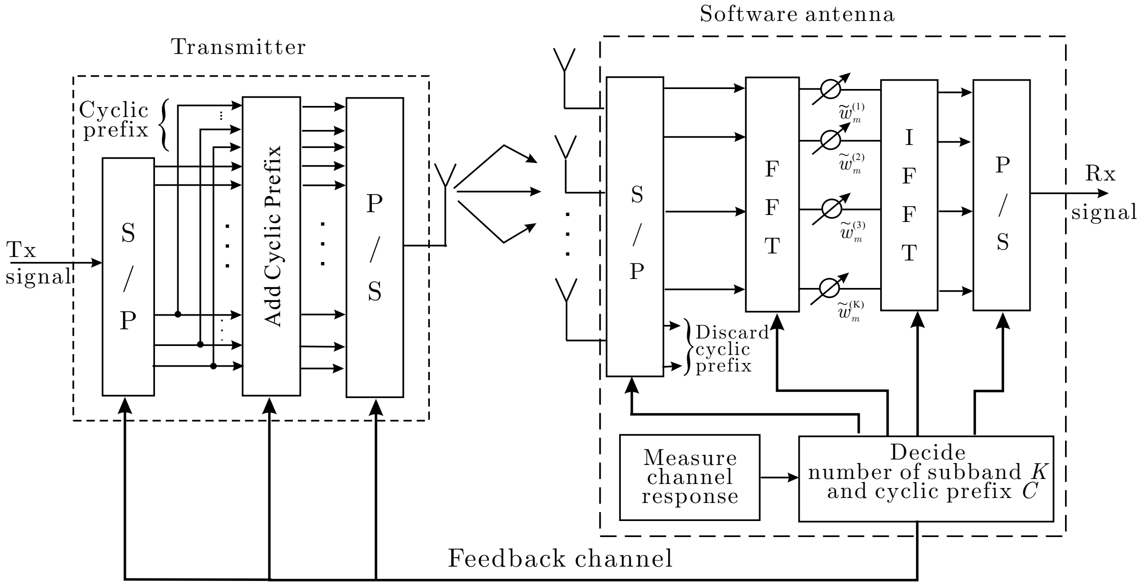

Figure 5.4: SBAA-CP as a software antenna reconfigurable to multipath fading.

5.6 Numerical and Simulation Results

5.6.1 Validation of Analysis

The validation of the analysis is done using a simulation model in Table 5.1.The multipath fading environment is assumed as in Table 5.2, where the relation between the delays of path 1 and path 2 are set according to the 4 cases which have been used in the earlier analysis. The element input SNR, which is defined by the power ratio of each multipath ray to the noise, is set equal to 0dB. The length of cyclic prefix is chosen as $L_{CP} = 4$ samples to give the efficiency about $\eta = 66.7\%$.

Figure 5.5 shows the array output SINRs for 4 different cases given in Table 5.2. The numerical results are shown to agree well with those by the simulation. It is realized that the output SINR of SBAA-CP is always equal or greater than that of the conventional SBAA for all the cases. For Case 2 and Case 3, the difference in the output SINRs of the two SBAA schemes reaches up to nearly 4dB. The only case in which the conventional SBAA can achieve the same performance with SBAA-CP is Case 1. The output SINR obtained in this case is about 11dB corresponding to the SINR estimated for the case all the paths are ideally combined, that is

$$\begin{aligned}\mathrm{SINR_{est}} &= 10\log_{10}(\mathrm{M}) + 10\log_{10}(\mathrm{P}) + \mathrm{SNR_{in}} \\ &= 10\log_{10}(4) + 10\log_{10}(3) + 0 = 10.79[\mathrm{dB}]. \end{aligned} \tag{5.37}$$

Table 5.1: Simulation model for SBAA-CP

Parameters	**Value**
Type of array	linear with $d = \lambda/2$
Number of antennas	$M = 4$
Number of subbands	$K = 8$
Cyclic prefix length	$L_{CP} = 4$
Type of modulation	BPSK
Signal length	10^4 symbols
Sampling type	T-spaced (1 sample/symbol)
Adaptive algorithm	SMI
Number of multipath rays	3 (see Table 5.2)
Input SNR	0dB

Table 5.2: Different cases to validate the analysis

Case	**Path 0** θ_0 [°]/L_0 [symbols]	**Path 1** θ_1 [°]/L_1 [symbols]	**Path 2** θ_2 [°]/L_2 [symbols]
Case 1	$0°/0$	$20°/0$	$-30°/0$
Case 2	$0°/0$	$20°/1$	$-30°/2$
Case 3	$0°/0$	$20°/4$	$-30°/5$
Case 4	$0°/0$	$20°/5$	$-30°/6$

5.6.2 Effect of Cyclic Prefix Length on the Output SINR.

In Figure 5.6, we illustrate the effect of using different cyclic prefix lengths on the output SINR of SBAA-CP. The delays of multipaths are set as $L_0 = 0$, $L_1 = L_2$ while the delay L_1 is varied from 0 to 7 to get the output SINR. Four values of cyclic prefix L_{CP} are taken into investigation as: $L_{CP} = 4$ ($\eta = 66.7\%$), $L_{CP} = 2$ ($\eta = 80\%$) and $L_{CP} = 0$ (conventional SBAA). It is seen that the longer the cyclic prefix length is utilized the better output SINR SBAA-CP can achieve. Therefore, in order to combine multipath rays with large delays, one would like to increase the length of cyclic prefix L_{CP}. However, in that case the efficiency of the cyclic prefix transmission scheme η defined in (5.36) should be maintained by enlarging the frame length K.

It is also interestingly noted from Figure 5.6 that *the output SINR of SBAA-CP when the delay of delayed paths is larger than the utilized cyclic prefix is actually the SINR of the conventional SBAA being shifted to the right by L_{CP} samples.* This calculation results support strongly our conclusion in Section 5.4.

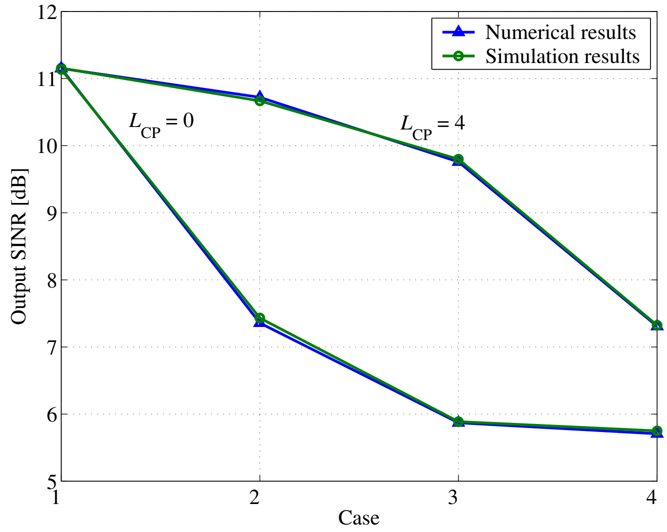

Figure 5.5: Output SINR of SBAA-CP for different cases. $M = 4$, $d = \lambda/2$, $K = 8$, 10^4 BPSK symbols, SMI algorithm, multipath parameters as in Table 5.2.

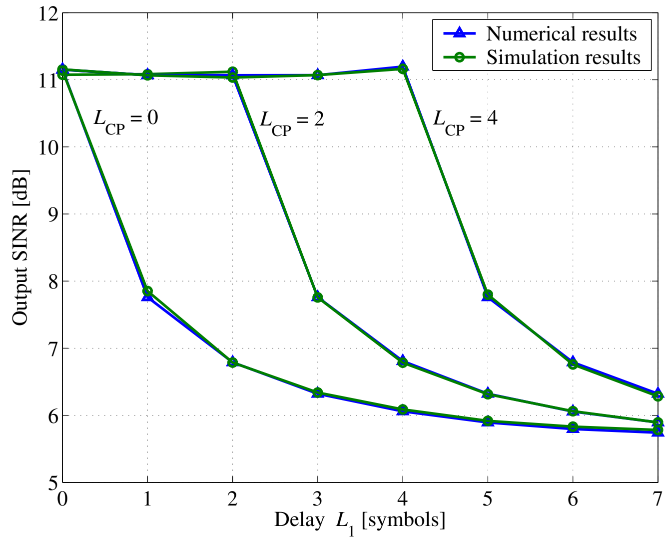

Figure 5.6: Effect of cyclic prefix on the output SINR of SBAA-CP. $M = 4$, $d = \lambda/2$, $K = 8$, 10^4 BPSK symbols, SMI algorithm. 3-path model: $\theta_0 = 0°$, $\theta_1 = 20°$, $\theta_2 = -30°$, $L_0 = 0$, $L_1 = L_2$.

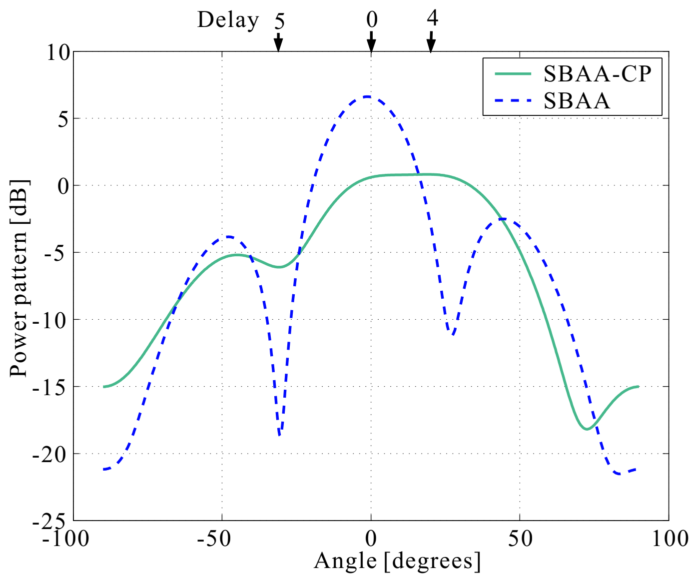

Figure 5.7: Average power patterns of SBAA-CP and SBAA. $M = 4$, $d = \lambda/2$, $K = 8$, 10^4 BPSK symbols, SMI algorithm, $L_{CP} = 4$, multipath parameters as Case 3 in Table 5.2.

5.6.3 SBAA-CP Beampattern Comparison with SBAA

Finally, the average power patterns of SBAA-CP and SBAA plotted for Case 3 in Table 5.2 are compared with each other in Figure 5.7. For both the SBAA schemes, the optimal weight vectors in subbands $\tilde{\boldsymbol{w}}^{(n)}$ are first calculated by the proposed theoretical method, then the power pattern of each subband is computed from the corresponding optimal weight vector. The average power pattern $P(\theta)$ is then obtained by averaging power patterns of all the subbands, that is

$$P(\theta) = \frac{1}{K}\sum_{n=1}^{K}\left|\boldsymbol{a}^{\mathsf{T}}(\theta)\tilde{\boldsymbol{w}}^{(n)}\right|^2, \tag{5.38}$$

$$P(\theta)[\text{dB}] = 10\log_{10} P(\theta), \tag{5.39}$$

where

$$\boldsymbol{a}(\theta) = \begin{bmatrix} 1 & e^{-j\frac{2\pi d}{\lambda}\sin\theta} & \ldots & e^{-j\frac{2(M-1)\pi d}{\lambda}\sin\theta} \end{bmatrix}^{\mathsf{T}}. \tag{5.40}$$

SBAA-CP is clearly shown to have better power pattern than that of the conventional SBAA in that it has capability to create an additional beam toward the first delayed ray θ_1.

5.7 Summary

We have presented detailed theoretical analysis of SBAA-CP under multipath fading condition. It is clearly shown that by using the cyclic prefix data transmission scheme, the performance of SBAA-CP is significantly improved over the conventional SBAA. Moreover, the output SINR of the SBAA-CP when the delay of the delayed path is larger than the utilized cyclic prefix is just simply the output SINR of SBAA being shifted L_{CP} samples to the right in time axis. We also discussed the applications of using SBAA-CP as a software antenna which has capability to reconfigure itself to adapt to multipath fading conditions so that the antenna performance is optimized. In conclusion, due to its advantages of having improved performance, reduced computation load, and capability to adapt to multipath conditions, SBAA-CP is thus considered an efficient scheme for software antenna.

Chapter 6

Subband Adaptive Array for DS-CDMA

In this chapter, we propose a novel scheme of subband adaptive array for DS-CDMA. The scheme exploits the spreading code and pilot signal as the reference signal to optimize its performance. We show that although its configuration is far different from that of 2D RAKEs the proposed scheme exhibits relatively equivalent performance of 2D RAKEs in multipath fading channel with small delay spread.

6.1 SBAA Configuration for DS-CDMA

The configuration of the scheme is shown in Figure 6.1. The subband structure of the scheme is similar with that introduced in [4]. However, in our approach, we use the critical sampling to reduce the complexity in generating the reference signal for the training process. Since critical sampling is assumed, the analysis filter works as a serial-to-parallel (S/P) converter and converts serial signal samples into parallel subband samples. These subband samples in time domain are then transformed into frequency domain subband samples using FFT.

In order to perform the adaptive signal processing in subbands, it is necessary that the reference signal also be converted into frequency domain subbands as to the received signal. In our proposed configuration of SBAA for DS-CDMA (SBAA-CDMA), the reference signal is generated from the desired user spreading code and the pilot signal. First, the user spreading code is transformed into frequency domain using the FFT transform, and then this frequency domain spreading code is used to spread the pilot signal. The result of this process is the frequency domain reference samples for each subband in the frequency domain.

The subband signals after being weighted by the optimal weights are combined according to each subband and IFFT is then performed on the subband combined signals $\widetilde{f}^{(n)}$ to give the array outputs $y_k(t)$ in time domain. To convert these array outputs to the serial signal a synthesis filter or a parallel-to-serial (P/S) converter for the case of the

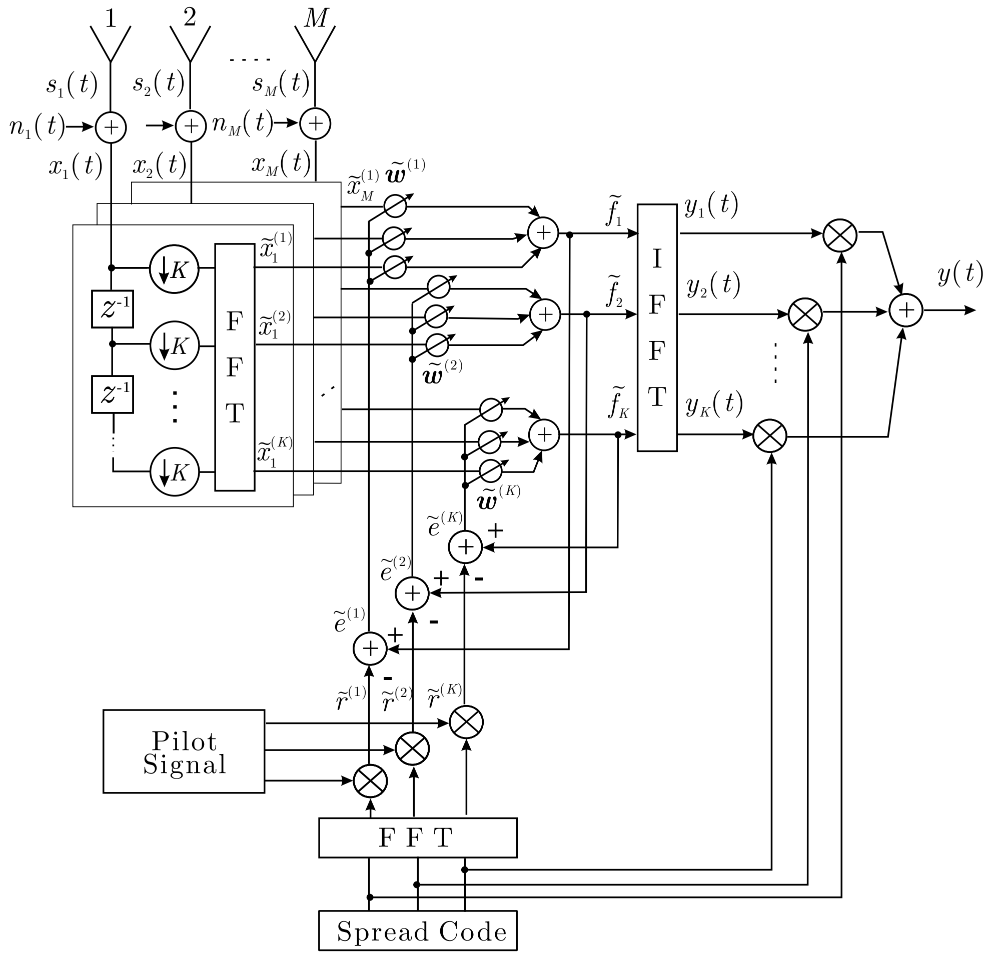

Figure 6.1: Subband adaptive array for DS-CDMA.

critical sampling SBAA is often needed [15], [16]. Since the SINR performance of SBAA does not depend on the synthesis filter [16] in our approach instead of converting $y_k(t)$ into serial signal $y(t)$ and then despreading this serial signal, we despread directly $y_k(t)$ by the desired user's spreading code $c_0(t)$ to save the synthesis filter bank. The role of this despreading part is the same with that of the correlator in the direct sequence spread BPSK receivers

6.2 Signal Model

Consider an asynchronous direct sequence spread BPSK system where after demodulation to remove the carrier frequency the received signal of the ith user is given by

$$s_i(t) = \alpha_i c_i(t) b_i(t), \tag{6.1}$$

where α_i is the complex amplitude of the received signal, $b_i(t)$ is the ith user's symbol given for BPSK modulation as

$$b_i(t) = b_u \in \{-1, 1\}, \quad uT_b \leq t < (u+1)T_b, \tag{6.2}$$

and $c_i(t)$ is the spreading code assigned to the ith user with

$$c_i(t) = c_v \in \{-1, 1\}, \quad vT_c \leq t < (v+1)T_c. \tag{6.3}$$

In (6.2) and (6.3) T_b and T_c are the bit and chip intervals, respectively. In the practical systems, T_b is often selected to be much larger than T_c to have high processing gain, *i.e.*, $P_G = T_b/T_c \gg 1$.

Assume that the system is affected by multipath fading where the received signal from the ith user contains P_i multipaths with different amplitudes $\alpha_{i,p}$, delays $\tau_{i,p}$ and arrival angles $\theta_{i,p}$. Taking into consideration the effect of all U users and local noise, the received signal at the array can be written as

$$\boldsymbol{x}(t) = \sum_{i=0}^{U-1} \sum_{p=0}^{P_i-1} \alpha_{i,p} b_i(t - \tau_{i,p}) c_i(t - \tau_{i,p}) \boldsymbol{a}(\theta_{i,p}) + \boldsymbol{n}(t), \tag{6.4}$$

where $\boldsymbol{a}(\theta_{i,p})$ is the array response vector corresponding to the pth path of the ith user's signal, and

$$\boldsymbol{n}(t) = \begin{bmatrix} n_1(t) & n_2(t) & \dots & n_M(t) \end{bmatrix}^{\mathsf{T}} \tag{6.5}$$

is the noise vector containing i.i.d. noise in each element. For a linear uniformly spaced array $\boldsymbol{a}(\theta_{i,p})$ is given by

$$\boldsymbol{a}(\theta_{i,p}) = \begin{bmatrix} 1 & e^{-j\frac{2\pi d}{\lambda}\sin\theta_{i,p}} & \dots & e^{-j\frac{2(M-1)\pi d}{\lambda}\sin\theta_{i,p}} \end{bmatrix}^{\mathsf{T}}. \tag{6.6}$$

Now if we define

$$\boldsymbol{s}_{i,p}(t) = \alpha_{i,p} b_i(t - \tau_{i,p}) c_i(t - \tau_{i,p}) \boldsymbol{a}(\theta_{i,p}) \tag{6.7}$$

as the signal vector received from the pth path of the ith user, then (6.4) can be rewritten as

$$\boldsymbol{x}(t) = \sum_{i=0}^{U-1} \sum_{p=0}^{P_i-1} \boldsymbol{s}_{i,p}(t) + \boldsymbol{n}(t). \tag{6.8}$$

Next, the received signal $\boldsymbol{x}(t)$ is decimated by a decimation factor K. These subband samples in time domain are then transformed into the frequency domain subband samples using FFT. Denote bold symbols with an overhead tilde as vectors containing samples in the frequency domain, the subband signal vectors at the nth subband in frequency domain are given by

$$\widetilde{\boldsymbol{x}}^{(n)} = \sum_{i=0}^{U-1} \sum_{p=0}^{P_i-1} \widetilde{\boldsymbol{s}}_{i,p}^{(n)} + \widetilde{\boldsymbol{n}}^{(n)}. \tag{6.9}$$

Denote the signal vector containing samples at subband n in the frequency domain as $\tilde{\boldsymbol{x}}^{(n)}$ then the covariance matrices in subbands are given by

$$\widetilde{\boldsymbol{R}}^{(n)} = \mathcal{E}\Big\{ \left(\widetilde{\boldsymbol{x}}^{(n)}\right)^* \left(\widetilde{\boldsymbol{x}}^{(n)}\right)^\mathsf{T} \Big\}. \tag{6.10}$$

Suppose that the 0th user is taken as the user of interest (desired user) while the rest $(U-1)$ users are uninterested (undesired) users. Assume that the pilot signal of the 0th user is $d_0(t)$, then the frequency domain reference samples at the nth subband are given by

$$\widetilde{r}^{(n)} = \sum_{k=1}^{K} c_0(t-[k-1]T_c) d_0(t) e^{-j\frac{2\pi}{K}(n-1)(k-1)}, \tag{6.11}$$

Since the local feedback is applied, the reference correlation vector is given by

$$\widetilde{\boldsymbol{p}}^{(n)} = \mathcal{E}\left\{ \widetilde{\boldsymbol{x}}^{(n)} \left(\widetilde{r}^{(n)}\right)^* \right\}. \tag{6.12}$$

If the mean square error (MSE) is taken as a criterion to optimize the array weights then the weight vectors in subbands are given by the Wiener-Hopf as

$$\widetilde{\boldsymbol{w}}^{(n)} = \left(\widetilde{\boldsymbol{R}}^{(n)}\right)^{-1} \widetilde{\boldsymbol{p}}^{(n)}. \tag{6.13}$$

The subband signals after being weighted by the optimal weights are combined according to each subband and the IFFT is then performed on the subband combined signals $\widetilde{f}^{(n)}$ to give signals $y_k(t)$ at the IFFT output taps. Arrange the IFFT output tap signals and spreading code for the 0th desired users in the vector form as

$$\boldsymbol{y}(t) = [y_1(t) \quad y_2(t) \quad \dots \quad y_K(t)]^\mathsf{T}, \tag{6.14}$$

$$\boldsymbol{c}_0 = [c_0(1) \quad c_0(2) \quad \dots \quad c_0(K)]^\mathsf{T}. \tag{6.15}$$

The parallel outputs $y_k(t)$ after being despread and combined are then given by

$$y_k(t) = \boldsymbol{y}^\mathsf{T}(t)\boldsymbol{c}_0^*. \tag{6.16}$$

Finally, the array output $y(t)$ is obtained by interpolating $y_k(t)$. For critical sampling, the interpolation is equivalent with parallel-to-serial (P/S) conversion.

6.3 Output SINR

The output SINR of the proposed configuration of SBAA for DS-CDMA is calculated via the cross-correlation coefficient given by (4.30)

$$\rho = \frac{\mathcal{E}\Big\{ \sum_{l=1}^{K} y_l(t) r_l^*(t) \Big\}}{\sqrt{\mathcal{E}\Big\{ \sum_{l=1}^{K} |y_l(t)|^2 \Big\} \mathcal{E}\Big\{ \sum_{l=1}^{K} |r_l(t)|^2 \Big\}}}, \tag{6.17}$$

where $r(t) = d_0(t)$ is the reference signal in time domain. The output SINR is finally computed via the correlation coefficient as

$$\mathrm{SINR}_{\mathrm{out}} = \frac{|\rho|^2}{1 - |\rho|^2}, \tag{6.18}$$

6.4 Performance Comparison with 2D RAKE

In this section, we compare the performance of the proposed SBAA-CDMA with that of the standard 2D RAKE. A standard RAKE receiver often employs a TDL with complex weights to coherently/incoherently combine delayed paths to maximize the output SINR [1]. This standard RAKE is also referred to as 1D RAKE since only the temporal structure of the received signal is exploited to estimate the channel response [53]. Due to the increasing research results on spatio-temporal processing, a new configuration of RAKE which is called the spatio-temporal RAKE receiver has been introduced in [53–55]. The spatio-temporal RAKE, which is also known as 2D RAKE receiver, is an extension of 1D RAKE where a conventional time domain RAKE receiver is combined with an adaptive array antenna to exploit both spatial and temporal structures of the received signal for maximum power combination of delayed paths. Due to the additional spatial dimension, both multipath fading and multiple access interference (MAI) are better mitigated leading to the increased channel capacity and improved output SINR [53]. When constructing 2D RAKE receivers for CDMA there exist different methods to integrate 1D RAKE with an adaptive array antenna resulting in different variations of 2D RAKE such as those in [53] to [55]. In this paper, for the purpose of comparing our proposed SBAA-CDMA with 2D RAKEs, we shall consider only the standard 2D RAKE given in Fig.6.2. This standard 2D RAKE is similar to the one introduced in [54].

The main difference between the SBAA-CDMA and the 2D RAKE receivers presented above [53]–[55] is in the beamforming method. While the 2D RAKE perform beamforming in the time domain, it is done in the subband frequency domain for the proposed SBAA-CDMA. However, despite this difference the two configurations have *relatively equivalent performance* in both single and multiple path fading environment.

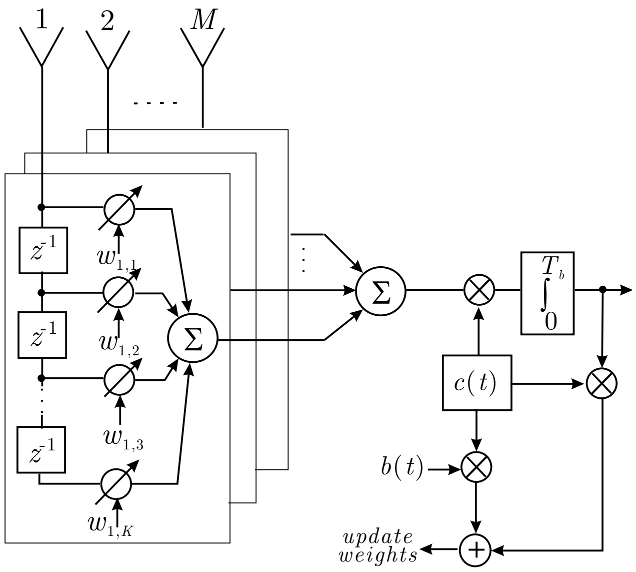

Figure 6.2: Standard 2D RAKE receiver for DS-CDMA.

Single path propagation channel

Since SBAA using FFT is a theoretically equivalent form of the TDLAA, the performance of both the adaptive arrays is relatively equal. In [43] Compton has shown that the output SINR of the TDLAA is identical to that of the SBAA using FFT provided that the number of taps in TDLs is the same with the number of samples used by FFT. Consequently, the performance of the proposed SBAA-CDMA is also the same with that of the standard 2D RAKE if the number of subbands K of the SBAA is the same with the number of employed taps in the standard 2D RAKE. This is true since in single path propagation channel the output SINRs of both the SBAA and the 2D RAKEs are independent of the number of taps K and given as a function of only the number of antennas M, the processing gain P_G and the input signal to noise ratio $\mathrm{SNR_{in}}$ as [16, 43]

$$\mathrm{SINR_{out}}[\mathrm{dB}] = 10\log_{10}(M) + 10\log_{10}(P_G) + \mathrm{SNR_{in}}[\mathrm{dB}]. \tag{6.19}$$

Multipath frequency selective fading channel

Assume that there are two multipaths with equal powers incident at the array: the direct path with AOA of 0° and the delayed path with AOA=30°. In this case, if the delay of the delayed path is smaller than the number of employed taps the output SINR of the standard 2D RAKE reaches the theoretical value given by

$$\mathrm{SINR}_{\mathrm{out}}[\mathrm{dB}] = 10\log_{10}(M) + 10\log_{10}(P_G) + 10\log_{10}(2) + \mathrm{SNR}_{\mathrm{in}}[\mathrm{dB}]. \tag{6.20}$$

Since the capability to enhance the multipath correlation of the SBAA increases with the number of subbands [2], use of a large number of subbands can increase the output SINR of the proposed SBAA-CDMA closely to the above theoretical value and thus obtain the same performance of the 2D RAKE. Due to this implicit RAKE combining function of the SBAA-CDMA, it is also referred to as *the implicit 2D RAKE* [18].

Computational complexity

This can be seen by comparing the processing methods of the implicit and standard 2D RAKE receivers. While the standard 2D RAKE processes the received signal in the chip-by-chip basis, this is done on block-by-block mode by the implicit 2D RAKE. As a result, the implicit 2D RAKE requires less mathematical operations than the standard 2D RAKE does. Recall from the subsection 3.2.2 that for a K tap and M element array antenna, the standard 2D RAKE employing the SMI algorithm requires $(KM)^3$ multiplications for each weight update. The proposed SBAA-CDMA with K subbands, on the other hand, needs only KM^3 multiplications [43]. Taking into account $2K\log_2 K$ multiplications due to both FFT and IFFT processing, the computational load required by the SBAA-CDMA is $K(M^3+2\log_2 K)$. Since DS-CDMA systems are often implemented with large processing gain P_G, then K is very large, and thus $(KM)^3 \gg K(M^3+2\log_2 K)$. Consequently, the proposed SBAA-CDMA can save a considerably large amount of computational load. From Figure 3.10, it can seen that for $K = 32$, in one iteration the 2D RAKE requires almost 14000 times more multiplications than the proposed SBAA.

It should be noted here for the case of 2D RAKE that, if the number of RAKE fingers is limited or the delay combining range is taken small enough then the amount of computational complexity will also become small. However, quantitative evaluation of the computational complexity in that case depends largely on system parameters, and thus will be spared for future research.

6.5 Simulation Results

In this section, we carry out the performance analysis of the proposed SBAA-CDMA using simulation results by computer programs. We shall focus our analysis mainly on two capabilities of the proposed SBAA-CDMA: (i) multipath combining capability and (ii) interference suppression capability. While interference suppression is the inherent capability of adaptive array antenna, multipath combining capability is gained thanks to

Table 6.1: Simulation model for the SBAA-CDMA.

Parameter	Value
Type of array	linear with $d = \lambda/2$
Number of antennas	$M = 4$
Number of subbands or TDLs	$K = 32$
Type of modulation	Direct Sequence BPSK
Data length	10^3 symbols
Spreading code	Gold code with $P_G = 31$
Adaptive algorithm	Sample Matrix Inversion (SMI)
Input SNR	0dB

use of subband signal processing. In order to make the RAKE function of the SBAA clear, we also show performance of the standard 2D RAKE as a reference. The simulation model is given in Table 6.1, where a simple CDMA network with short spread codes of 31 chip length is assumed. For the comparison purpose, we set the number of TDLs in the 2D RAKE and the number of subbands in the proposed SBAA the same and equal to 32. The spread codes are padded with either a "0" or "1" to have 32-chip length.

For simplicity, when performing the simulation we assume perfect synchronization of the pilot signal and use the recalculation method to obtain the output SINR. The 10^3 BPSK symbols are first used as the training symbols to obtain the optimal weights by SMI algorithm. These symbols are then used again as the data symbols to calculate the output SINR.

6.5.1 Multipath Combining Capability

The multipath combining capability of the SBAA-CDMA is illustrated in Figures 6.3 to 6.5. In Figure 6.3, two multipaths with the following parameters are assumed incident at the array: the direct path with $\theta_{0,0}$=0°, delay $\tau_{0,0} = 0$ chip, and the delayed path with $\theta_{0,1} = 30°$ and delay $\tau_{0,1}$ varying from 0 to 20 chips. It is noticed that the output SINR of the SBAA-CDMA decreases gradually between the 2 theoretical limits as the delay of the delayed path increases. The upper limit is the SINR value when the two paths are completely correlated calculated using (6.20) while the lower limit is the SINR value calculated using (6.19) corresponding to the case in which the two paths are totally uncorrelated. The performance of the standard 2D RAKE is shown better than that of the SBAA-CDMA in that the output SINR of the standard 2D RAKE is kept almost constant at the upper theoretical limit whereas the output SINR of the SBAA-CDMA gradually decreases from the upper to the lower theoretical limit. However, we should strongly noted that practical DS-CDMA systems always employ longer spread code than that used

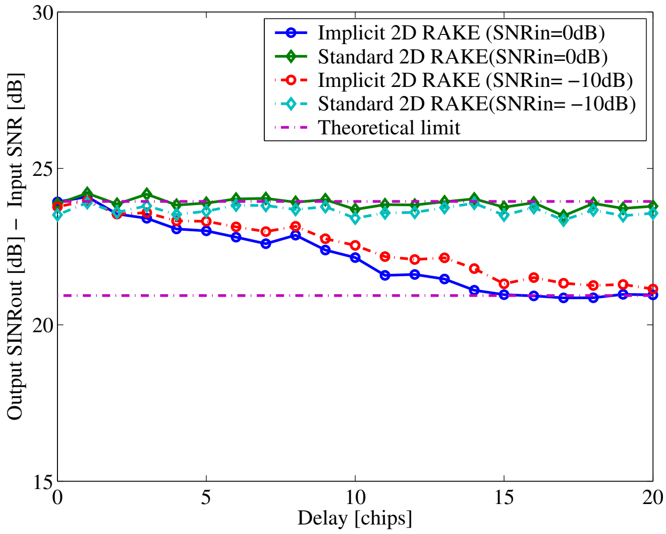

Figure 6.3: SINR of SBAA-CDMA versus delay of delayed path. $M = 4$, $d = \lambda/2$, $K = 32$, 10^3 BPSK symbols, SMI algorithm. 2-path model: $\theta_{0,0} = 0°$, $\tau_{0,0} = 0$ chip, $\theta_{0,1} = 30°$.

in the simulation to have high processing gain. Consequently, a larger number of subbands will be used leading to increased multipath correlation and thus better output SINR is expected. Moreover, in CDMA networks such as in the 3G of mobile communications, it is shown that the propagation channel is often of several chip order. As a result, the output SINRs of the SBAA-CDMA and 2D RAKE are comparatively equivalent, particularly, at low input SNRs.

Figure 6.4 shows the output SINRs as the AOA of the delayed ray $\theta_{0,1}$ varies. It is seen that if the delayed ray arrives at the array from an AOA significantly different from the direct ray then better output SINR can be achieved by both the schemes. The reason for this is that when the difference of the AOAs of the 2 paths is large enough the adaptive array can produce a supplementary lobe with a certain gain pointing towards the AOA of the delayed ray. By doing so the power of the delayed ray is optimally combined to maximize the output SINR. Whereas when the difference of the AOAs is small, the adaptive array cannot create the additional lobe causing the two paths to share the same main lobe, and thus the power of the delayed path cannot be optimally combined leading to the poorer output SINR. It is particularly noted that when the delay of the delayed path is small, namely, when $\tau_{0,1} = 1$ chip the performances of the SBAA-CDMA and the standard 2D RAKE are the same. However, as the delay of the delayed path increases, the performance of the SBAA-CDMA becomes worse than that of the standard 2D RAKE. For $\tau_{0,1} = 5$ chips the standard 2D RAKE can achieve approximately 1.7 dB better output SINR than the SBAA-CDMA for spread codes of 32 chip length.

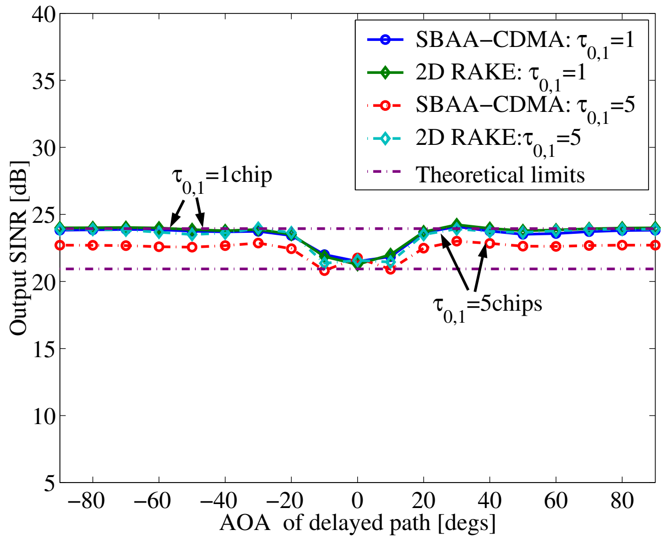

Figure 6.4: SINR of SBAA-CDMA versus AOA of delayed path. $M = 4$, $d = \lambda/2$, $K = 32$, 10^3 BPSK symbols, Input SNR=0dB, SMI algorithm. 2–path model: $\theta_{0,0} = 0°$, $\tau_{0,0} = 0$ chip, $\tau_{0,1} = 1$ and 5 chips.

Figure 6.5 compares the performances of the SBAA-CDMA and the standard 2D RAKE for different number of antenna elements and input SNRs. In this case, the received signal is assumed to contain 3 multipaths: the direct path with $\theta_{0,0} = 0°/\tau_{0,0} = 0$ chip, the first delayed path with $\theta_{0,1} = 15°/\tau_{0,1} = 1$ chip, and the second delayed path with $\theta_{0,2} = -20°/\tau_{0,2} = 2$ chips. The input SNR, which is defined by the power ratio of each path to the noise, is in turn set as -10dB, 0dB and 10dB. It is seen from Figure 6.5 that the performances of the SBAA-CDMA and 2D RAKE are relatively equivalent, particularly, for low input SNRs. The reason why the SBAA-CDMA cannot obtain the same output SINR as the standard 2D RAKE does at high input SNRs can be explained as follows. Since the signal power at the array output includes both the power of the desired signal and an amount of desired signal power correlated in the multipaths, the difference between output SINRs of the two schemes depends mainly on the capability to extract the correlated signal power from multipaths. At low input SNRs, since noise power is dominant thus the output SINRs of both the 2 schemes are similar. However, at higher input SNRs the signal and the correlated signal power become dominant. Since the standard 2D RAKE has been shown to combine multipaths better, the correlated power it can extract from multipaths is thus larger than that the SBAA-CDMA can do. Consequently, the SINR performance of the standard 2D RAKE is better than that of the SBAA-CDMA at high input SNRs.

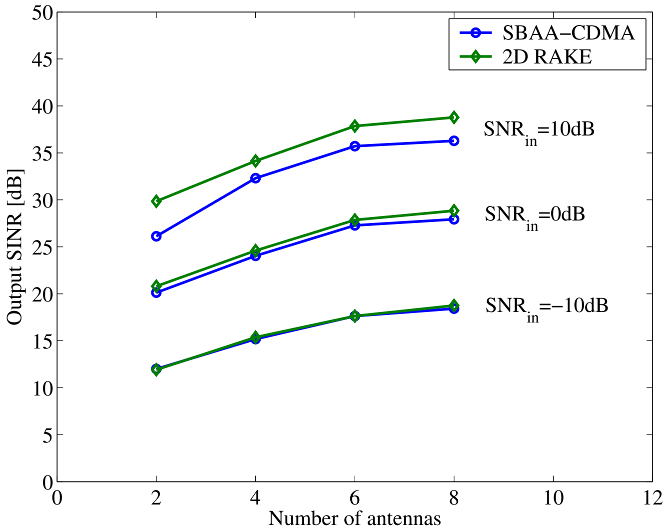

Figure 6.5: SINR of SBAA-CDMA versus number of antennas. $d = \lambda/2$, $K = 32$, 10^3 BPSK symbols, SMI algorithm. 3-path model: $\theta_{0,0} = 0°$, $\tau_{0,0} = 0$ chip, $\theta_{0,1} = 15°$, $\tau_{0,1} = 1$ chip, and $\theta_{0,2} = -20°$, $\tau_{0,2} = 2$ chips.

6.5.2 Interference Suppression Capability

We now compare the MAI cancellation capabilities of the SBAA-CDMA and the standard 2D RAKE. The propagation model is set up with 1 desired user and 3 other undesired users with interference to noise ratio INR=0dB as MAI sources. For each user's signal it is assumed that there are 1 direct ray and 2 delayed rays with AOAs and delays as given in Figure 6.6. In the figure, the denotation $a°/d$ means that the path is incident at the array from arrival angle $a°$ with d chip delay. When there are no multipaths in all user's signals, *i.e.*, each user's signal contains only the direct path (with 0 delay), the propagation environment is called the interference only; whereas if there are multipaths it is defined as the interference plus multipath environment.

The interference suppression capability of the two 2D RAKE schemes is shown in Figure 6.7, where the solid and the dotted lines denote the output SINRs of the interference plus multipath and the interference only environment, respectively. It is noticed that in the interference only environment, both the two schemes have the same interference suppression capability. However, when there exist multipaths, the performance of the SBAA-CDMA deteriorates about 1.5dB compared with that of the standard 2D RAKE. Therefore, it is concluded that although the proposed SBAA-CDMA achieves the same interference suppression capability of the standard 2D RAKE, it suffers the problem of multipaths of the interferences more seriously than the standard 2D RAKE does.

The normalized power patterns of the two schemes corresponding to Case 4 of Figure

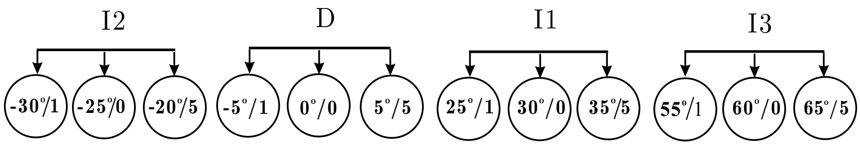

Case 1: D

Case 2: D + I1

Case 3: D + I1 + I2

Case 4: D + I1 + I2 + I3

Figure 6.6: Propagation model with MAIs for SBAA-CDMA.

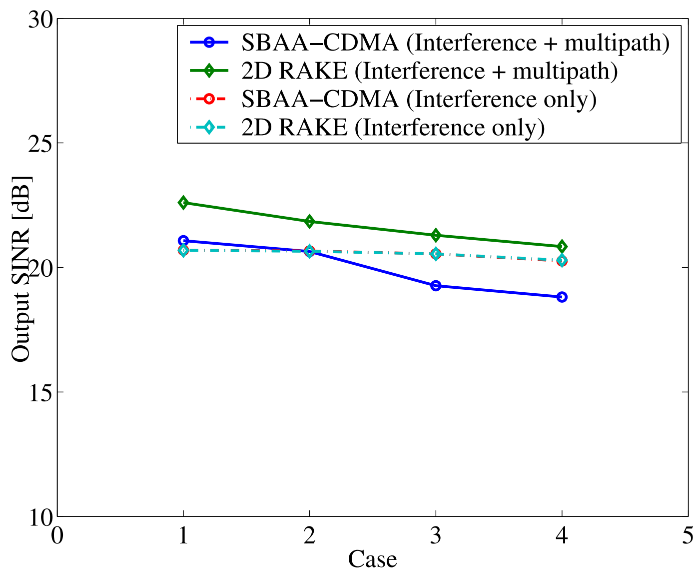

Figure 6.7: MAI cancellation capabilities of SBAA-CDMA. $M = 4$, $d = \lambda/2$, $K = 32$, 10^3 BPSK symbols, Input SNR=0dB, Input INR=0dB, SMI algorithm.

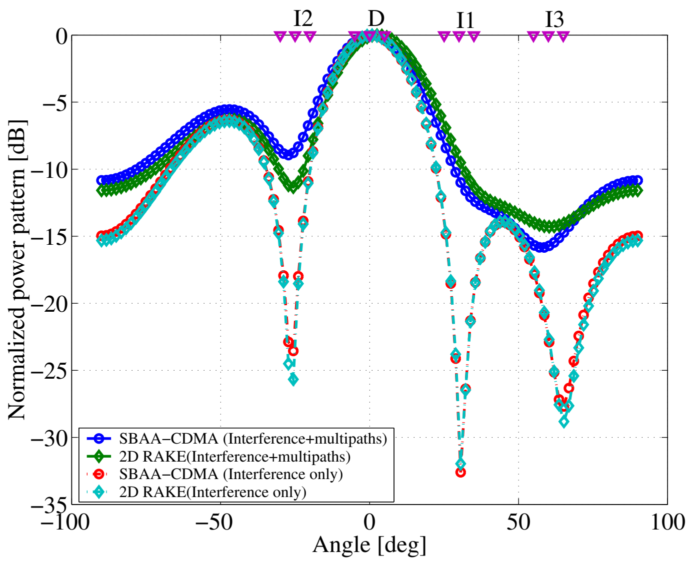

Figure 6.8: Normalized power patterns of SBAA-CDMA and 2D RAKE. $M = 4$, $d = \lambda/2$, $K = 32$, 10^3 BPSK symbols, Input SNR=0dB, Input INR=0dB, SMI algorithm. Case 4 of Fig. 6.6.

6.6 are compared in Figure 6.8. It is observed that the two schemes produce the same power patterns in the interference only environment. However, when there are multipaths the power pattern of the SBAA-CDMA becomes slightly worse in that its nulls toward the direct path of interferences are shifted to the left causing the poorer performance.

6.6 Summary

We have presented a novel configuration of subband adaptive array for DS-CDMA mobile radio which have a 2D RAKE function and thus is called the implicit 2D RAKE. The proposed SBAA-CDMA was shown to obtain comparatively equivalent performance as the standard 2D RAKE does while saving a large amount of computational load due to using subband signal processing. The proposed configuration therefore can be well applied for DS-CDMA systems to maximize the performance benefits.

It should be noted here that the performance of the proposed SBAA-CDMA be improved to be the same with that of the standard 2D RAKE by combining with cyclic prefix data transmission scheme [19] as we introduce in the following chapter.

Chapter 7

Subband Adaptive Array for Multirate Multicode DS-CDMA

A novel scheme of subband adaptive array for multicode wideband DS-CDMA is proposed in this chapter. The proposed scheme has a flexible configuration which allows basestation to be able to dynamically adapt to multirate transmission requests from subscribers. It is shown that the novel scheme can effectively suppress multiple access interferences (MAI) by appropriately forming main beam toward the desired user while pointing beampattern nulls toward MAI sources. Moreover, the combination of the subband adaptive array with the so-called cyclic prefix spreading code CDMA is also proposed to mitigate multipath fading and maximize diversity gain in multipath fading environment.

7.1 Multirate Multicode DS-CDMA Model

In multicode DS-CDMA systems [56] transmission data of high rate users is decomposed into streams of a basic rate which is often chosen to be the data rate of the user with the lowest rate. These streams are then spread and transmitted by different codes of the same length. The implementation of the multicode system thus can be done in the same way as in a single rate DS-CDMA system. An example of a dual rate multicode DS-CDMA system is shown in Figure 7.1.

Consider a multirate multicode DS-CDMA system supporting Q different data rates which correspond to Q classes of services. Those with the lowest data rate (basic rate) R_1 are called class 1 users. Assume that the user of class q has its data rate $R_q = qR_1$, where q is an integer. The data symbol duration of class q user is then given by $T_q = 1/R_q$. Denote the lth user of the class q and its spreading code as (l, q) and $c_{l,q}(t)$, respectively. In multirate multicode CDMA systems, transmission data of user (l, q) is decomposed into q streams, where each stream has the same data rate with that of the class 1 user. The ith data stream of user (l, q) is considered transmission data from *effective user* (i, l, q) [57].

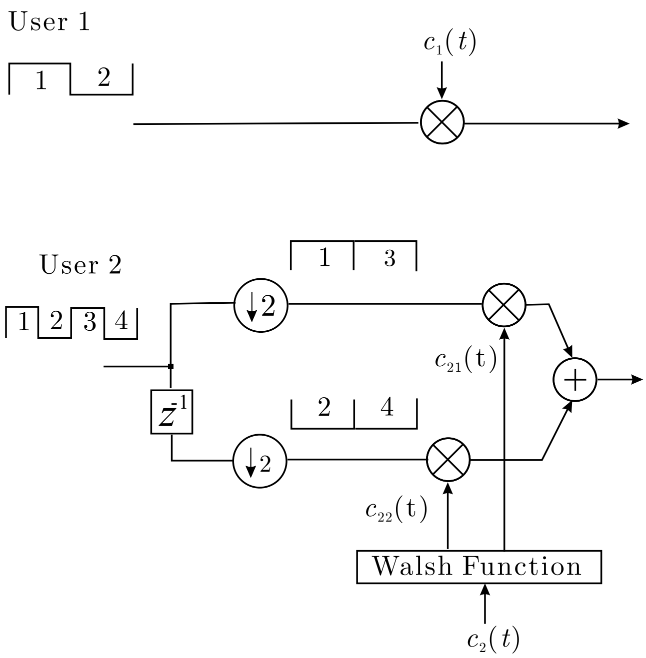

Figure 7.1: Example of a dual rate multicode DS-CDMA system.

Thus a *physical user* (l, q) is said to contain q effective users [57]. In order to spread these q effective user signals, the subcode concatenation process should be applied to create q subcodes from the primary code assigned to physical user (l, q). Since the primary codes assigned to users in DS-CDMA systems are pseudo-noise (PN) codes and in effect not orthogonal, use of PN codes directly for effective users will cause self-interference for a physical user comprised of several effective users, *i.e.*, users with high rate data. The purpose of the subcode concatenation process is to create q orthogonal subcodes for user (l, q) in which $c_{i,l,q} \perp c_{l,l,q}$ for $i \neq l$ [56]. The function of the subcode concatenate block is thus the same with the Walsh function. Denote the ith data stream of user (l, q), *i.e.*, data from effective user (i, l, q), as $b_{i,l,q}(t)$, the transmit signal from user (l, q) is given by

$$s_{l,q}(t) = \sum_{i=1}^{q} b_{i,l,q}(t) c_{i,l,q}(t) \tag{7.1}$$

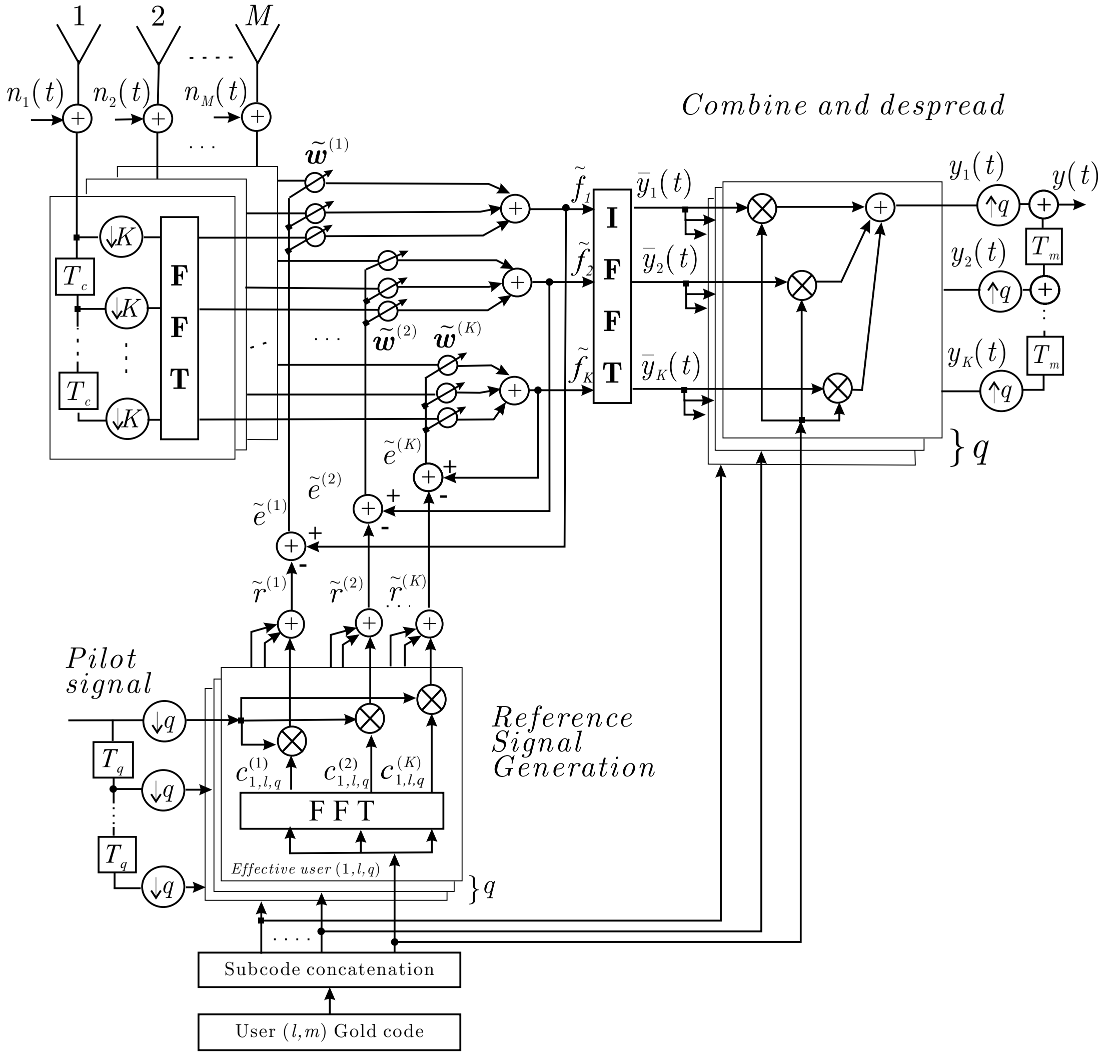

Figure 7.2: Configuration of SBAA for multirate multicode DS-CDMA systems.

7.2 SBAA Configuration for Multicode DS-CDMA

In this section, we present the novel configuration of SBAA for multirate multicode wideband DS-CDMA systems. The proposed configuration, illustrated in Figure 7.2, is an extension of the SBAA for DS-CDMA [18] presented in Chapter 6 to multirate multicode DS-CDMA. The main difference is in the so-called "Reference Signal Generation" and "Combine and Despread" blocks. These two blocks are designed in stacks using a critical sampling analysis filter with decimation/expansion rate equal to the class index q. When a user wants to transmit using class q service, for example, it sends a request to the basestation. The basestation then sets q accordingly in both Reference Signal Generation and Combine and Despread blocks to adapt to the request. The proposed configuration for multicode CDMA is thus flexible and capable of dynamical adaptation to the multirate transmission requests from subscribers (mobile stations)

7.3 Signal Model

In order to explore the performance of the configuration in multipath frequency selective fading channel, we assume that the signal from user (l,q) is incident at the basestation array with $P_{l,q}$ paths in which path p ($p \in 0,1,2,...,P_{l,q}-1$) has amplitude $\alpha_{p,l,q}$, delay $\tau_{p,l,q}$ and arrival angle $\theta_{p,l,q}$. Also, in order to realize the effect of MAIs, particularly, the effect of high rate users on the low rate users, we assume that there are K_q users in use for class q. Considering the effect of all users and noise, the received signal at the array is given by

$$\boldsymbol{x}(t) = \sum_{q=1}^{Q}\sum_{l=1}^{K_q}\sum_{p=1}^{P_{l,q}} \alpha_{p,l,q} s_{p,l,q}(t-\tau_{p,l,q})\boldsymbol{a}(\theta_{p,l,q}) + \boldsymbol{n}(t). \tag{7.2}$$

where $s_{p,l,q}(t-\tau_{p,l,q})$ and $\boldsymbol{a}(\theta_{p,l,q})$ are the signal and array response corresponding to path p of user (l,q), respectively. For a linear array antenna, $\boldsymbol{a}(\theta_{p,l,q})$ is given by

$$\boldsymbol{a}(\theta_{p,l,q}) = \begin{bmatrix}1 & e^{-j\frac{2\pi d}{\lambda}\sin\theta_{p,l,q}} \dots e^{-j\frac{2(N-1)\pi d}{\lambda}\sin\theta_{p,l,q}}\end{bmatrix}^{\mathsf{T}} \tag{7.3}$$

In equation (7.2), $\boldsymbol{n}(t)$ is the noise vector containing i.i.d element noises given by

$$\boldsymbol{n}(t) = \begin{bmatrix} n_1(t) & n_2(t) & \dots & n_M(t)\end{bmatrix}^{\mathsf{T}}. \tag{7.4}$$

To perform adaptive signal processing in subbands, the received signal $\boldsymbol{x}(t)$ is decomposed into subbands using analysis filter. The analysis filter employed in the proposed configuration utilizes critical sampling, *i.e.*, the received signal at each array element is decimated with maximum rate K as for the SBAA-CDMA presented in the previous chapter.

Now if we denote the signal vector containing samples at subband n in the frequency domain as $\tilde{\boldsymbol{x}}^{(n)}$ then the covariance matrices in subbands are given by

$$\widetilde{\boldsymbol{R}}^{(n)} = \mathcal{E}\Big\{\Big(\widetilde{\boldsymbol{x}}^{(n)}\Big)^{*}\Big(\widetilde{\boldsymbol{x}}^{(n)}\Big)^{\mathsf{T}}\Big\}. \tag{7.5}$$

In order to generate the receive antenna weights, one may use either a blind (reference signal is created from the received signal) or a pilot training (reference signal is created from a known training sequence). In this work, for simplicity we utilize the training method, in which the training data sequence is assumed to be *a priori* known at both the mobile and base stations.

Assume that user (l, q) is taken as the desired user and its assigned spread code is $c_{l,q}(t)$. After performing subcode concatenation, we obtain orthogonal subcodes $c_{i,l,q}(t)$ as explained in the above section. After taking FFT the spread subcode of the effective user (i, l, q) in frequency domain becomes

$$\tilde{c}_{i,l,q}^{(n)} = \sum_{k=1}^{K} c_{i,l,q}(t - [k-1]T_c) e^{-j\frac{2\pi}{K}(n-1)(k-1)}. \tag{7.6}$$

where T_c is the chip interval. Assume that the training data sequence of the user (l, q) is $d_{l,q}(t)$ and thus the data training sequence of the effective user (i, l, q) after decimation is $d_{i,l,q}(t)$. The reference signal for the effective user (i, l, q) at subband n then is given by

$$\begin{aligned} \tilde{r}_{i,l,q}^{(n)} &= d_{i,l,q}(t)\tilde{c}_{i,l,q}^{(n)} \\ &= \sum_{k=1}^{K} d_{i,l,q}(t) c_{i,l,q}(t - [k-1]T_c) e^{-j\frac{2\pi}{K}(n-1)(k-1)}. \end{aligned} \tag{7.7}$$

Finally, the reference signal in frequency domain for the desired user (l, q) is given by

$$\tilde{r}_{l,q}^{(n)} = \sum_{i=1}^{K_q} \sum_{k=1}^{K} d_{i,l,q}(t) c_{i,l,q}(t - [k-1]T_c) e^{-j\frac{2\pi}{K}(n-1)(k-1)}. \tag{7.8}$$

Since the localized feedback is applied, the reference correlation vector is given by

$$\widetilde{\boldsymbol{p}}^{(n)} = \mathcal{E}\left\{ \widetilde{\boldsymbol{x}}^{(n)} \left(\widetilde{r}_{l,q}^{(n)} \right)^* \right\}. \tag{7.9}$$

If the MSE is taken as a criterion to optimize the array weights then the weight vectors in subbands are given by the Wiener-Hopf as

$$\widetilde{\boldsymbol{w}}^{(n)} = \left(\widetilde{\boldsymbol{R}}^{(n)} \right)^{-1} \widetilde{\boldsymbol{p}}^{(n)}. \tag{7.10}$$

The subband signals after being weighted by the optimal weights are combined according to each subband and the IFFT is then performed on the subband combined signals $\widetilde{f}^{(n)}$ to give signals $\bar{y}_k(t)$ at the IFFT output taps. Let us arrange the IFFT output tap signals and subcodes for effective users in the vector form as

$$\bar{\boldsymbol{y}}(t) = [\bar{y}_1(t) \quad \bar{y}_2(t) \quad \ldots \quad \bar{y}_K(t)]^{\mathsf{T}}, \tag{7.11}$$

$$\boldsymbol{c}_{i,l,q} = [c_{i,l,m}(1) \quad c_{i,l,q}(2) \quad \ldots \quad c_{i,l,q}(K)]^{\mathsf{T}}. \tag{7.12}$$

The parallel outputs $y_k(t)$ after being despread and combined are then given by

$$y_k(t) = \sum_{i=1}^{K_q} \bar{\boldsymbol{y}}^{\mathsf{T}}(t)\boldsymbol{c}_{i,l,q}^{*}. \tag{7.13}$$

Finally, the array output $y(t)$ is obtained by interpolating $y_k(t)$. For critical sampling, the interpolation is equivalent with P/S conversion.

7.4 Output SINR

The output SINR of the proposed configuration of SBAA for multirate multicode DS-CDMA is calculated via the cross-correlation coefficient given by (4.30)

$$\rho = \frac{\mathcal{E}\Big\{ \sum_{l=1}^{K} y_l(t) r_l^*(t) \Big\}}{\sqrt{\mathcal{E}\Big\{ \sum_{l=1}^{K} |y_l(t)|^2 \Big\} \mathcal{E}\Big\{ \sum_{l=1}^{K} |r_l(t)|^2 \Big\}}}, \tag{7.14}$$

where $r(t)$ is the reference signal in time domain. Since user (l, m) is taken as the desired user, $r(t)$ is given by

$$r(t) = s_{l,m}(t). \tag{7.15}$$

The output SINR is finally computed via the correlation coefficient as

$$\mathrm{SINR}_{\mathrm{out}} = \frac{|\rho|^2}{1 - |\rho|^2}, \tag{7.16}$$

7.5 Diversity Gain Maximization using Cyclic Prefix Spread Code.

In wideband multirate CDMA systems, delay spread caused by multipath frequency selective fading is the factor that limits high data rate transmission. When data rate increases, the effect of ISI becomes more severe and thus combating multipath fading must be taken seriously.

Subband adaptive array as we presented so far has been shown to be able to mitigate multipath fading [2, 16]. However, the performance of SBAA degrades as the delay spread increases [16] and thus multipaths with large delay are not mitigated (refer to Chapter 6). In this section we propose a new scheme of CDMA, where different from the conventional DS-CDMA there is a cyclic prefix inserted in the user spreading code. We call the scheme cyclic prefix spreading code DS-CDMA. The combination of the SBAA

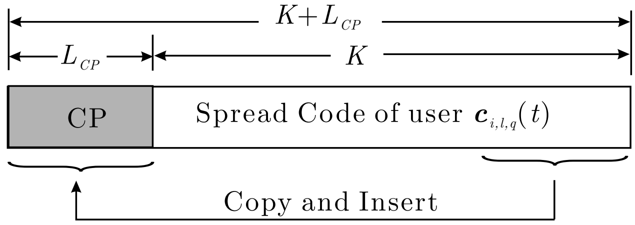

Figure 7.3: Cyclic Prefix Spreading Code for DS-CDMA.

configuration presented in the above section with cyclic prefix spreading code DS-CDMA in order to mitigate multipath fading and achieve maximum diversity gain in multipath fading environment is presented below.

Consider a multirate multicode DS-CDMA system where user (l, q) is assigned a unique code $c_{l,q}(t)$. After the subcode concatenation process the class q physical user has q subcodes for its q effective users as described in the previous section. The subcode for the effective user (i, l, q) is recalled from (7.12).

Assume that the channel suffers from multipath frequency selective fading with maximum delay of L chips and that L_{CP} chip cyclic prefix is utilized in the spreading code, the new subcode of length $(K + L_{CP}) \times 1$ for user (i, l, q) is given by

$$\begin{aligned}\hat{\boldsymbol{c}}_{i,l,m} =& [c_{i,l,m}(K - L_{CP} + 1) \dots c_{i,l,m}(K) \\ & c_{i,l,m}(1) \quad c_{i,l,m}(2) \dots \\ & \quad c_{i,l,m}(K - L_{CP} + 1) \dots c_{i,l,m}(K)]^{\mathrm{T}},\end{aligned} \tag{7.17}$$

where the last L_{CP} chips in the spreading code have been copied and inserted into the front of the code vector. The idea of inserting a cyclic prefix into the spreading code is similar with that used for single carrier frequency domain equalization [48, 49] and frequency domain beamforming [12, 15, 50] in Chapter 5. However, the method of implementation and its application to multicode DS-CDMA are novel. We shall call this new code scheme *the cyclic prefix spreading code.* The illustration of the cyclic prefix spreading code is given in Figure 7.3

When the cyclic prefix spreading code is used in the transmit side (subscriber's side), the proposed SBAA configuration of Figure 7.2 needs only small modification in the analysis filter, which is similar to that explained in [15]. Besides this modification, no other changes are necessary to implement the combination of the proposed SBAA with the cyclic prefix spreading code.

Using this proposed cyclic prefix spreading code may cost some losses in the transmission efficiency, however, the diversity gain can be maximized as we shall see from simulation results in the next section.

Table 7.1: Simulation model for SBAA for multicode DS-CDMA.

Parameter	Value
Type of array	linear with $d = \lambda/2$
Number of antennas	$M = 4$
Number of subbands	$K = 32$
Type of modulation	DS-BPSK
Data length	640 symbols per effective user
User code	Gold code with $P_G = 31$
Classes of services	Class 1, Class 2 and Class 3
Number of user per class	1 user
Adaptive algorithm	Sample Matrix Inversion (SMI)
Input SNR	0dB for effective user
Subcode concatenation	Walsh function

7.6 Simulation Results.

We now explore the performance of the proposed scheme of SBAA for multirate multicode DS-CDMA using computer simulation. We set up a simulation with parameters as shown in Table 7.1. In our simulation, each of 3 class users is assigned a unique PN Gold code. The subcode concatenation is done using Walsh function. Since new orthogonal subcodes require length of order 2 and the number of subbands used for simulation is $K = 32$, either one "0" or "1" is padded to the Gold code sequence. The selection of "0" or "1" to be padded depends on the balance between the number of "0" and "1" in the Gold code sequence. In the following simulations we always assume perfect synchronization and power control in the system. Here the perfect power control assumption means that signals from all users in the same cell site arrive at the basestation with the same power.

7.6.1 MAI Cancellation Performance

We first investigate the interference cancelling capability of the proposed scheme of SBAA for multirate multicode CDMA. A single path propagation environment is assumed with 3 different class users, namely, class 1, class 2 and class 3 users. The received signals from class 1 to class 3 users arrive at the array from $0°$, $-25°$ and $30°$, respectively. The array beampattern and output SINR for each class user are shown in Figure 7.4. It is seen that the array can appropriately create main beam toward the desired user while pointing beampattern nulls toward MAI sources. Moreover, the same output SINRs obtained for all three class users reveal that the effect of high data rate users on low rate users is resolved by using the proposed configuration.

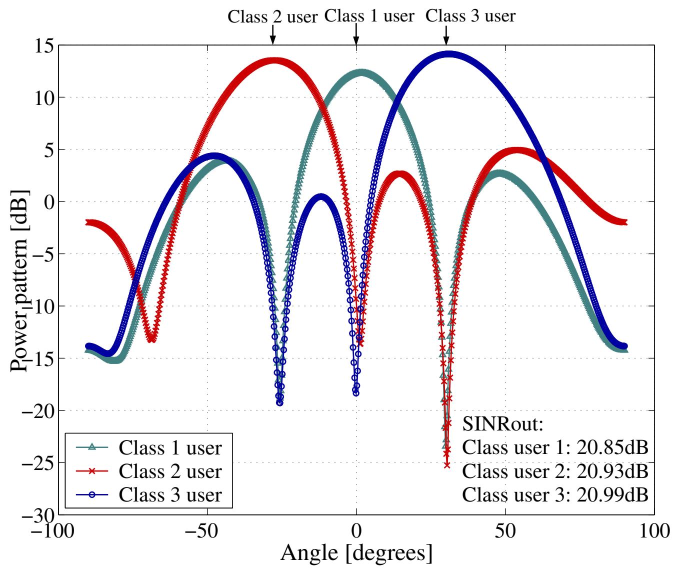

Figure 7.4: Beampatterns and output SINRs in single path environment. $M = 4$, $d = \lambda/2$, $K = 32$, 640 BPSK symbols per effective user, Input SNR=0dB, SMI algorithm.

7.6.2 Effect of Cyclic Prefix Spreading Code in Multipath Frequency Selective Fading Channel

In order to show how the proposed cyclic prefix spreading code can maximize the diversity gain in multipath frequency selective fading channel, we assume a typically simple 2 path model for all 3 class users, where there are one direct and one delayed path incident at the array from 0° and 30°, respectively. The delay of the direct path is set to 0 while that of the delayed ray is varied to obtain output SINRs versus delay of delayed ray. The output SINRs obtained for the 3 class users for $L_{CP} = 0$ and $L_{CP} = 8$ chips are illustrated in Figure 7.5. It is noticed that when the cyclic prefix is employed in the spreading code, the output SINR is maximized to the upper theoretical limit

$$\begin{aligned} \text{SINR}_{\text{out}}[\text{dB}] =& 10\log_{10}(N) + 10\log_{10}(K) + 10\log_{10}(2) \\ =& 24.08\text{dB}. \end{aligned} \tag{7.18}$$

Whereas, if cyclic prefix is not utilized or if the delay of the delayed path exceeds the employed cyclic prefix then the 3dB path diversity gain is not achieved. In that case, the output SINR decreases to the lower theoretical limit of 21dB as the delay of delayed ray increases. We also see that the output SINR is slightly better for low rate users. The reason for this is that SBAA often gives better SINR gain for low power users, which was

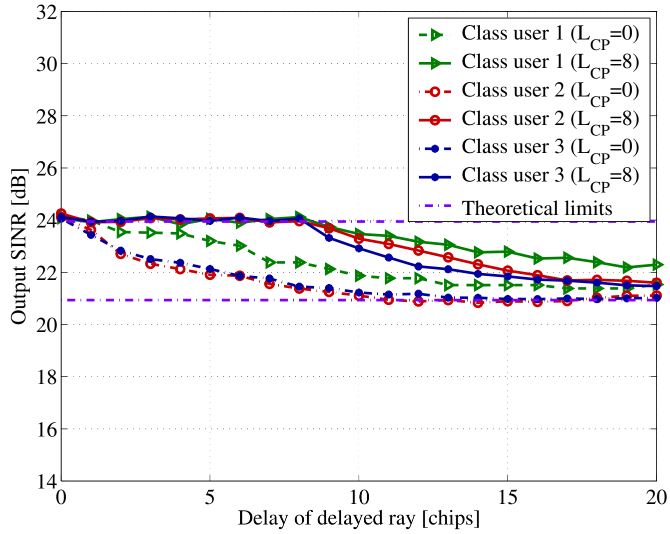

Figure 7.5: Output SINR versus delay of delayed ray. $M = 4$, $d = \lambda/2$, $K = 32$, 640 BPSK symbols per effective user, Input SNR=0dB, SMI algorithm, 2-path model.

clearly shown in Chapter 4.

The effect of use of cyclic prefix spreading code on beampattern and output SINR for each class user in a more practical multipath fading environment is shown through Figures 7.6.(a) to 7.6.(c). The assumed propagation environment is similar to that used in Figure 7.4. However, in the received signal of each class user it is assumed that there are 2 more delayed rays with the same delay of 7 chips incident at $-5°$ and $+5°$ apart from the direct path. In the simulation, we assume that both the two delayed rays have the same power as that of the corresponding direct ray. The figures show that use of cyclic prefix spreading code helps to improve array beampatterns in that the main beam with larger gain is created toward the desired user while still keeping the pattern nulls deeply pointed toward MAI sources. Consequently, the output SINRs for all class users are maximized to around 24dB. It is also noticed that the SINR gains achieved for class 2 and class 3 users are better than that for class user 1. This observation coincides with that revealed from Figure 7.5. In order to show whether incident directions affect the obtained SINR gains of different class users, we swapped positions of the 3 class users for one another. We have found that in spite of its incident direction, the SINR gain achieved for the class 1 user is always about 6dB (25dB with CP and 19dB without CP); whereas those obtained for class 2 and 3 users are 10dB (24dB with CP and 14dB without CP). This implies that those with multiple codes can have better SINR gains that of the single code user.

Next, the output SINRs of the proposed configuration against the number of array

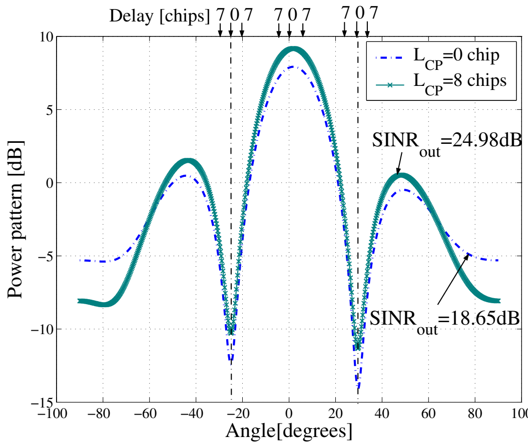

(a) Beampattern of class 1 user

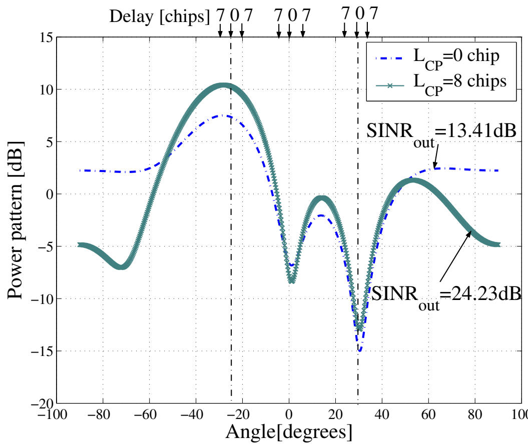

(b) Beampattern of class 2 user

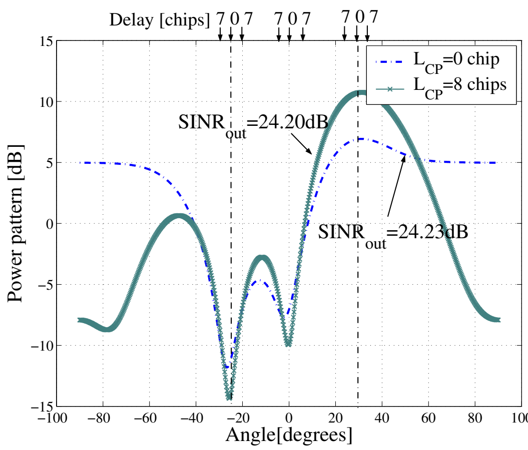

(c) Beampattern of class 3 user

Figure 7.6: Beampatterns in multipath fading environment. $M = 4$, $d = \lambda/2$, $K = 32$, 640 BPSK symbols per effective user, Input SNR=0dB, SMI algorithm, 3-path model.

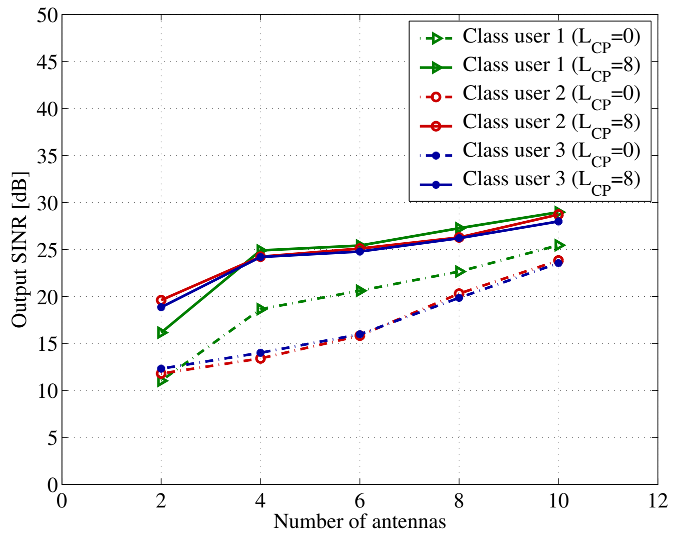

Figure 7.7: Output SINR versus number of array elements. $d = \lambda/2$, $K = 32$, 640 BPSK symbols per effective user, Input SNR=0dB, SMI algorithm.

elements in the above assumed multipath fading environment are shown in Figure 7.7. It is clearly shown that the more array elements are used the larger space diversity can be achieved, and thus better output SINR is obtained. Another interesting observation from Figure 7.7 is that the SINR gain due to cyclic prefix spreading code is better obtained for array with smaller number of elements. This can be explained by the fact that when the number of employed array elements is small the path diversity gain obtained by the array is also small and thus the difference between obtained and the maximum SINRs is large. Therefore, the effect of cyclic prefix spreading code is apparent. However, as the number of array elements increases the path diversity gain is improved accordingly causing the obtained output SINR to reach closely the maximum value. Consequently, the effect of cyclic prefix spreading code is clearly smaller in this case.

7.6.3 BER Performance in Multiuser Frequency Selective Channel

Bit error rates (BERs) of different class users are illustrated in Figure 7.8. In order to obtain the BERs, we obtained the signal model in Figure 7.6 and generated 9 more users (3 users per each class) with random angles of arrival. In each user signal, as in the above simulations we assume that there 2 more delayed paths incident at $+5^\circ$ and -5° apart from the center path with random delays but smaller than the utilized cyclic prefix length. Moreover, powers of all the direct and delayed paths are set equal. For each class, we take

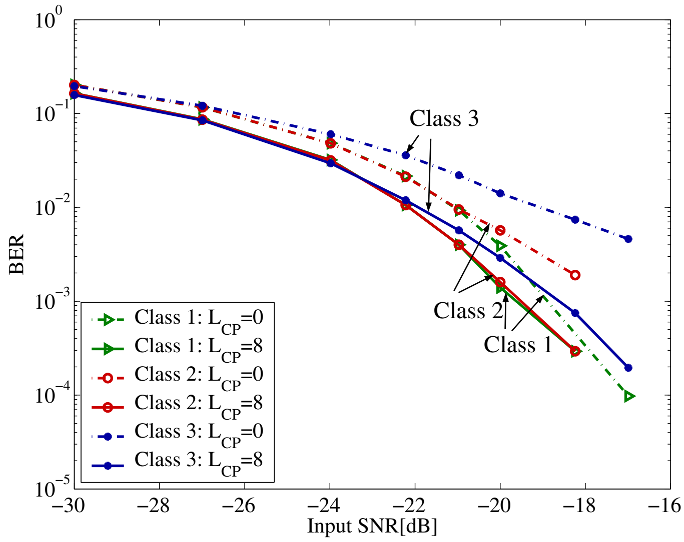

Figure 7.8: BERs of different class users. $M = 4$, $d = \lambda/2$, $K = 32$, SMI algorithm, 4 users$\times$3 classes.

a user with the same parameters used for Figure 7.6 as the desired user into investigation. Simulations are then carried out for 30 times. The obtained BERs are then averaged and plotted versus the input SNRs before combining and despreading. It is easy to realize that use of cyclic prefix spreading code can improve BER performance of SBAA for multicode CDMA, particularly, for class 3 user.

Diversity Gain versus Transmission Efficiency

We have shown that by using cyclic prefix spreading code, the diversity gain can be maximized and thus large amount of diversity gain can be achieved. The longer the cyclic prefix is, the better diversity gain can be gained depending on the channel order. However, as we stated above adding a cyclic prefix into the spreading code would lead to a decrease in transmission efficiency. Thus the transmission efficiency, defined in (5.36)

$$\eta = \frac{K}{K + L_{CP}} \tag{7.19}$$

should be considered to balance the cyclic prefix and diversity gain. In our simulation, since 8 chips were inserted into 32 chip code sequence, the efficiency is $\eta = \frac{32}{32+8} = 80\%$ which is equivalent to the transmission efficiency loss of about $10 \log_{10} \frac{32+8}{32} \simeq 1$dB. However, at least 3dB diversity gain was obtained for the simple case of 1 direct and 1 delayed ray in Figure 7.5. For a richer scattering environment such as with 2 delayed rays in Figure 7.6, it may be possible to get up to 10dB gain as revealed from Figure 7.6.(b) and Figure 7.6.(c). Clearly, it is deserved to sacrifice 1dB loss in transmission efficiency to receipt of 10dB diversity gain. Since the practical propagation environment often contains a large number of delayed rays, and thus larger diversity gain can be expected by using cyclic prefix spreading code.

7.7 Summary

We have proposed a novel configuration of SBAA for multirate multicode DS-CDMA systems. It was shown that the proposed configuration can effectively suppress MAIs and eliminate the effect of high rate users on low rate users which often happens in multirate CDMA systems. We have also proposed a new scheme of DS-CDMA with cyclic prefix spreading code. Simulation results showed that the combination of the proposed SBAA with the cyclic prefix spreading code CDMA helps to maximize diversity gain in multipath fading environment.

Chapter 8

Conclusion and Future Work

This chapter summarizes the results of this work and describes open topics for the future research. Finally, conclusion of the work is included.

8.1 Conclusions

In this work, the fundamentals of adaptive array were reviewed in Chapter 2. Chapter 3 described basic operations and components of SBAA and discussed the configuration SBAA as well as the motivations to use SBAA in mobile communications. Performance of SBAA and SBAA-CP were analyzed using theoretical method in Chapter 4 and Chapter 5, respectively. Finally, two novel configurations of SBAA for DS-CDMA in Chapter 6 and for the wideband multirate multicode DS-CDMA in Chapter 7.

According to the numerical and simulation results shown in this work, the following concluding remarks are obtained

- **Performance of SBAA**

  1. Detailed mathematical models for performance analysis of both SBAA and SBAA-CP were successfully developed. The models give exact expressions for subband signals, subband optimum weights, array output and the output SINR. The developed models are simple and can be applied for various types of adaptive array.
  2. It was shown that the output SINR of SBAA and TDLAA are the same in single path propagation environment. However, in multipath frequency selective fading channel provided that the same number of TDLs and subbands are utilized, performance of SBAA is slightly worse than that of TDLAA depending on the input SNR and delay spread of the channel. SBAA is however, superior to TDLAA in having significantly reduced computational complexity.

3. Combining with cyclic prefix data transmission scheme, SBAA-CP can achieve the same performance of TDLAA in trade-off of the transmission efficiency. The configuration of SBAA-CP can be developed to become a software antenna which can be reconfigurable to adapt to the multipath fading channel.
4. Performance of SBAA-CP when the delay spread is larger than the cyclic prefix length is simply the performance of SBAA shifted by L_{CP} samples in the time axis.

- **Applications of SBAA to DS-CDMA**

  1. A novel generalized configuration of SBAA for DS-CDMA was proposed. The proposed configuration has implicitly RAKE function and expresses comparatively equivalent performance of the 2D-RAKE while outperforming 2D-RAKE in computation complexity. The configuration is thus can be well applied for DS-CDMA, particularly, in the frequency selective channel with small delay spread.
  2. A novel generalized configuration of SBAA for multirate multicode DS-CDMA was proposed. The configuration is flexible, which allows the array to easily adapt to multirate requests from subscribers. Both MAI and interference by high data rate users on low data rate users are suppressed using the the configuration.
  3. Use of cyclic prefix spreading code can maximized diversity gain of SBAA for DS-CDMA in the multipath frequency selective fading channel.

- **Applications of cyclic prefix in wideband multipath frequency selective fading channel.**

  1. Single carrier cyclic prefix data transmission and cyclic prefix spreading code are effective methods to maximize diversity gain in the wideband multipath frequency selective fading channel.

8.2 Future Work

Referring to the above conclusions, there are several areas of this work which could be extended for future research.

1. In this work SINR was taken as the performance criterion for analysis. Further analysis using other criteria such as frame error rate (FER) or BER would probably provide better understanding on the SBAA performance.

2. Analysis in Chapters 4 and 5 focused mainly on the effects of multipath fading on the performance of SBAA. Additional analysis under multipath fading plus interference would provide additional insight into the performance of SBAA.

3. Performance of the two proposed configurations of SBAA for DS-CDMA and the multicode DS-CDMA was investigated using computer simulation. Analysis of the configurations using theoretical method is still opened for further research.

4. Almost all configurations of SBAA were introduced for forward link beamforming. Applications of SBAA to downlink beamforming and MIMO systems could be an interesting topic for further study.

5. Cyclic prefix is an effective method to improve the array performance in the frequency selective channel. Recently, applications of cyclic prefix in single carrier frequency domain equalization for space-time block code were also proposed in [58, 59]. It is possible to replace the frequency domain equalizer by a SBAA-CP. How to modify SBAA-CP configurations for space-time block code and performance results of the combined space-time code and SBAA-CP would be of particularly interesting.

6. Due to the similarity in the configuration of SBAA and adaptive array for OFDM, using the analytical model for SBAA to analyze performance of adaptive array for OFDM may be an interesting topic.

References

[1] A. J. Paulraj and C. B. Paradias, "Space-time processing for wireless communications", *IEEE Signal Procesing Magazine*, vol. 14, no. 6, pp. 49–83, November 1997.

[2] Y. Zhang, K. Yang, and M. G. Amin, "Adaptive array procesing for multipath fading mitigation via exploitation of filter banks", *IEEE Transactions on Antennas and Propagation*, vol. 49, no. 4, pp. 505–516, April 2001.

[3] K. Yang, Y. Zhang, and Y. Mizuguchi, "A signal subspace-based subband approach to space-time adaptive processing for mobile communications", *IEEE Transaction on Signal Processing*, vol. 49, no. 2, pp. 401–413, February 2001.

[4] J. M. Khalab and M. K. Ibrahim, "Novel multirate adaptive beamforming", *Electronics Letters*, vol. 30, no. 15, pp. 1194–1195, July 1994.

[5] Y. Zhang K. Yang and Y. Mizuguchi, "Subband realization of space-time adaptive processing for mobile communications", in *Proc. The 10th IEEE International Symposium on Personal, Indoor and Mobile Communications (PIMRC)*, Osaka, Japan, 1999, pp. 785–791.

[6] Y. Kamiya, S. Denno, Y. Mizuguchi, M. Katayama, A. Ogawa, and Y. Karasawa, "Development of an adaptive array based on subband signal processing", in *Proc. The fifth International Symposium on Antennas and Propagation EM Theory (ISAPE)*, Beijing, China, August, 2000.

[7] T. Sekiguchi and Y. Karasawa, "CMA adaptive array antennas using analysis and synthesis filter banks", *IEICE Transaction on Fundamentals*, vol. E81-A, no. 8, pp. 1570–1577, August 1998.

[8] Y. Zhang, K. Yang, and M. G. Amin, "Adaptive subband arrays for multipath fading mitigation", in *Proc. IEEE Antennas and Propagation Society International Symposium*, Atlanta, GA, 1998, pp. 380–383.

[9] Y. Zhang, K. Yang, and Y. Karasawa, "Subband CMA adaptive arrays in multipath fading environment", *IEICE Transaction on Communications (Japanese Edition)*, vol. J82-B, no. 1, pp. 97–108, January 1999.

[10] Y. Zhang, K. Yang, M. G. Amin, and Y. Karasawa, "Performance analysis of subband arrays", *IEICE Transaction on Communications*, vol. E84-B, no. 09, pp. 2507–2515, September 2001.

[11] Y. Zhang, K. Yang, and M. G. Amin, "Convergence performance of subband arrays for spatio-temporal equalization", in *Proc. IEEE Workshop on Statistical Signal Processing*, Singapore, August 2001.

[12] Y. Karasawa and M. Shinozawa, "Subband signal processing adaptive array with a data transmission scheme inserting a cyclic prefix", *IEICE Transaction on Communications (Japanese Edition)*, vol. J85-B, no. 1, pp. 90–99, January 2002.

[13] T. Taniguchi, X. N. Tran, and Y. Karasawa, "Analysis and evaluation of subband adaptive array under multipath fading environment", in *Proc. The IEEE Semiannual Vehicular Technology Conference*, Birmingham, Alabama, May 2002.

[14] X. N. Tran, T. Taniguchi, and Y. Karasawa, "Performance analysis of subband adaptive array in multipath fading environment", in *Proc. The 2002 IEEE AP-S International Symposium and USNC/URSI National Radio Science Meeting*, San Antonio, Texas, USA, June 2002, pp. 610–613.

[15] X. N. Tran, T. Taniguchi, and Y. Karasawa, "Theoretical analysis of subband adaptive array combining cyclic prefix data transmission scheme", *IEICE Transaction on Communications*, vol. E85-B, no. 12, pp. 2610–2621, December 2002.

[16] X. N. Tran, T. Taniguchi, and Y. Karasawa, "Performance analysis of subband adaptive array in multipath fading environment", *IEICE Transaction on Fundamentals*, vol. E85-A, no. 8, pp. 1798–1806, August 2002.

[17] X. N. Tran, T. Taniguchi, and Y. Karasawa, "Theoretical analysis of subband adaptive array combining cyclic prefix data transmission scheme", in *Proc. The 8th IEEE International Conference on Communication Systems (ICCS)*, Singapore, November 2002.

[18] X. N. Tran, T. Omata, T. Taniguchi, and Y. Karasawa, "Subband adaptive array for DS-CDMA mobile radio", in *Proc. 2002 Interim International Symposium on Antennas and Propagation*, Yokosuka Reserach Park, Japan, November 2002.

[19] X. N. Tran, T. Taniguchi, and Y. Karasawa, "Subband adaptive array for multirate multicode DS-CDMA systems", *IEICE Transaction on Fundamentals*, vol. E–86A, no. 7, pp. 1611–1618, July 2003.

[20] S. Weiss, *On Adaptive Filter in Oversampled Subbands*, PhD thesis, University of Strathclyde, 1988.

[21] B. Widrow, P. E. Mantey, L. J. Griffiths, and B. B. Goode, "Adaptive antenna systems", *Proceedings of IEEE*, vol. 55, pp. 2143–2159, December 1967.

[22] W. F. Gabriel, "Adaptive array – an introduction", *Proceedings of IEEE*, vol. 64, pp. 239–272, February 1976.

[23] J. E. Hudson, *Adaptive Array Principle*, Peter Peregrinus Ltd., 1981.

[24] R. T. Compton, *Adaptive Antennas: Concepts and Performance*, Prentice Hall, 1988.

[25] P. H. Lehne and M. Pettersen, "An overview of smart antenna technology for mobile communications systems", *IEEE Communications Survey*, vol. 2, no. 4, pp. 2–13, Fourth Quarter 1999.

[26] B. D. Van Veen and K. M. Buckley, "Beamforming: A versatile approach to spatial filtering", *IEEE Signal Processing Magazine*, pp. 4–24, April 1988.

[27] R. A. Monzingo and T. W. Miller, *Introduction to Adaptive Arrays*, John Wiley & Sons, 1980.

[28] L. C. Godara, "Application of antenna arrays to mobile communications, part 2: Beam-forming and direction-of-arrival considerations,", *Proceedings of the IEEE*, vol. 85, no. 8, pp. 1193–1245, August 1997.

[29] J. Litva and T. K.-Y. Lo, *Digital Beamforming in Wireless Communications*, Artech House, 1996.

[30] R. B. Ertel, *Antenna Array Systems: Propagation and Performance*, Ph.D. Thesis, Virginia Polytechnic Institute and State University, 1999.

[31] B. Widrow and S. D. Stearns, *Adaptive Signal Processing*, Prentice Hall, 1985.

[32] N. Kikuma, *Adaptive Signal Processing with Array Antenna*, Science and Technology Publishing Co., Ltd., Japan, 1999.

[33] S. Haykin, *Adaptive Filter Theory*, 4th edition., Prentice Hall, 2002.

[34] G. V. Tsoulos, "Smart antennas for mobile communication systems", *Electronics and Communication Engineering Journal*, vol. 11, no. 2, pp. 84–94, April 1999.

[35] J. H. Winters, "Smart antennas for wireless systems", *IEEE Personal Communications*, vol. 5, no. 1, pp. 23–27, February 1988.

[36] P. P. Vaidyanathan, “Multirate digital filters, filter banks, polyphase networks, and aplications: A tutorial”, *Proceeding of IEEE*, vol. 78, no. 1, pp. 56–93, January 1990.

[37] A. J. Coulson, “A generalization of nonuniform bandpass sampling”, *IEEE Transactions on Signal Processing*, vol. 43, no. 3, pp. 694–704, March 1995.

[38] A. Gilloire and M. Vetterli, “Adaptive filter in subbands with critical sampling: Analysis, experiments, and application to acoustic echo cancellation”, *IEEE Transactions on Signal Processing*, vol. 40, no. 8, pp. 1862–1875, August 1992.

[39] M. D. Courville and P. Duhamel, “Adaptive filtering in subbands using a weighted criterion”, *IEEE Transactions on Signal Processing*, vol. 46, no. 9, pp. 2359–2371, September 1998.

[40] S. S. Pradhan and V. U. Reddy, “A new approach to subband adaptive filtering”, *IEEE Transactions on Signal Processing*, vol. 47, no. 3, pp. 655–664, March 1999.

[41] M. K. Sridharan, “Subband adaptive filtering: Oversampling approach”, *Signal Processing*, vol. 71, pp. 101–104, 1998.

[42] R. E. Crochiere and L. R. Ranbiner, *Multirate Digital Signal Processing*, Prentice Hall, 1983.

[43] R. T. Compton, “The relationship between tapped delay-line and FFT processing in adaptive arrays”, *Transactions on Antennas and Propagation*, vol. 36, no. 1, pp. 15–26, January 1988.

[44] S. Weiss, R. W. Stewart, M. Schabert, I. K. Proudler, and M. W. Hoffman, “An efficient scheme for broadband adaptive beamforming”, in *Proc. The 33rd Asilomar Conference on Signals, Systems, and Computers*, Monterey, CA, 1999.

[45] M. Schabert, “Subband adaptive beamforming”, Master’s thesis, University of Strathclyde, 1999.

[46] J. R. Treichler, I. Fijalkow, and Jr. C. R. Johnson, “Fractionally spaced equalizers: How long should they really be”, *IEEE Signal Prococessing Magazine*, vol. 13, no. 3, pp. 65–81, May 1996.

[47] R. V. Nee and R. Prasad, *OFDM for Wireless Multimedia Communications*, Artech House, 2000.

[48] S. Sari, G. Karam, and I. Jeanclaude, “Frequency domain equalization of mobile radio and terrestrial broadcast channels”, in *Proc. IEEE Global Telecommunications Conference (GLOBECOM)*, San Francisco, CA, 1994.

[49] A. Czylwik, "Comparison between adaptive OFDM and single carrier modulation with frequency domain equalization", in *Proc. IEEE Vehicular Technology Conference*, Phoenix, May 1997.

[50] M. V. Clark, "Adaptive frequency domain equalization and diversity combining for broadband wireless communications", *IEEE Journal on Selected Areas in Communications*, vol. 16, no. 8, pp. 1385–1395, October 1998.

[51] Y. Karasawa, T. Sekiguchi, and T. Inoue, "The software antenna: A new concept of kaleidoscopic antenna in multimedia radio and mobile computing era", *IEICE Transaction on Communications*, vol. E80–B, no. 8, pp. 1214–1217, August 1997.

[52] Y. Karasawa, Y. Kamiya, T. Inoue, and S. Denno, "Algorithm diversity in a software antenna", *IEICE Transaction on Communications*, vol. E83–B, no. 6, pp. 1229–1236, July 2000.

[53] B. H. Khalaj, A. J. Paulraj, and T. Kailath, "2D RAKE receivers for CDMA cellular systems", in *Proc. IEEE Global Telecommunications Conference (GLOBECOM)*, San Francisco, USA, 1994, pp. 400–404.

[54] A. Stephene and B. Champagne, "Improving the performance of blind CDMA 2D RAKE receivers with phase ambiguity in the bit decision variable", in *Proc. The 32th Asilomar Conference on Signals, Systems and Computers*, California, USA, November 1998, pp. 1882–1886.

[55] T. Inoue and Y. Karasawa, "Two-dimensional RAKE reception scheme for DS/CDMA systems in beam space digital beam forming antenna configuration", *IEICE Transaction on Communications*, vol. E81-B, no. 7, pp. 1374–1383, July 1998.

[56] C. L. I and R. D. Gitlin, "Multi-code CDMA wireless personal communications networks", in *Proc. IEEE International Conference on Communications*, Seattle, AW, USA, 1995, pp. 1060–1064.

[57] M. Juntti, "System concept comparisons for multirate CDMA with multiuser detection", in *Proc. IEEE Vehicular Technology Conference*, Ottawa, Canada, 1998, pp. 31–35.

[58] F. W. Vook and T. A. Thomas, "Transmit diversity schemes for broadband communication systems", in *Proc. IEEE Vehicular Technology Conference*, 2000, pp. 2523–2529.

[59] N. Al-Dhahir and T. A. Thomas, "Single-carrier frequency-domain equalization for space-time-coded transmissions over broadband wireless channels", in *Proc. International Symposium on Personal, Indoor and Mobile Radio Communications (PIMRC)*, September 2001, pp. 143–146.

Appendix A

Derivation of $R_{mv,pp}^{(n)}$ for SBAA-CP

Assume that there are multipath 2 paths, for example, paths p and q, incident at the array. For simplicity, let us consider the case $m \neq v$ so that noise components are uncorrelated with signals and does not appear in our calculation. In this case, $\varepsilon_{mv}^{(n)}$ are given by

$$\begin{aligned}\varepsilon_{mv}^{(n)} = \mathcal{E}\Bigg\{ &\sum_{k=1}^{K} \Big(s_{1,p}(t-[k-1]T_s)e^{-j(m-1)\psi_p} + s_{1,q}(t-[k-1]T_s)e^{-j(m-1)\psi_q} \Big)^* E_{n,k}^* \\ &\sum_{k=1}^{K} \Big(s_{1,p}(t-[k-1]T_s)e^{-j(v-1)\psi_p} + s_{1,q}(t-[k-1]T_s)e^{-j(v-1)\psi_q} \Big) E_{n,k} \Bigg\}. \end{aligned} \tag{A.1}$$

Using (5.6) we can express (A.1) as

$$\begin{aligned}\varepsilon_{mv}^{(n)} &= \mathcal{E}\Bigg\{ \sum_{k=1}^{K} s_{1,p}^*(t-[k-1]T_s)e^{j(m-1)\psi_p} E_{n,k}^* \sum_{k=1}^{K} s_{1,p}(t-[k-1]T_s)e^{-j(v-1)\psi_p} E_{n,k} \Bigg\} \\ &+ \mathcal{E}\Bigg\{ \sum_{k=1}^{K} s_{1,p}^*(t-[k-1]T_s)e^{j(m-1)\psi_p} E_{n,k}^* \sum_{k=1}^{K} s_{1,q}(t-[k-1]T_s)e^{-j(v-1)\psi_q} E_{n,k} \\ &+ \sum_{k=1}^{K} s_{1,q}^*(t-[k-1]T_s)e^{j(m-1)\psi_q} E_{n,k}^* \sum_{k=1}^{K} s_{1,p}(t-[k-1]T_s)e^{-j(v-1)\psi_p} E_{n,k} \Bigg\} \\ &+ \mathcal{E}\Bigg\{ \sum_{k=1}^{K} s_{1,q}^*(t-[k-1]T_s)e^{j(m-1)\psi_q} E_{n,k}^* \sum_{k=1}^{K} s_{1,q}(t-[k-1]T_s)e^{-j(v-1)\psi_q} E_{n,k} \Bigg\} \\ &= R_{mv,pp}^{(n)} + R_{mv,pq}^{(n)} + R_{mv,qq}^{(n)}. \end{aligned} \tag{A.2}$$

The closed form of $R_{mv,pq}^{(n)}$ is calculated for different cases as follows.

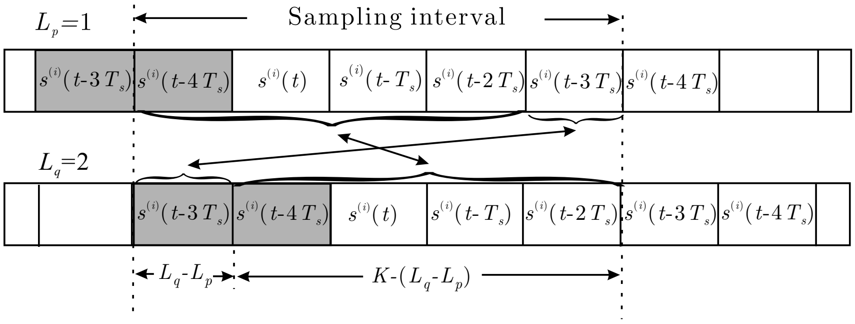

Figure A.1: Illustration of correlation between 2 multipaths. Case 2: $K = 5$, $L_{CP} = 2$, $L_p = 1$, $L_q = 2$.

A.1 Case 1: $p = q$

In this case, it is straightforward from (A.2) that

$$R^{(n)}_{mv,pp} = K\xi_p^2 e^{j(m-v)\psi_p}. \tag{A.3}$$

A.2 Case 2: $p \neq q$ and $L_p \leq L_{CP}$, $L_q \leq L_{CP}$

Denote frame i of the transmit signal as $s^{(i)}(t)$, $s^{(i)}(t - T_s)$, ..., $s^{(i)}(t - [K-1]T_s)$. Note that the signals of paths p and q can be expressed as $s_p(t) = \xi_p s(t - L_pT_s)$ and $s_q(t) = \xi_q s(t - L_qT_s)$, respectively. Now let us consider the first term of $R^{(n)}_{mv,pq}$ which is given by

$$\begin{aligned}
&\mathcal{E}\Bigg\{\sum_{k=1}^{K} s^*_{1,p}(t-[k-1]T_s)e^{j(m-1)\psi_p}E^*_{n,k}\cdot\sum_{k=1}^{K} s_{1,q}(t-[k-1]T_s)e^{-j(v-1)\psi_q}E_{n,k}\Bigg\}\\
&=\mathcal{E}\Bigg\{\xi_p\Big[s^*(t-[K-L_p]T_s)+\ldots+s^*(t-[K-1]T_s)e^{j\frac{2\pi}{K}(n-1)L_p}+s^*(t)e^{j\frac{2\pi}{K}(n-1)(L_p+1)}\\
&+s^*(t-[K-L_p-1]T_s)e^{j\frac{2\pi}{K}(n-1)(K-1)}\Big]\xi_q\Big[\ldots+s(t-[K-L_p-1]T_s)e^{-j\frac{2\pi}{K}(n-1)(L_q-L_p-1)}\\
&+s(t-[K-L_p]T_s)e^{-j\frac{2\pi}{K}(n-1)(L_q-L_p)}+\ldots+s(t-[K-1]T_s)e^{-j\frac{2\pi}{K}(n-1)L_q}\\
&+s(t)e^{-j\frac{2\pi}{K}n-1(L_q+1)}+\ldots\Big]\Bigg\}e^{j\{(m-1)\psi_p-(v-1)\psi_q\}}e^{j\{(m-1)\psi_p-(v-1)\psi_q\}}.
\end{aligned}\tag{A.4}$$

Using the illustration in Figure A.1 and noting that $e^{j\frac{2\pi}{K}(n-1)K} = e^{-j\frac{2\pi}{K}(n-1)K} = 1, \forall n$, after some mathematical manipulations (A.4) becomes

$$\begin{aligned}
&\mathcal{E}\{\sum_{k=1}^{K} s^*_{1,p}(t-[k-1]T_s)e^{j(m-1)\psi_p}E^*_{n,k}\sum_{k=1}^{K} s_{1,q}(t-[k-1]T_s)e^{-j(v-1)\psi_q}E_{n,k}\Big\} \\
&= \xi_p\xi_q\Big\{\big[K-(L_q-L_p)\big]e^{-j\frac{2\pi}{K}(n-1)(L_q-L_p)} + (L_q-L_p)e^{j\frac{2\pi}{K}(n-1)[K-(L_q-L_p)]}\Big\} \\
&\qquad\qquad\qquad\qquad\qquad\qquad\qquad\qquad \cdot e^{j\{(m-1)\psi_p-(v-1)\psi_q\}} \\
&= K\xi_p\xi_q e^{-j\frac{2\pi}{K}(n-1)(L_q-L_p)}e^{j\{(m-1)\psi_q-(v-1)\psi_p\}}
\end{aligned} \tag{A.5}$$

Following the calculation in (A.4) and (A.5), the second term of $R^{(n)}_{mv,pq}$ can be found as

$$\begin{aligned}
&\mathcal{E}\Big\{\sum_{k=1}^{K} s^*_{1,q}(t-[k-1]T_s)e^{j(m-1)\psi_q}E^*_{n,k}\cdot\sum_{k=1}^{K} s_{1,p}(t-[k-1]T_s)e^{-j(v-1)\psi_p}E_{n,k}\Big\} \\
&= K\xi_p\xi_q e^{j\frac{2\pi}{K}(n-1)(L_q-L_p)}e^{j\{(m-1)\psi_p-(v-1)\psi_q\}}
\end{aligned} \tag{A.6}$$

Combining (A.5) and (A.6) we can obtain $R^{(n)}_{mv,pq}$ as

$$R^{(n)}_{mv,pq} = 2K\xi_p\xi_q e^{j\frac{(m-v)(\psi_p+\psi_q)}{2}}\cos\left[\frac{(m+v-2)(\psi_q-\psi_p)}{2} - \frac{2\pi}{K}(n-1)(L_q-L_p)\right]. \tag{A.7}$$

A.3 Case 3: $p \neq q$ and $L_p \leq L_{CP}$, $L_q > L_{CP}$

By doing similarly as for Case 2, $R^{(n)}_{mv,pq}$ is obtained as

$$\begin{aligned}
R^{(n)}_{mv,pq} &= \xi_p\xi_q\Big\{[K-(L_q-L_p)]e^{-j\frac{2\pi}{K}(n-1)(L_q-L_p)} + (L_{CP}-L_p)e^{j\frac{2\pi}{K}(n-1)[K-(L_q-L_p)]}\Big\} \\
&\qquad \cdot e^{j\{(m-1)\psi_q-(v-1)\psi_p)\}} + \xi_p\xi_q\Big\{[K-(L_q-L_p)]e^{j\frac{2\pi}{K}(n-1)(L_q-L_p)} \\
&\qquad + (L_{CP}-L_p)e^{-j\frac{2\pi}{K}(n-1)[K-(L_q-L_p)]}\Big\}e^{j\{(m-1)\psi_p-(v-1)\psi_q)\}}
\end{aligned} \tag{A.8}$$

which finally becomes

$$\begin{aligned}
R^{(n)}_{mv,pq} &= 2(K-L_q+L_{CP})\xi_p\xi_q e^{j\frac{(m-v)(\psi_p+\psi_q)}{2}} \\
&\qquad \cdot\cos\left[\frac{(m+v-2)(\psi_q-\psi_p)}{2} - \frac{2\pi}{K}(n-1)(L_q-L_p)\right].
\end{aligned} \tag{A.9}$$

A.4 Case 4: $p \neq q$ and $L_p > L_{CP}$, $L_q > L_{CP}$

Using the calculation in Case 2, $R^{(n)}_{mv,pq}$ in this case is given by

$$\begin{aligned} R^{(n)}_{mv,pq} &= \xi_p \xi_q \big[K - (L_q - L_p)\big] e^{-j\frac{2\pi}{K}(n-1)(L_q-L_p)} e^{j\{(m-1)\psi_q-(v-1)\psi_p\}} \\ &\qquad + \xi_p \xi_q \big[K - (L_q - L_p)\big] e^{j\{(m-1)\psi_p-(v-1)\psi_q\}} e^{j\frac{2\pi}{K}(n-1)(L_q-L_p)} \\ &= 2(K - L_q + L_p)\xi_p \xi_q e^{j\frac{(m-v)(\psi_p+\psi_q)}{2}} \\ &\qquad \cdot \cos\left[\frac{(m+v-2)(\psi_q-\psi_p)}{2} - \frac{2\pi}{K}(n-1)(L_q-L_p)\right]. \end{aligned} \tag{A.10}$$

List of Original Publications

Journal Papers

Journal Papers Directly Related to the Dissertation

1. X. N. Tran, T. Taniguchi and Y. Karasawa, "Performance analysis of subband adaptive array in multipath fading environment", *IEICE Transaction on Fundamentals,* Special section on Digital Signal Processing, vol. E85–A, no. 8, pp. 1798–1806, August 2002. (Related to the contents of Chapter 4)

2. X. N. Tran, T. Taniguchi and Y. Karasawa, "Theoretical analysis of subband adaptive array combining cyclic prefix data transmission scheme,"*IEICE Transaction on Communications,* Special Issue on Software Defined Radio Technology and Its Applications, vol. E85–B, no. 12, pp. 2610-2621, December 2002. (Related to the contents of Chapter 5)

3. X. N. Tran, T. Taniguchi and Y. Karasawa, "Subband adaptive array for multirate multicode DS-CDMA systems,"*IEICE Transaction on Fundamentals,* Special Section on Multi-dimensional Mobile Information Networks, vol. E.86–A, no. 7, pp. 1611–1618, July 2003. (Related to the contents of Chapter 7)

Journal Papers Used for Reference

4. X. N. Tran, "A comprehensive method to analyse and design Cassegrain antennas for satellite earth stations," *DGPT–Post and Telecommunications Journal*, no.1, pp. 29–35, July 1999, Vietnam (in English).

5. X. N. Tran, "A computational method to obtain the sum and difference pattern of the conical corrugated horn for satellite tracking," *DGPT–Post and Telecommunications Journal,* no.2, pp. 47–53, December 1999, Vietnam (in Vietnamese).

6. X. N. Tran, "Effects of the design parameters on the efficiency of Cassegrain antenna in Ka-band," *Science and Technique,* Le Qui Don Technical University, No.87(II-1999), pp.12-19, 1999, Vietnam (in English).

International Conference Papers

1. T. Taniguchi, X. N. Tran and Y. Karasawa, "Analysis and evaluation of subband adaptive array under multipath fading environment," in *Proc. The IEEE Semiannual Vehicular Technology Conference,* Birmingham, Alabama, USA, May 2002.(Related to the contents of Chapter 4 and Chapter 5)

2. X. N. Tran, T. Taniguchi and Y. Karasawa, "Performance analysis of subband adaptive array in multipath fading environment," in *Proc. The 2002 IEEE AP-S International Symposium and USNC/URSI National Radio Science Meeting,* San Antonio, Texas, USA, June 2002. (Related to the contents of Chapter 4)

3. X. N. Tran, T. Omata, T. Taniguchi and Y. Karasawa, "Subband adaptive array for DS-CDMA mobile radio," in *Proc. The 2002 Interim International Symposium on Antennas and Propagation,* Yokosuka Reserach Park, Yokosuka, Japan , November 2002. (Related to the contents of Chapter 6)

4. X. N. Tran, T. Taniguchi and Y Karasawa, "Theoretical analysis of subband adaptive array combining cyclic prefix data transmission scheme," in *Proc. 8th IEEE International Conference on Communication Systems (ICCS'02)*, Singapore, November 2002. (Related to the contents of Chapter 5)

5. X. N. Tran, T. Taniguchi and Y Karasawa, "Subband adaptive array for multirate multicode DS-CDMA," in *Proc. 2003 IEEE AP-S Topical Conference on Wireless Communications Technology*, Honolulu, Hawaii, USA, October 2003. (Related to the contents of Chapter 7)

Other Conference Papers and Presentations

1. X. N. Tran, T. Taniguchi and Y. Karasawa, "Performance analysis of subband adaptive array in multipath fading environment," *Technical Report of IEICE*, AP2001-109, pp. 129–134, October 2001.

2. X. N. Tran, T. Taniguchi and Y. Karasawa, "Improvement of subband adaptive array performance using a novel data transmission scheme adding a cyclic prefix: theoretical analysis," *Technical Report of IEICE*, AP2001-148, pp.27–32, Nov. 2001.

3. X. N. Tran, T. Taniguchi and Y. Karasawa, "Analysis of the optimal weight vector of the subband adaptive array using data transmission scheme with cyclic prefix," *IEICE General Conference,* Waseda University, Tokyo, Japan, March 2002.

4. T. Taniguchi, X. N. Tran and Y. Karasawa, "Performance analysis and evaluation of subband adaptive array using data transmission with cyclic prefix under multipath fading environment," *Technical Report of IEICE,* RCS2002-49, April 2002.

5. X. N. Tran, T. Omata, T. Taniguchi and Y. Karasawa, "Subband adaptive array for DS-CDMA Mobile Radio," *IEICE Society Conference*, Symposium on Multiple Access and Signal Processing Transmission Technique for Next Generation Mobile Communications, SB-12-7, 10-12 September 2002, Miyazaki University, Kyushyu, Japan.

6. X. N. Tran, T. Taniguchi and Y. Karasawa, "Subband adaptive array for multirate multicode DS-CDMA systems," *Technical Report of IEICE,* AP2002-171, vol. 102, no. 166, pp. 69–74, March 2002.

7. X. N. Tran, T. Taniguchi and Y. Karasawa, "Subband adaptive array for multi-rate multicode DS-CDMA Systems," *IEICE General Conference*, Symposium on Advanced Radio Link Control Techniques for Broadband Wireless Access, SB-12-2, Tohoku University, Sendai, Japan, March 2003.

8. T. Taniguchi, R. Takemoto, X. N. Tran and Y. Karasawa, "A design method of MIMO communication system with robustness to eigenvector mismatch problem," *Technical Report of IEICE,* AP2003-9, pp. 51–55, April 2003.

9. X. N. Tran, T. Taniguchi and Y. Karasawa, "A novel adaptive beamforming for space-time block codes," *Technical Report of IEICE,* AP2003, August 2003.

10. X. N. Tran, T. Taniguchi and Y. Karasawa, "Adaptive beamforming for multiuser space-time block code," *IEICE Society Conference*, Niigata University, Niigata, Japan, September 2003.

Author Biography

Xuan Nam Tran (*Trần Xuân Nam*) was born in Thanh Hoa, Vietnam on the 8th September 1971. He received Bachelor of Engineering in Radio-electronics from Hanoi University of Technology, Vietnam in 1993 and Master of Engineering in telecommunications engineering from University of Technology, Sydney, Australia in 1998. From October 2000 to September 2003 he was a doctorate candidate in the Department of Electronic Engineering, The University of Electro-Communications, Tokyo, Japan. He was also a research assistant at the same department from April 2002 to September 2003. His research interests are in the areas of adaptive arrays, subband signal processing for adaptive arrays, code division multiple access (CDMA), wideband multiple-input multiple-output (MIMO) and space-time codes.

Mr. Tran is a student member of the Institute of Electronics, Information and Communications Engineering (IEICE), Japan and the Institute of Electrical and Electronics Engineers (IEEE).